The Synthesis and Reactivity of Novel $[Co(L)(PMG)]^{n+}$ Complexes

A thesis submitted in partial fulfilment
of the requirements for the degree
of
Master of Science in Chemistry
at the
University of Canterbury
by
Andrea L. Cusiel

April 2005

Abstract

Glyphosate (*N*-(phosphonomethyl)glycine) is the phytotoxic reagent in the widely used Roundup® herbicide. Its mode of action in plants is the disruption of the Shikimate pathway, part of an important route to the biosynthesis of essential aromatic amino acids. It is well documented that glyphosate can be degraded by soil microorganisms after contact of the herbicide solution with the soil. It is also accepted that glyphosate, an excellent ligand, is readily absorbed to metal ions, such as Fe(III), that can be abundant in soils.

There have been many accounts on the microbial degradation of glyphosate, and several metal-glyphosate complexes have been synthesised and characterised. Surprisingly, given the degree of adsorption to metal ions in the soil, there have not, to date, been any reports in the literature on the reactivity of metal-glyphosate complexes. The behaviour of these types of complexes under various reaction conditions may give us an insight into the mechanisms present when glyphosate degrades.

In order to explore the behaviour of metal-glyphosate adducts, we have prepared several new cobalt-PMG complexes in the lab. These complexes have been characterised by NMR, mass spectrometry, elemental analysis, and in some cases X-ray crystal structure determination. We chose to synthesise complexes where the PMG ligand is bidentate or tridentate, filling the remaining four or three (respectively) coordination sites with an ancillary, nitrogen-containing ligand.

We have subjected the complexes to photolytic and basic conditions, as we are interested in ascertaining how coordinated PMG might behave when irradiated with UV light, and when it is C-deprotonated. Metal-glyphosate complexes in nature may be exposed to UV light, so we are concerned with how the coordinated ligand might react under these circumstances. We have found that the prepared cobalt-PMG complexes are reactive when exposed to UV light, and that this appears to result in the degradation of the complex, and in some cases, the PMG ligand itself.

The reactivity of C-deprotonated PMG is also an area of interest to us. It is possible that elevations in soil pH can lead to C-deprotonation of glyphosate, then further reactivity that may contribute to the degradation of the compound. Furthermore, when the herbicide is held in the active site of an enzyme within a microbe, it may become deprotonated, and this may aid in its microbial degradation. We have found that, under basic conditions, the reactivity of the prepared PMG complexes depends on the ancillary ligand attached - π-acidic, pyridine-containing ancillary ligands appear to increase the reactivity of coordinated PMG. It seems that amine-containing ligands hinder the reactivity of the coordinated PMG such that the complex remains intact.

It is hoped that the results of the research described in this thesis will assist in the future investigations into the reactivity of the herbicide glyphosate.

Acknowledgements

The research presented in this thesis is the culmination of two years of work, and I have many people to express my gratitude to.

First and foremost, my thanks go to my supervisor, Dr Richard Hartshorn, for his continual encouragement, commitment to excellence, and his open-door policy. Richard invests countless hours in making his students' post-graduate research experiences successful and fulfilling.

I would especially like to thank my husband-to-be, Andy Kitchingman, who has supported me financially, spiritually, and mathematically during the marathon that is a Masters Degree. Even when the going got tough his support of my gaining a good university education never faltered.

My thanks go to Mum (Diane Cusiel) and Dad (Hans Cusiel) for not questioning my choice to pack in a reasonably good job and become a student at the ripe old age of 28, and for always offering food.

The members of the Hartshorn group, change as they may from year to year, have been a great team to work with. There are too many to name, but all have made post-grad life quite an agreeable experience.

The staff of the University of Canterbury Chemistry Department have been invaluable. Thanks to:

- Professor Ward Robinson for his expertise in solving my X-ray crystal structures.
- Wayne McKay for fixing my rotovap pumps.
- Rewi Thompson for rescuing me on many occasions when running those darned phosphorus NMRs!
- Rob McGregor for glassblowing my columns back to life.
- Bruce Clark for running my mass spectrum analyses.

I must also thank my late grandmothers:

- Thanks to Nanna Pugh for exclaiming in horror "But you've GOT to go to university!" when I told her at age 18 that I wasn't. The £1000 legacy she left me was well spent on the fees for the first year of my tertiary education.

- Thanks to Oma Cusiel for saying time and time again in her thick Dutch twang: "Cooking is not a nice job for a girl". I finally got the message.

Abbreviations

2,4-D	2,4-dichlorophenoxyacetic acid
aa	amino acid
ala	alanine
AMPA	aminomethylphosphonic acid
bamp	2,6-bis(aminomethyl)pyridine
bpa	bis(2-picolyl)amine
conc	concentrated
dien	diethylene triamine
dpg	*N,N*-bis(2-pyridylmethyl)glycinate
EDTA	ethylenediaminetetraacetate
EPSP	5-enolpyruvylshikimate 3-phosphate
fac	facial
gly	glycine
HSAB	Hard-Soft-Acid-Base
IDA	iminodiacetate
IR	infra-red
L	ligand
LMCT	ligand-to-metal-charge-transfer
mer	meridional
nm	nanometre
NMR	Nuclear Magnetic Resonance
PEP	5-enolpyruvylshikimic acid 3-phosphate
phen	1,10-phenanthroline
P_i	inorganic phosphate
PMG	*N*-(phosphonomethyl)glycine
ppm	parts per million
R_1	refinement factor
S3P	shikimic acid 3-phosphate
tacn	1,4,7-triazacyclononane
tpa	tris(2-picolyl)amine
TPMS	trimethylsilyl-1-propane sulfonate

tren	tris(2-aminoethylamine)
Ts	tosylate
UV	ultra-violet light
vis	visible light
λ_{max}	wavelength at maximum absorbance
ε_{max}	extinction coefficient at maximum absorbance

Chapter 1 - Introduction

1.1 Introduction to the Herbicide Glyphosate

The intention of the research undertaken during the course of this work has been to synthesise and characterise new cobalt-glyphosate* complexes before subjecting them to chemical and photochemical reaction conditions. This has been carried out with the hope of revealing what kinds of mechanisms may occur when the herbicide decomposes in natural situations.

This chapter endeavours to introduce the compound glyphosate and its use as a herbicide. Aside from the brief outline of its discovery, commercial synthesis, and mode of action when absorbed into plants, a reasonable proportion of this chapter has been assigned to summarising the information available in the literature concerning the fate of the herbicide once it has made contact with the soil.

This latter topic is considered important in the context of this thesis, given the idea that this work has been based on: glyphosate, a good ligand, forms complexes with metal ions that reside in the soil. It is of interest to explore the reactivity of such metal-glyphosate complexes in the lab, and to ascertain what reaction conditions the complexes may be susceptible to. The topic of metal-glyphosate complexes that have, to date, been fully characterised is covered, plus an introduction to the types of metal-glyphosate complexes to be synthesised, characterised, and studied in this research.

---

* In this thesis, the term "glyphosate" refers to the active ingredient in Roundup® herbicide. When mentioned in the text, "PMG" (*N*-(phosphonomethyl)glycine) is a generic term for the ligand used in the synthesis of the $[Co(L)(PMG)]^{n+}$ complexes, and refers to all protonation states. However, in the naming of the complexes, "PMG" refers to the dianionic ligand, that has a phosphonate proton and a carboxylate proton removed. "PMGH", meanwhile, represents the monoanionic ligand, that is deprotonated at the carboxylate oxygen atom only.

1.1.1 What is glyphosate?

Glyphosate is the organophosphate constituent of Roundup® herbicide and is responsible for the herbicide's phytotoxic properties.[1] It is employed in a multitude of agricultural situations where systemic, broad spectrum, non-selective, post-emergence control of annual and perennial weeds is required.[2] In forestry it is used to prevent grasses and shrubs competing with planted seedlings,[3] and in rubber, oil palm, or cocoa plantations for control of grasses and broadleaf weeds.[4] It can be absorbed quickly through the foliage or roots of plants and translocated *via* the phloem and xylem to all regions of the organism,[5] after which plant death occurs over several days or weeks.[6]

The herbicidal properties of glyphosate were discovered by scientists working for Monsanto Company in the late 1960s,[7] and the compound is now manufactured by several other companies. In recent years, two factors have generated increasing interest in glyphosate: (1) the introduction of genetically modified, glyphosate-tolerant crops,[8] and (2) the expiry of Monsanto Company's glyphosate patent which now gives any chemical company the right to produce and sell the herbicide, resulting in price reductions for the consumer.[4] These two factors may have induced the recently observed escalation in the use of glyphosate, and consequent environmental concerns associated with its use. The commercial success of glyphosate as a herbicide has led to much interest in its environmental fate, and has thus stimulated many studies on its behaviour in soils including its effects on soil microorganisms, processes of degradation, and soil persistence.

Glyphosate is considered non-toxic to humans and animals, as it has been shown to possess little or no carcinogenic, mutagenic,[9] or neuro-toxic activities.[10] The isopropyl ammonium salt of glyphosate, the derivative of glyphosate commonly used in its herbicide preparations, is very water-soluble and does not partition into animal fats. Thus, biological amplification of the herbicide into fish or other animals is not observed.[11] However, accounts of glyphosate's low toxicity to animals should not be considered watertight, as recent research has reported the existence of secondary effects, such as reproductive dysfunctions, in some animals.[12] Other studies have shown that fish and invertebrates are sensitive to commercial preparations of the herbicide[13] but this is

possibly because of the other ingredients in the formulation, such as surfactants,[7] that may act as irritants.

1.1.2 Discovery of glyphosate as a herbicide

The mid-1940s witnessed the beginning of a new era in weed control with the advent of 2,4-dichlorophenoxyacetic acid (2,4-D) (Figure 1.1) as a selective herbicide, *i.e.* phytotoxic towards weeds but not crops.[6] At this stage in herbicide science, control of annual weeds with contact herbicides was successful and progressive, but many perennial weeds, with their well established root systems, were either controlled poorly by the herbicides on the market or not at all.[6] What was needed was a systemic, rather than a contact, herbicide, that could kill the intricate root systems of perennial weeds.

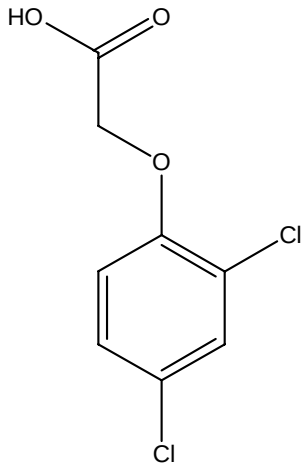

Figure 1.1: The structure of 2,4-D.

At Monsanto Company in the 1960s, a long term study was begun in an attempt to satisfy the need for a commercially acceptable perennial herbicide that was both highly effective and compatible with mammals and the environment.[6] The study involved determining the herbicidal properties of various tertiary aminomethylphosphonic acids derived from primary and secondary amines.[7] Only two of the compounds prepared, Compound A and Compound B depicted in Figure 1.2, exhibited any herbicidal qualities, but their unit activities, *i.e.* herbicidal activity per volume of compound applied, were low.[7] The compounds needed to be five times as effective before either could be considered a market-worthy herbicide.[6]

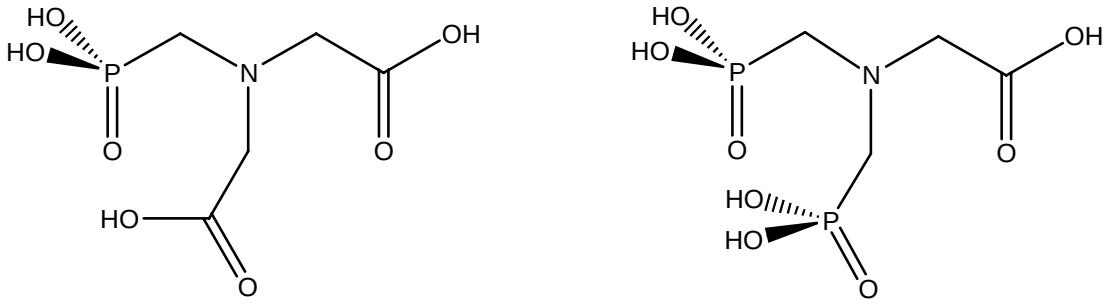

Compound A Compound B

Figure 1.2: The two compounds that showed low herbicidal activity.[14]

As far as the phytotoxic activities of the compounds were concerned, it was suggested that both were metabolised within the trial plants to a smaller, common metabolite with herbicidal properties.[7] At the time, this theory flew in the face of the common belief that metabolism always led to less toxic substances. It was postulated that one or more of several possible metabolites, of which glyphosate (Figure 1.3) was one, might be responsible for the herbicidal activity observed.[6]

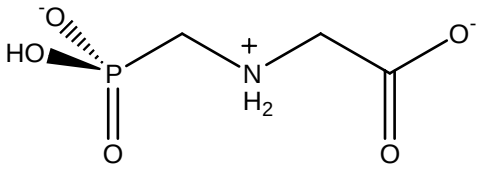

Figure 1.3: The structure of monoanionic glyphosate, the predominant species in Roundup® herbicide.

The conversion from Compound A or Compound B to glyphosate within plants would involve the loss of a carboxymethyl group from Compound A and the loss of a phosphonomethyl group from compound B.[14] The researchers involved in the study thought it unlikely that a single mode of metabolism, such as the selective elimination of one of the substituents of Compound A and of Compound B, could exist and lead to equal amounts of one herbicidal metabolite, *i.e.* glyphosate.[6] However, it seemed certain that this process was indeed in place, as the synthesis and testing of all the postulated metabolites found that only glyphosate had high herbicidal activity.[6] So impressed was Dr Douglas Baird, the plant physiologist who analysed the field trial results, that his report to Monsanto management was simply titled "EUREKA".[6]

Contrary to the belief of the researchers at Monsanto, glyphosate was not a new compound.[6] It had first been synthesised in 1950 by Dr Henri Martin, who worked for Cilag, a small pharmaceutical company in Switzerland, although the compound had been of no interest to his employers. Coincidentally, in 1958, Dr Martin began work on the synthesis of new herbicides while under the employ of another company, but never tested glyphosate for herbicidal activity.[6] The Monsanto Company also found that the patent for the compound had been issued to the Stauffer Chemical Company in 1964, although there were no claims to its herbicidal activity. The compound was also found advertised for sale in the 1966 edition of The Aldrich Library of Rare Chemicals.

Instead of what could have been a serendipitous discovery by Dr Martin, the ability of glyphosate to act as a herbicide was only revealed when Monsanto implemented a structured, synthetic program in herbicide research. The commercial preparation of the glyphosate-containing Roundup® herbicide was initiated soon after. The herbicide was released into several world markets in 1974 where it has been used extensively since.[6]

During the investigations into Compounds A and B, Compound B was found by Monsanto scientists to have the ability to increase the sucrose content of fruit. Hence, since the 1970s this compound had been marketed as “Polaris”, a sugar cane ripener.[6]

1.1.3 Commercial synthesis of glyphosate

In the 1970s few chemical methods were known for the synthesis of molecules such as glyphosate, and even fewer methods were efficient enough to be used in large-scale preparations of the compound. Since then hundreds of patents for the synthesis of glyphosate have been issued. The large numbers of syntheses of glyphosate are possibly because of the stability of the compound in the presence of acid, base, and strong reductants or oxidants. These properties give rise to the many and varied methods of its preparation. Glyphosate analogues have also been developed and patented in an attempt to produce a herbicide that is economically more viable: however, none of these compounds have been commercialised with a cost advantage over glyphosate.[6]

The reported syntheses of glyphosate employ three bond-forming strategies, including the formation of the C_β-N, P-C_β-N, and C_α-N bonds (Figure 1.4).[6]

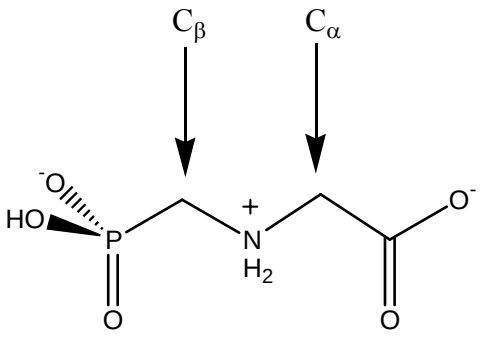

Figure 1.4: The atom-labelling scheme for synthetic approaches to glyphosate. Note that although the structure above is monoanionic, the protonation states of glyphosate can differ depending on the synthetic method used.

The formation of these bonds can be represented retrosynthetically (Figure 1.5).

1.1.3.1 Formation of the C_β-N bond

The first methods of making glyphosate involved the formation of the C_β-N bond.[6] The construction of this bond involves the use of equivalent reagents that correspond to synthons A and B in Figure 1.5. In the following example, methylphosphate derivatives and glycine or its sodium salt represent synthons A and B, respectively.

Initial attempts at making glyphosate followed a procedure as shown in Figure 1.6.[6] This reaction sees glycine reacting with α-chloromethylphosphonic acid under basic conditions.

However, this nucleophilic substitution reaction results in only poor yields of glyphosate, particularly if excess glycine is used. A significant improvement in yield can be achieved if the more reactive α-chloromethylphosphinic acid is used (Figure 1.7). Reported yields for this synthesis are around 80 %.[6] Unfortunately, however, this method involves mercury(II) chloride as an oxidising agent. It is unfavourable to use mercury compounds in synthetic chemistry due to their toxicity, and this detail makes the preparation according to Figure 1.7 questionable.

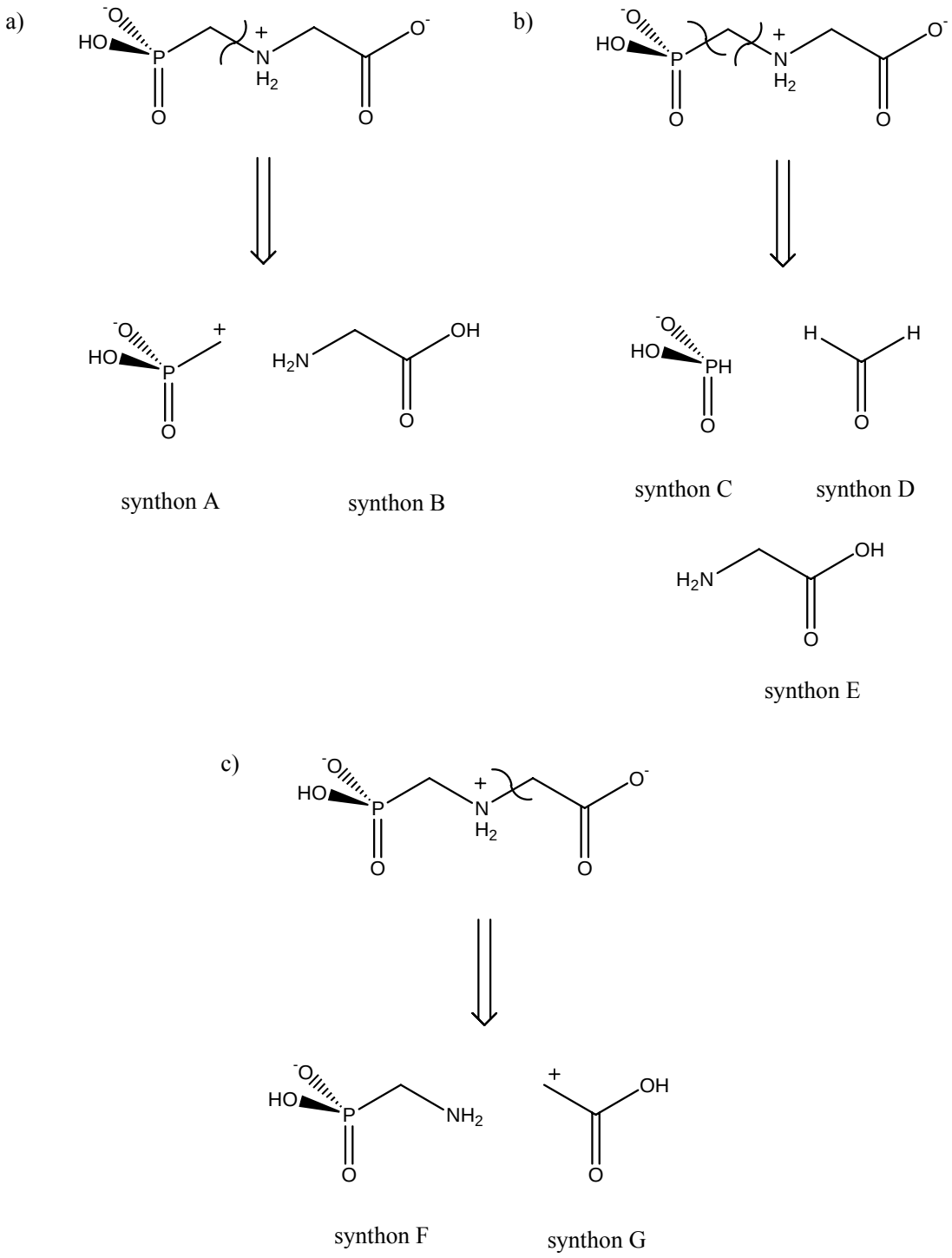

Figure 1.5: The retrosynthetic representation of the formation of the a) C_β-N, b) P-C_β-N, and c) C_α-N bonds. Disconnections and the corresponding synthons are shown. The protonation states of the glyphosate varies with pH.

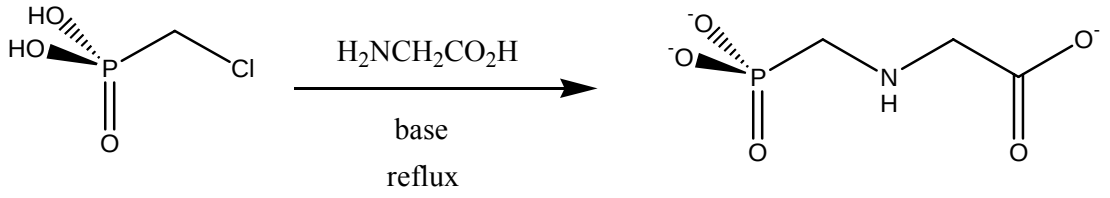

Figure 1.6: The synthesis of glyphosate from α-chloromethylphosphonic acid and glycine.

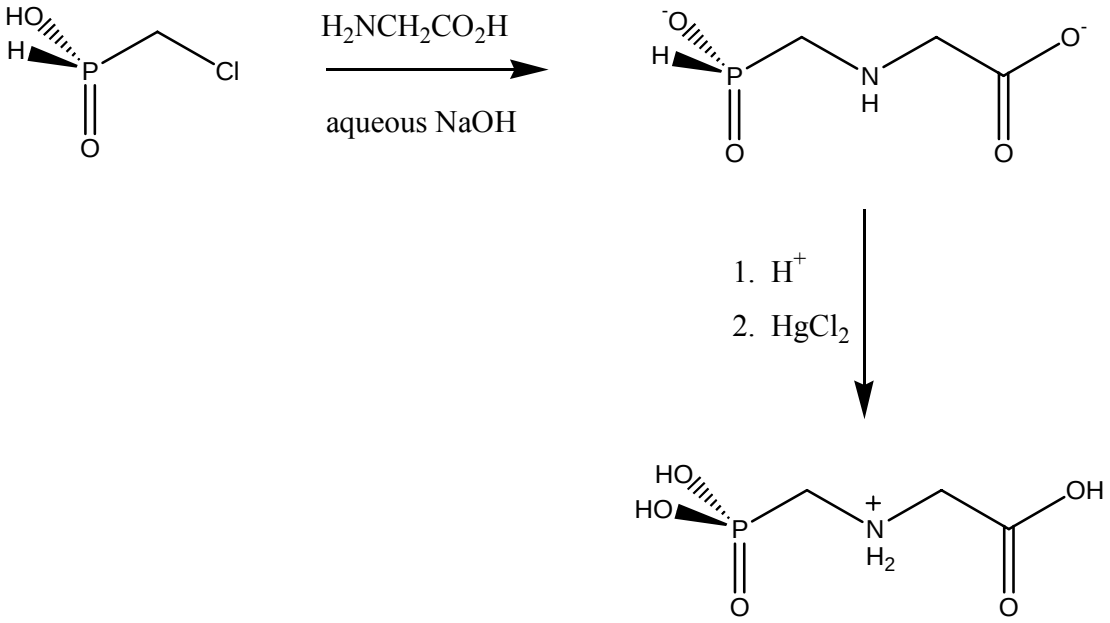

Figure 1.7: The synthesis of glyphosate from α-chloromethylphosphonic acid and glycine.

A more recent and very efficient method of preparing glyphosate is by the reaction of the electrophilic phosphonomethyl triflate with sodium glycinate (Figure 1.8).[6] The reaction yields an aminomethylphosphonate ester which then undergoes acid hydrolysis with HBr to remove the ester groups, giving a good yield of glyphosate.

1.1.3.2 Formation of the P-C$_\beta$-N bonds

The assembly of the P-C$_\beta$ and the C$_\beta$-N bonds appear among the most important synthetic strategies in the commercial production of glyphosate.[6] The construction of these bonds utilise equivalent reagents that correspond to synthons C, D and E in Figure 1.5. In all the examples that follow, the equivalent reagent, formaldehyde, replaces synthon D. Synthon

C is primarily phosphorus acid or a dialkyl phosphite, while Synthon E is glycine or one of its derivatives.

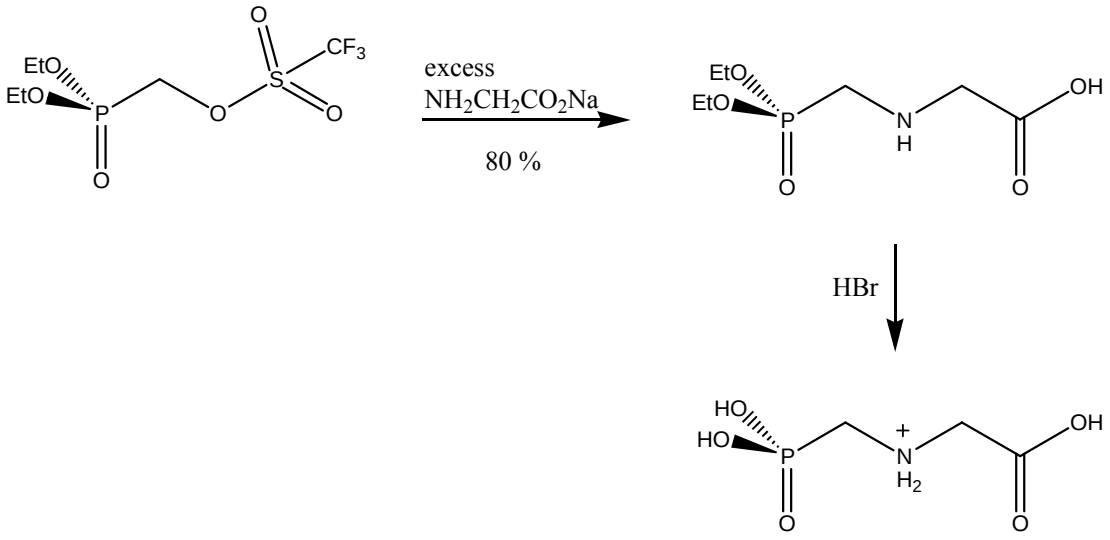

Figure 1.8: The synthesis of glyphosate from a phosphonomethyl triflate and sodium glycinate.

This bond-forming process can be achieved through a modification of the traditional Mannich reaction (Figure 1.9). In the synthesis of glyphosate, the phosphorus-containing reagent replaces the keto/enol species.

The synthesis of glyphosate from phosphorus acid, formaldehyde and glycine is shown in Figure 1.10. Low yields of glyphosate are obtained when this procedure is followed, even when a 1:1:1 ratio of phosphorus acid, formaldehyde and glycine are used.[6] The bis-phosphonomethyl adduct predominates (65 % yield), although this is a possible synthetic route to the sugar cane ripener, Polaris, which was first isolated by Monsanto chemists *en route* to their glyphosate discovery (also see Compound B, Figure 1.2).

An alternative method of glyphosate production involves a variant of the Mannich reaction and is a one-pot, two-step process (Figure 1.11). In this case, a dialkyl phosphite is used rather than phosphorus acid. Various glyphosate-dialkyl phosphonate esters are formed during this synthesis and a further acid hydrolysis is necessary to yield the glyphosate species.[6] This reaction yields 65-67 % of glyphosate from its starting materials.

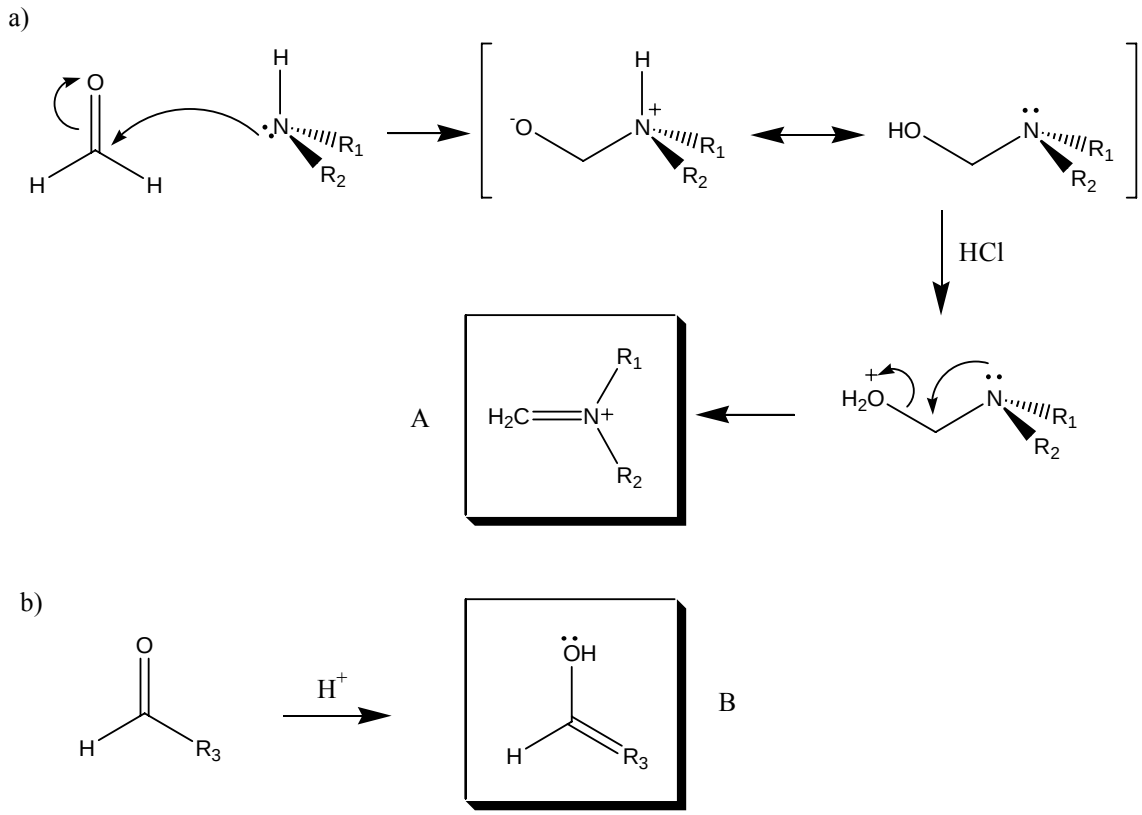

A and B may now react to form a new carbon-carbon bond:

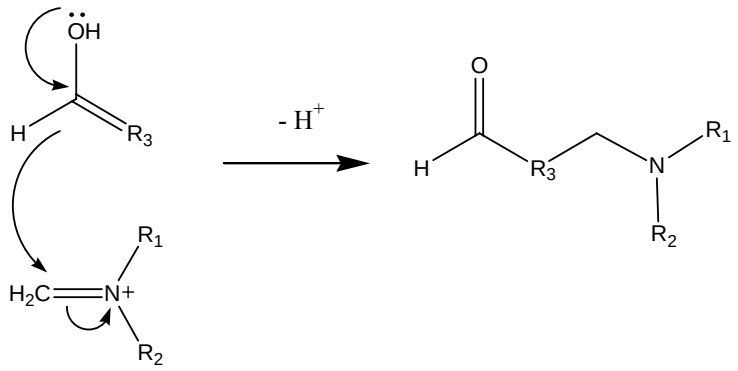

Figure 1.9: A generalisation of the Mannich reaction.

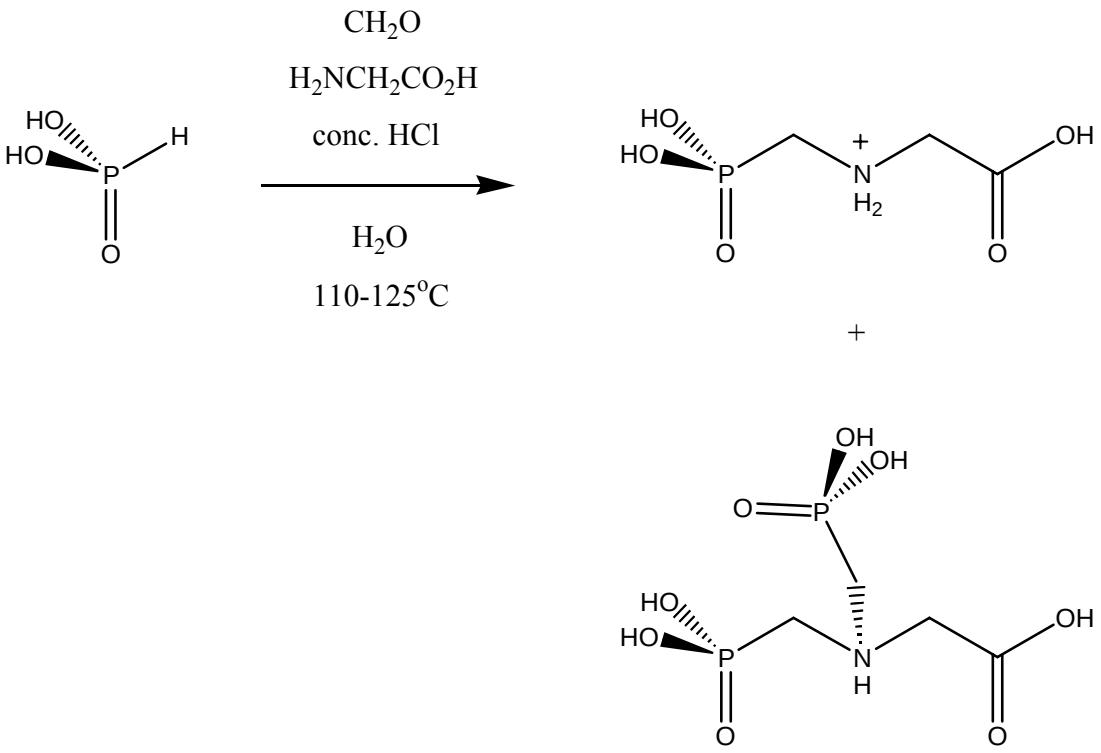

Figure 1.10: The synthesis of glyphosate from phosphorus acid, formaldehyde and glycine.

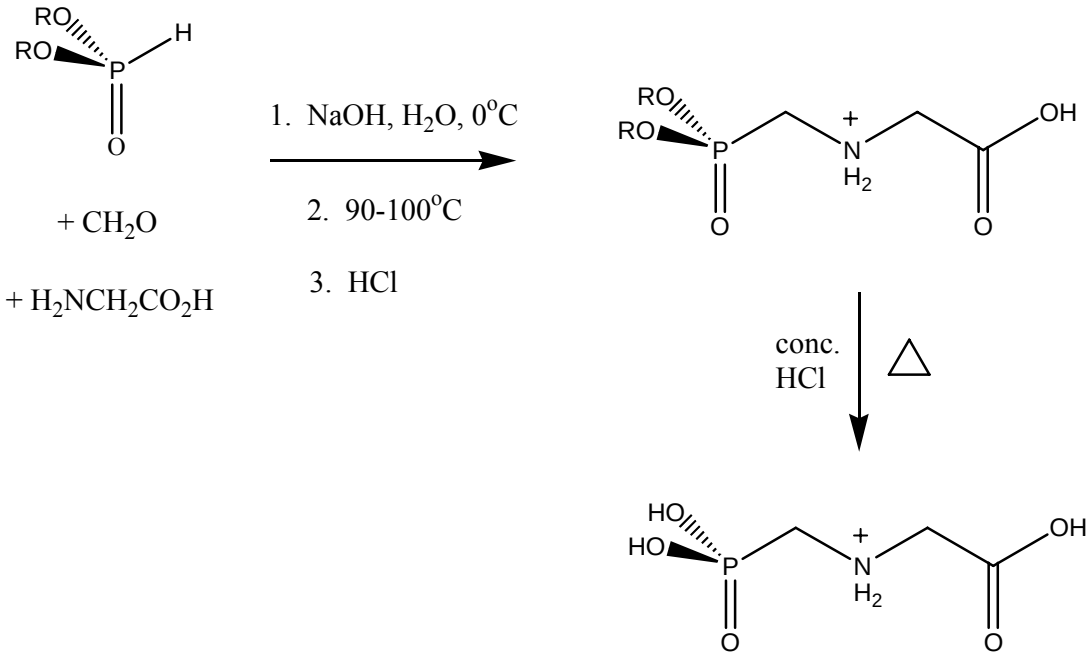

Figure 1.11: The synthesis of glyphosate from a dialkyl phosphite, formaldehyde and glycine.

The use of iminodiacetic acid (IDA) features in one of the most important commercial methods of preparing glyphosate,[6] and is another example of a Mannich reaction approach (Figure 1.12). The dicarboxymethyl species that results can be oxidised by dioxygen with a carbon catalyst, or by other means such as treatment with fuming sulfuric acid or hydrogen peroxide, to yield the glyphosate molecule. The yields obtained from this method of glyphosate preparation are reported to be very good.

Aside from the Mannich reaction process, it is also viable to prepare glyphosate *via* a hexahydro-1,3,5-triazine (HHT) reaction.[6] In these ring-opening reactions, the HHT is protonated by the weakly acidic phosphite compound. This initiates the ring-opening process which constructs the glyphosate backbone. Figure 1.13 illustrates the formation of the trimeric HHT derivative from glycine, and the subsequent reaction of the HHT component with diethyl phosphite and HCl to yield a phosphonoester species. This species is then treated with HBr to hydrolyse the esters to obtain approximately a 63 % yield of glyphosate.

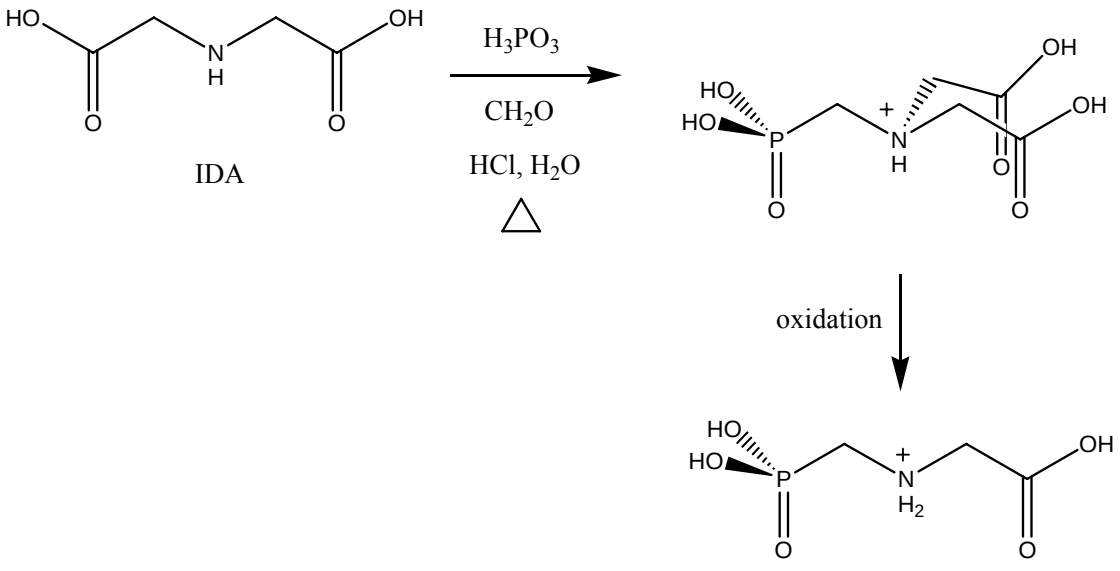

Figure 1.12: The synthesis of glyphosate from IDA, phosphorus acid and formaldehyde.

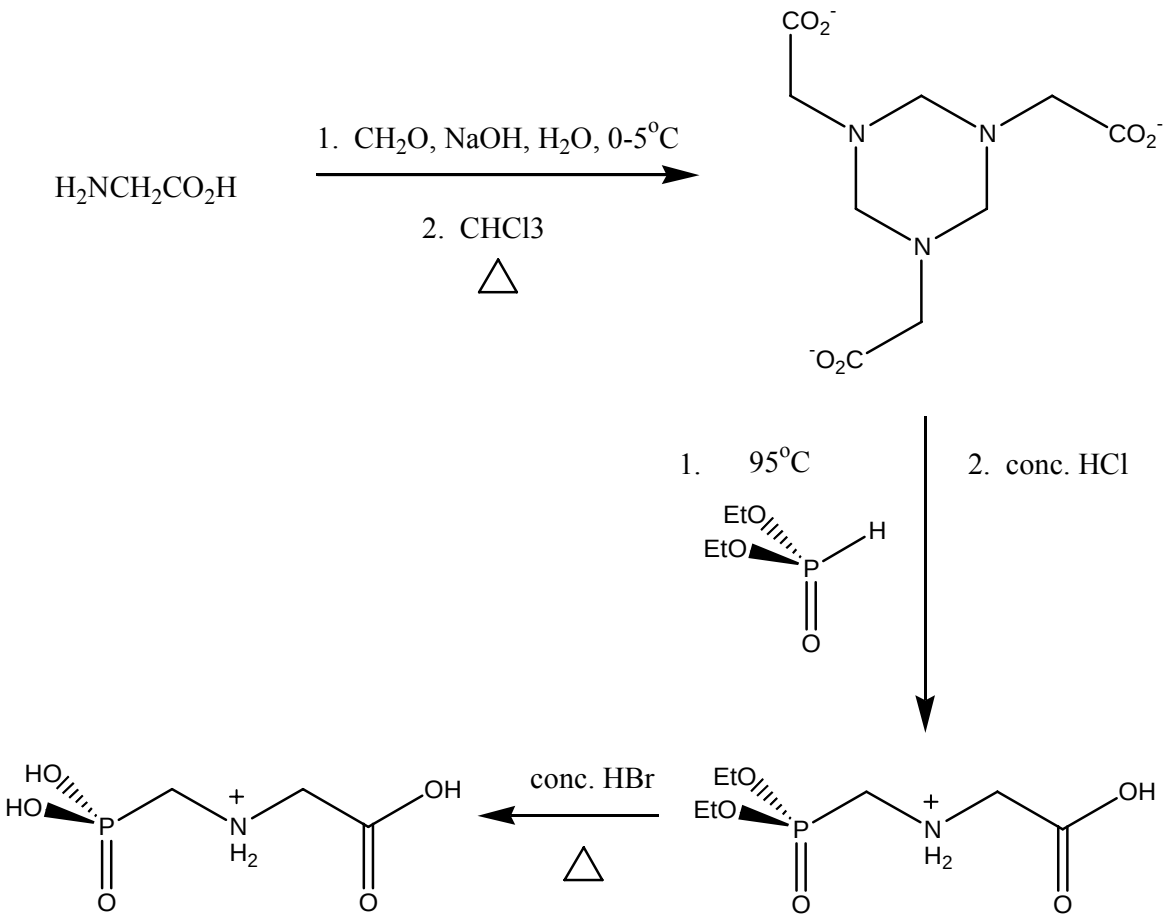

Figure 1.13: The synthesis of glyphosate from a trimeric HHT derivative intermediate.

1.1.3.3 Formation of the C_α-N bond

Few syntheses using the construction of this bond have been employed commercially.[6] In general, one of the starting materials for this procedure is aminomethylphosphonic acid (AMPA), which fulfils the role of synthon F in Figure 1.5. The transformation to the glyphosate molecule involves the formation of the C_α-N bond *via* direct alkylation or reductive alkylation.[6] Synthon G can be represented by the equivalent reagent glyoxylic acid, and an efficient synthesis of glyphosate *via* this route is depicted in Figure 1.14. This synthesis proceeds through an imine intermediate, resulting from the condensation of AMPA with glyoxylic acid. The imine can be reduced by catalytic hydrogenation, electrochemically or with other chemical reducing agents to give the disodium salt of glyphosate.

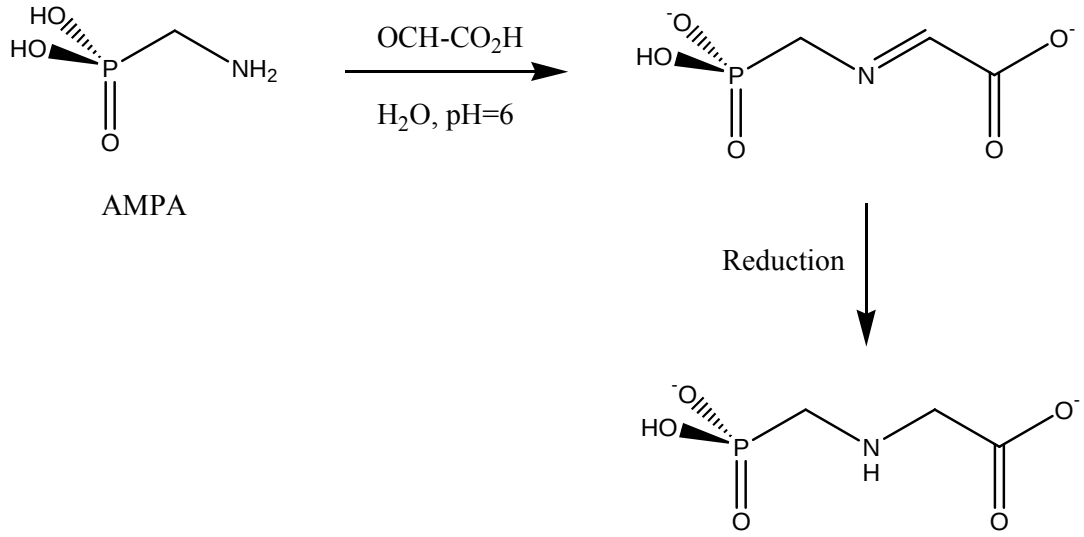

Figure 1.14: The synthesis of glyphosate from AMPA and glyoxylic acid.

1.1.4 Properties of glyphosate and its salts

Glyphosate is a white, odourless, crystalline solid that exists as a zwitterion in its solid state.[14] The compound is a relatively strong acid,[6] the pH of a 1 weight % solution of glyphosate being about 2.[6] It has low solubility in water, *i.e.* 1.2 to 8.0 weight % at 25-100^{o}C [14] due to very strong intermolecular forces between the molecules in the solid structure, and is insoluble in organic solvents.[6] However, it dissolves readily in strong aqueous acids and dilute aqueous bases to form ions of various charge.[6] When subjected to temperatures of 200-230^{o}C, glyphosate undergoes dehydration and dimerisation to give a diketo-piperazine compound (Figure 1.15).[6]

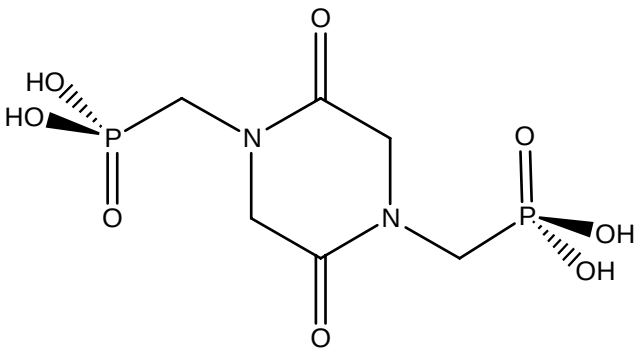

Figure 1.15: Dimerisation of glyphosate.

Glyphosate possesses three acidic protons, and can exist as the cation, or the monoanionic, dianionic, or trianionic salts, depending on the pH of the parent solution (Figure 1.16).[6]

1.1.5 Commercial formulations of Roundup® herbicide

Due to the insolubility of glyphosate in water, it is necessary that its herbicidal preparations contain a salt of the compound. The herbicide is sold as the monoanionic, isopropyl ammonium salt. During the studies of glyphosate as a potential herbicide, Monsanto tested hundreds of glyphosate derivatives including esters, hydrazides, and amides, for water solubility,[14] but it has never been disclosed why the company chose to manufacture glyphosate as the isopropyl ammonium salt.

Roundup® herbicide formulations include a surfactant that lowers the surface tension of the aqueous carrier solution to increase spreading and penetrating power. The surfactant used in the herbicide is typically polyethoxylated tallowamine.[11]

Roundup® generally has the following composition:[6]

Ingredient	% weight of formulation
Isopropyl ammonium salt of glyphosate	41
Polyethoxylated tallowamine	7-8
Related organic acids of glyphosate	1.5
Water	49

Table 1.1: The composition of Roundup® formulations.

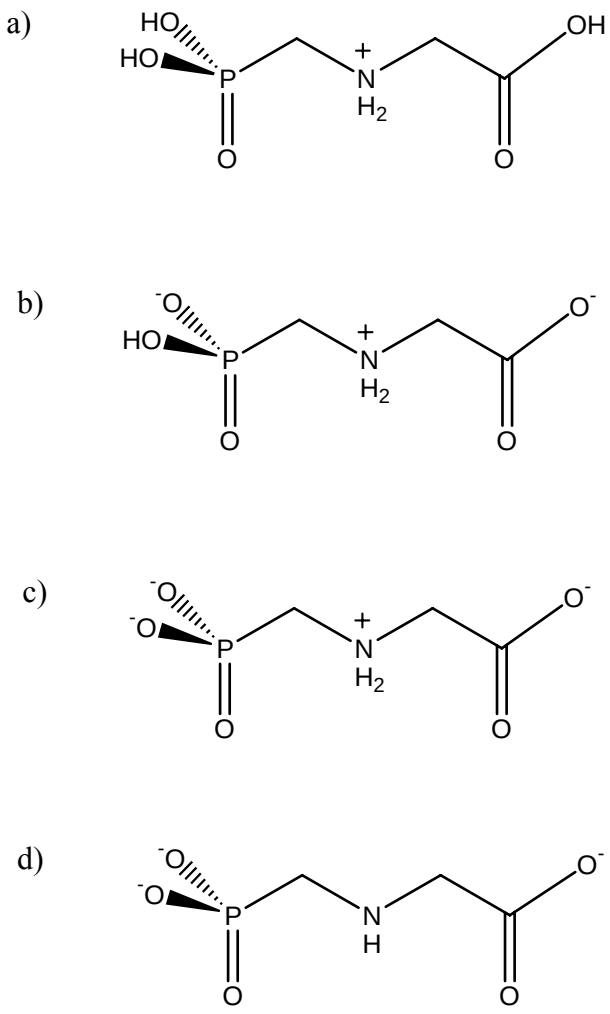

Figure 1.16: Ionic forms of glyphosate: a) cation; b) monoanion; c) dianion; d) trianion.

1.1.6 Absorption and translocation of glyphosate in plants

When a herbicide is applied to a plant the first barrier to absorption is the cuticle, a waxy substance which covers all plant foliage with the main purpose of protecting the plant from water loss and pathogen invasion.[6] The absorption is initially rapid and is thought to be facilitated by the steep concentration gradient of glyphosate across the cuticle,[6] and proceeds *via* a hydrophilic pathway.[6] As the concentration gradient of glyphosate across the cuticle diminishes, so too does the rate of absorption.

After absorption from the aerial parts of the plant such as the stems and leaves, glyphosate is translocated throughout the plant *via* the phloem, the portion of the vascular system responsible for sugar transport,[15] and the xylem, the water- and mineral-carrying segments

of the vascular system.[15] The herbicide is then unloaded at the "sinks" which include the apical meristems,[6] the growing points of the plant that exist both above and below the ground.[6] The translocation process from leaf to apical meristem is usually rapid and this is the dominant factor behind glyphosate's reputation as an effective, systemic herbicide.[6]

Once the glyphosate has been translocated throughout the plant, passive diffusion into the cells through the cell wall occurs.[9] This process is generally slow, possibly because the negatively charged groups in the cell wall and the cell membrane repel the anionic glyphosate.[6] The interior of the cell is about 150 to 200 mV more negative than the exterior of the cell, and this potential across the cell membrane is also a factor in the inhibition of glyphosate entrance into the cell.[6]

Although plants have the capacity to absorb glyphosate through their roots, absorption *via* this pathway from soils is a less significant mode of uptake since the herbicide tends to form stable complexes with metal cations in the soil soon after application.[6]

Due to the wide diversity in the chemical and biochemical makeup amongst plant species, each responds to glyphosate in an individual fashion. These chemical differences between plants are responsible for the observed variation in interception, retention, penetration, and transport of the herbicide.[6] Other factors can affect the mode and extent of glyphosate uptake by plants and these include the age of the plant, water status, light levels, temperature, method of application and the concentrations of glyphosate and surfactants used.[6]

1.1.7 Mode of action of glyphosate

"Mode of action" in the context of herbicide activity describes the sequence of events leading to injury or elimination of a plant after herbicide treatment.[6] The term can include such processes as absorption, translocation, metabolism, as well as biochemical targets of the herbicide and growth and structural changes that take place in the plant after herbicide application.[6] From a biochemical point of view, however, "mode of action" can relate just to the processes that occur after translocation to the sites inside the plant that are susceptible to herbicide treatment.

Within plant cells, glyphosate selectively targets and inhibits 5-enolpyruvylshikimate 3-phosphate synthase (EPSP synthase). This enzyme is responsible for the conversion of shikimic acid 3-phosphate (S3P) and phosphoenolpyruvate (PEP) into 5-enolpyruvylshikimic acid 3-phosphate in the Shikimate pathway (Figure 1.17).[1]

Glyphosate is a potent, reversible and competitive inhibitor with respect to PEP,[6] and is non-competitive with respect to S3P.[7] S3P and EPSP synthase must form a binary complex before either glyphosate or PEP can bind at the active site, which results in a ternary complex.[6] These S3P-EPSP-PEP and S3P-EPSP-glyphosate ternary complexes have been extracted from plants and characterised using biophysical methods.[6] In almost all cases studied, it has been found that glyphosate binds more tightly to the EPSP synthase active site than does PEP.[6]

The binding of glyphosate to EPSP synthase causes the inhibition of the enzyme, leading to the eventual disruption of the biosynthesis of chorismate. It has been estimated that up to 35% of dry plant mass consists of essential aromatic molecules, such as tyrosine and phenylalanine; and these are synthesised from chorismate.[6] With this in mind, it becomes apparent why chorismate is so essential to plant life, and why disruption of its biosynthesis results in complete plant death.

It is possible that glyphosate targets other sites within plants too: in one study, treatment of soybean seedlings with the herbicide resulted in plant injury but not significantly reduced aromatic amino acid concentrations.[6] This result suggests that EPSP synthase was not fully inhibited by glyphosate, since after glyphosate treatment, chorismate and its consequent aromatic amino acids continued to be biosynthesised, *i.e.* another mode of action must have been in place to cause the plant injury. For this reason, the targeting of EPSP synthase by glyphosate may be regarded as the compound's primary, but not exclusive, mode of action.[6]

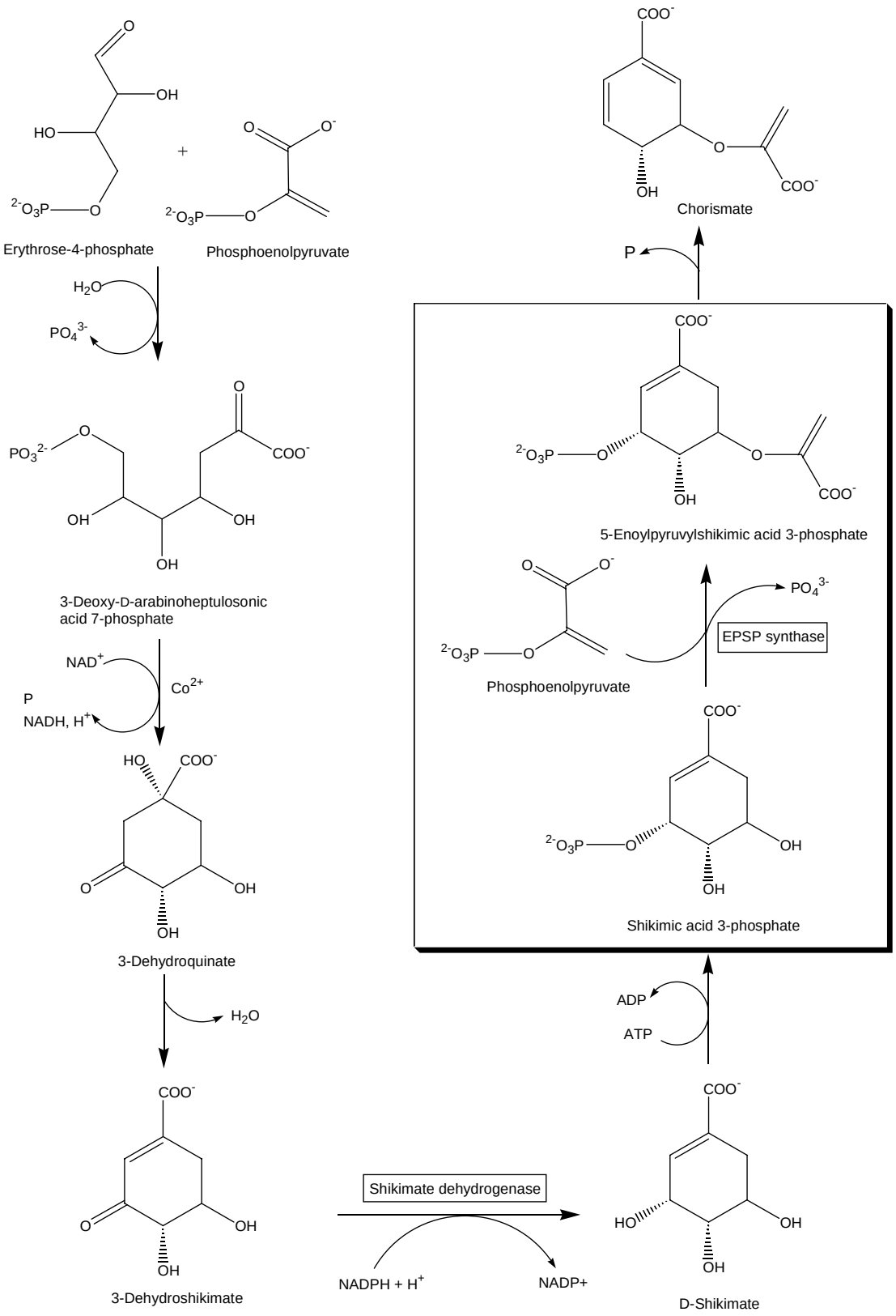

Figure 1.17: The Shikimate pathway. The step targeted by glyphosate is highlighted by a box.[1]

It is conceivable that the chelating properties of glyphosate contribute to its herbicidal effects, since the compound has the ability to bind, within plants, to metal cations that are essential in the execution of biological processes. For example, it has been observed that the synthesis of 5-aminolevulenic acid, a precursor to the synthesis of all porphyrin-containing compounds, is hindered by glyphosate. The synthesis of this acid is iron-dependent, and is inhibited when glyphosate coordinates to the iron metal centres. A similar compound, the cobalt-dependent dehydroquinate synthase, may also be a casualty of glyphosate's chelating abilities.[7]

Studies have shown that disruption of enzymes unrelated to the Shikimate pathway can occur when treated with glyphosate. However, most of these cases are not thought to account for the toxicity of glyphosate, since high levels of the herbicide are required to inhibit a sufficient quantity of enzymes such that a phytotoxic effect is observed.[7]

Insects, birds, fish, and mammals do not rely on the Shikimate pathway for the synthesis of essential amino acids, *i.e.* they obtain them from their diets, therefore glyphosate is commonly thought to be relatively non-toxic to such organisms.[6] The Shikimate pathway is, however, present in some microorganisms, *e.g.* in *Escherichia coli*, where EPSP synthase has been overexpressed and readily available to study. Due to this abundant supply of the enzyme, EPSP synthase is the only herbicide target to have been so thoroughly characterised.[6]

No other post-emergence herbicides share glyphosate's mode of action.[6] It is the lack of the Shikimate pathway in non-plant life that has earned glyphosate its reputation for being relatively non-toxic to such organisms; on the other hand, it is the widespread occurrence of the pathway in plant life that accords glyphosate its reputation as an effective herbicide.

1.2 The Fate of Glyphosate in the Environment

The interest in glyphosate amongst the chemical community is mainly due to issues such as contamination of aquifers by glyphosate, persistence of it in soils, and its effects on soil microbial populations. These concerns have prompted many studies of the herbicide over the last 25 years, the majority of research concentrating on the fate of glyphosate once it

has made soil contact. The consensus appears to be that microbial activity provides the main route to degradation in soils. Chemical and photochemical degradation play a minor role in this medium, but in aqueous systems the photochemical pathway seems to be major.[6,7,12]

Of course, glyphosate is not applied deliberately to the soil: herbicide solution runoff from foliage application is a major contributor to glyphosate levels in soils. When the compound makes contact with the soil, it is believed that two processes occur: a quantity of the glyphosate is utilised by soil microbes and is degraded to its metabolites, and the remainder of the herbicide is rapidly complexed to metal cations residing in the soil. Generally, microbes, *via* mineralisation processes, degrade only a small fraction of glyphosate before the remaining free glyphosate molecules can adsorb to metal cations. This adsorption renders the herbicide non-phytotoxic, and unavailable to microbes.

This phenomenon of the herbicide being unavailable for microbial metabolism when bound to metal cations can be explained by consideration of the phase associated with adsorption. When glyphosate first makes contact with the soil, the herbicide is in solution (as are the microbes that degrade it). If the compound is adsorbed to the soil it no longer exists in the liquid phase, but becomes part of an insoluble solid. It is probably this absence of "being in solution" that causes glyphosate to be unavailable to microbes.

Only when the bound glyphosate is released from the metal-glyphosate complex can microbial degradation continue. The efficiency of the adsorption, desorption, and degradation processes in soils appears to be reliant on a combination of factors, including temperature, microbial species present, pH, species of metal ions present, organic substrate availability, nutrient levels, moisture levels, and levels of inorganic phosphate.

1.2.1 Metal complexation of glyphosate in soils

It was first shown by Sprankle *et al* that wheat seedlings can easily absorb glyphosate through their roots from nutrient solution.[16] However, in spite of this viable mode of entry into the organisms, the seedlings did not suffer injury when they were planted in soil that had recently been treated with the herbicide. It was postulated by Sprankle *et al*[16] that the

low herbicidal activity of glyphosate in soils is not due to the inability of plants to absorb it *via* their roots, but because the compound undergoes rapid microbial degradation, chemical degradation, or adsorption to the soil after contact is made. The subsequent studies of the researchers went on to determine the reasons behind the rapid inactivation of glyphosate in soils.

To test if microbial degradation may be responsible for the inactivation of glyphosate in soils, seedlings were grown in autoclaved (*i.e.* sterile) soil treated with glyphosate, and in autoclaved soil that was left untreated (the control).[16] The crop grown in the sterile, glyphosate-treated soil did not show any herbicidal injury. Thus, the glyphosate had somehow been inactivated – microbial degradation was ruled out as a cause due to the soil having been autoclaved.

To assess whether or not glyphosate undergoes chemical degradation in soils, the researchers compared plant dry weight between plants grown in (1) soils pre-treated with glyphosate and phosphate, and (2) soils pre-treated with glyphosate alone.[16] The plant dry weight from sample (1) had much less dry plant weight than sample (2), *i.e.* glyphosate plus phosphate combined had a greater herbicidal effect than glyphosate treatment alone. The researchers suggested that the phosphate anions compete with glyphosate for binding sites on soil particles. This renders the herbicide free in the soil, leading to the observed herbicidal effect. Since glyphosate was available in the soil to compete with phosphate and to act phytotoxically, it was concluded that the herbicide had not been chemically degraded, and that such degradation is not responsible for the rapid inactivation of glyphosate in soils. This experiment also led to the conclusion that when glyphosate binds to soil particles, the herbicide is likely to be bound through its phosphonate group. The theory of glyphosate binding to soils through its phosphonate group has been supported by other researchers.[10,11]

Consequently, it was proposed by Sprankle *et al*[16] that the rapid inactivation of glyphosate in soils is not due to microbial degradation, chemical degradation, or the inability of plants to absorb glyphosate through their roots, but some other factor. The researchers concluded that the observed immediate inactivation of glyphosate is due to adsorbance onto soil particles.

It is now widely accepted that adsorption by metals residing in the soil is an important factor in predicting the fate of herbicides in the soil.[17] The soil type governs the level of adsorption of glyphosate to soils,[16] and the rate of degradation of glyphosate in soils is generally inversely proportional to the degree of soil adsorption,[4] *i.e.* in soils that exhibit a high degree of glyphosate adsorption a slow rate of degradation of the herbicide is observed. It has been found that clays saturated with Fe(III) and Al(III) adsorb more glyphosate than clays saturated with Na(I) and Ca(II).[18] This finding has been supported by Hensley *et al*,[17] who found no herbicidal activity of glyphosate in soils that contained Fe(III) or Al(III). These researchers postulated that the ionic radii of the metal ions influence the strength of the glyphosate-metal binding (Table 1.2).

Metal Ion	Ionic Radii (Å)
Na^{+}	0.97
K^{+}	1.33
Ca^{2+}	0.99
Fe^{3+}	0.64
Al^{3+}	0.51

Table 1.2: The ionic radii of some relevant metal ions.[19]

In the same study,[17] the presence of Ca(II), Na(I), and K(I) was found to have no effect on the activity of glyphosate, and it was suggested that this is because of the large ionic radii of the metal ions which prevents the glyphosate from wrapping around to form one or more chelate rings. On the other hand, Fe(III) and Al(III) are relatively small and can facilitate coordination such that one or more chelate rings can occur. Keeping in mind the stability of metal complexes that contain chelate rings, it becomes evident why the presence of small ions such as Fe(III) and Al(III) can have an inhibitory effect on glyphosate, while their larger counterparts, Ca(II), Na(I) and K(I) might not. In the case of Ca(II), Na(I) and K(I), the binding of glyphosate to the metal centre may not result in chelation. Thus, the resulting adduct would be less thermodynamically stable than a chelated species and more prone to decomposition to the free metal and free glyphosate. This would explain the higher herbicidal effects of glyphosate when Ca(II), Na(I) and K(I) were present in the soils, compared to when glyphosate was added to soils lacking these metal ions.

The results of the research by Hensley *et al*[17] have also been supported by studies into the effects of spray solution composition on glyphosate phytotoxicity.[20] Stahlman and Phillips found that the addition of Fe(III) and Al(III) to glyphosate solutions greatly reduce the herbicidal effect, while the addition of Na(I) and K(I) causes little or no reduction in herbicidal activity.

However, contrary to the study carried out by Hensley *et al*,[17] glyphosate showed reduced activity when applied to plants in a Ca(II)-containing carrier solution,[21] implying that the herbicide was in fact being bound firmly to the metal ion. The herbicidal activity of glyphosate was reinstated when ethylenediaminetetraacetate (EDTA), known for its chelating abilities, was added to the solution. The addition of a compound with such chelating properties would have promoted the substitution of glyphosate for EDTA, due to the relative stability of the Co-glyphosate and Co-EDTA species. EDTA can form five five-membered chelate rings when coordinated to a metal centre, and the resulting complex is very stable. It was shown by Smith and Raymond[22] that the Ca-glyphosate adduct contains no five-membered chelate rings (this topic is described in more detail in Section 1.3.1.). Therefore, the Ca-EDTA complex will be the species that predominates in solution. This renders the glyphosate free to act phytotoxically.

The ability of glyphosate to bind to Ca(II) is supported by Smith and Raymond,[22] whose crystal structure of the Ca-glyphosate polymer showed that glyphosate binds to the metal centre through two oxygen atoms of the phosphonate group, *i.e,* it forms a four-membered chelate ring. This result contrasts to what we would expect according to the research by Hensley *et al.*[17] These researchers put forward that the large size of Ca(II) inhibited the glyphosate from coordinating to the metal ion. But the synthesis of a Ca(II)-glyphosate complex, by Smith and Raymond,[22] with an apparently stable four-membered ring suggests that the size of the metal ion is not the only factor influencing the coordination of glyphosate to metal ions.

Due to the chemical differences amongst soils allegedly of the same type, some comparable studies show contrasting results with respect to their glyphosate adsorbing properties. Sprankle *et al*[18] calculated the adsorptive capacity of two clays, illite and kaolinite, and found that kaolinite adsorbed approximately twice as much glyphosate as

illite did. When Glass[23] repeated the experiment, the adsorptive capacity of glyphosate was calculated to be exponentially higher for illite than for kaolinite. Glass suggested that the purity and origin of the clays are responsible for the differences. This is a reasonable explanation for the observed differences, since the categorisation of soils does not take into account the amount of free metal ions present. Rather, it is based on the relative amounts of clay, silt, and sand present.

The observation of low herbicidal activity of glyphosate when applied to soils has been supported by other researchers,[5,11,17,24] but other studies have found that glyphosate present in soils can have some herbicidal activity.[25] Salazar and Appleby found that glyphosate applied to the foliage of wheat can be released into the soil through the roots and cause damage to corn seedlings grown in the same soil.[25] The same authors also found that the pre-emergence application of glyphosate to moist soil after planting wheat seedlings can result in plant damage. In this case, the soil used was sandy loam which is now known to have low levels of adsorptive materials,[4] hence the glyphosate would have been free in the soil to be absorbed into the roots of the wheat seedlings.

1.2.2 Biodegradation of glyphosate by soil-dwelling microorganisms

Although Sprankle *et al*[16] stated that adsorption to soil particles is the reason behind the rapid inactivation of glyphosate, they by no means suggested that this is the fate of glyphosate in soils. In a subsequent study by the same researchers[18] it was shown that microbial activity is a major contributor to glyphosate degradation in soils. Soil microorganisms are heterotrophic (they acquire energy from the intake and digestion of plant or animal tissues)[26] and acquire carbon and nitrogen for growth by decomposing organic materials in the soil.[27] Glyphosate has a high C:N ratio of 3:1 which is ideal for such microbial mineralisation, and treatment of soils with the herbicide can have an immediate, favourable effect on soil-microbe activity.[27]

During the studies by Sprankle *et al* the amount of $^{14}CO_2$ emitted from soils was measured after the application of 1-^{14}C-glyphosate (labelled at the carboxylate carbon atom).[18] It was found, from the rates at which $^{14}CO_2$ was released from the soil, that the glyphosate was degraded rapidly at first, followed by a slower, quasi steady state of degradation. This

phenomenon can be explained by the initial microbial metabolism of free glyphosate, then the subsequent degradation of the metal-bound glyphosate[18] (recall from Section 1.2 that metal-bound glyphosate is unavailable to microbes due to its phase: bound herbicide is part of a solid, while free glyphosate is in solution within the soil, as are the microbes). This is an equilibrium process: as the free glyphosate in the soil is degraded by microbes, a quantity of metal-bound glyphosate is released from the metal ions back into the soil such that a state of equilibrium is achieved.

Differences in degradation rates between the different types of soils, as observed by Sprankle *et al*,[18] were believed to be due to variations in microbe populations and the tenacity of glyphosate binding. The stability of the metal-phosphonate complex is influenced by the type of metal ions present the soil, and is the main contributor to the unavailability of glyphosate to microbial catabolism,[28] and may be governed by the species of metal ions present in the soil.

Further research has supported the hypothesis put forward by Sprankle *et al*[18] regarding the microbial degradation of glyphosate: it was found by Moshier and Penner[29] that sterilised soils treated with glyphosate emit very little $^{14}CO_2$ compared with their non-sterilised counterparts, confirming that microbes are at work in the degradation process.

As convenient as these results may be in the context of microbial degradation of glyphosate, it has been suggested that it is unlikely that the utilisation of the compound in its entirety by microbes as a nutrient source would occur in most natural situations, as these usually contain sufficient elements for microbial growth.[9] The research undertaken by Klimek *et al* in their study shows that when other organic sources of nitrogen are made available, glyphosate utilisation by *Penicillium chrysogenum* is either significantly reduced or completely inhibited.[9]

1.2.3 Pathways to glyphosate biodegradation and its resulting metabolites

The formation of ammonium, phosphate, carbon dioxide, and glyoxylate has been observed from the breakdown of glyphosate, plus other compounds resulting from the glyoxylate cycle (Figure 1.18).[6] More recent research into the metabolism[9] has revealed

the possibility of acetylation of AMPA then cleavage of the C-P bond (hashed arrow in Figure 1.18).

Later research[6] has documented a second possible pathway for the degradation of glyphosate in soils (Figure 1.19), resulting in sarcosine as a primary metabolite.

Which species of microorganisms are present in the soil governs the pathway by which glyphosate degradation occurs. For example, microorganisms that are able to utilise glyphosate as their sole phosphorus source, including *Rhizobium* and *Agrobacterium* organisms, degrade the herbicide *via* the sarcosine pathway.[6]

As well as in soil, glyphosate can also be degraded in plants, although on the whole this process is very slow.[6] A comprehensive study utilising maize, soybean, cotton, and wheat was undertaken to determine the degradation of glyphosate within plants.[6] It was found that the main metabolite (in maize) is AMPA, and the pathway proposed is similar to that illustrated in Figure 1.18.

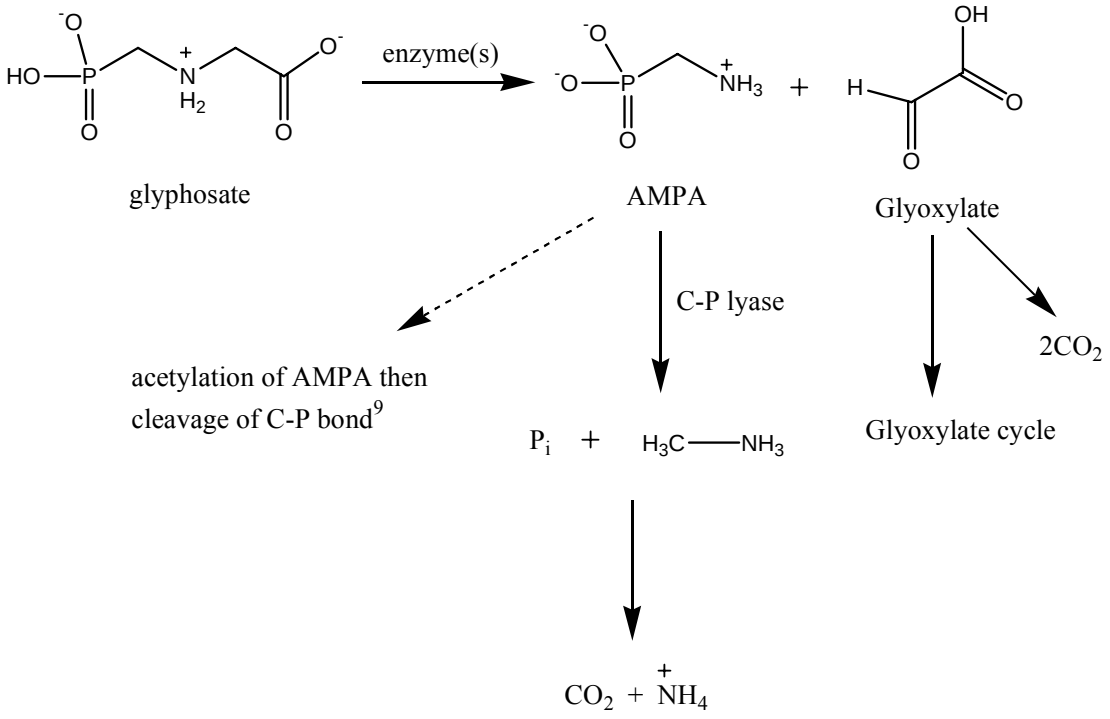

Figure 1.18: Possible pathways for the degradation of glyphosate in soils.

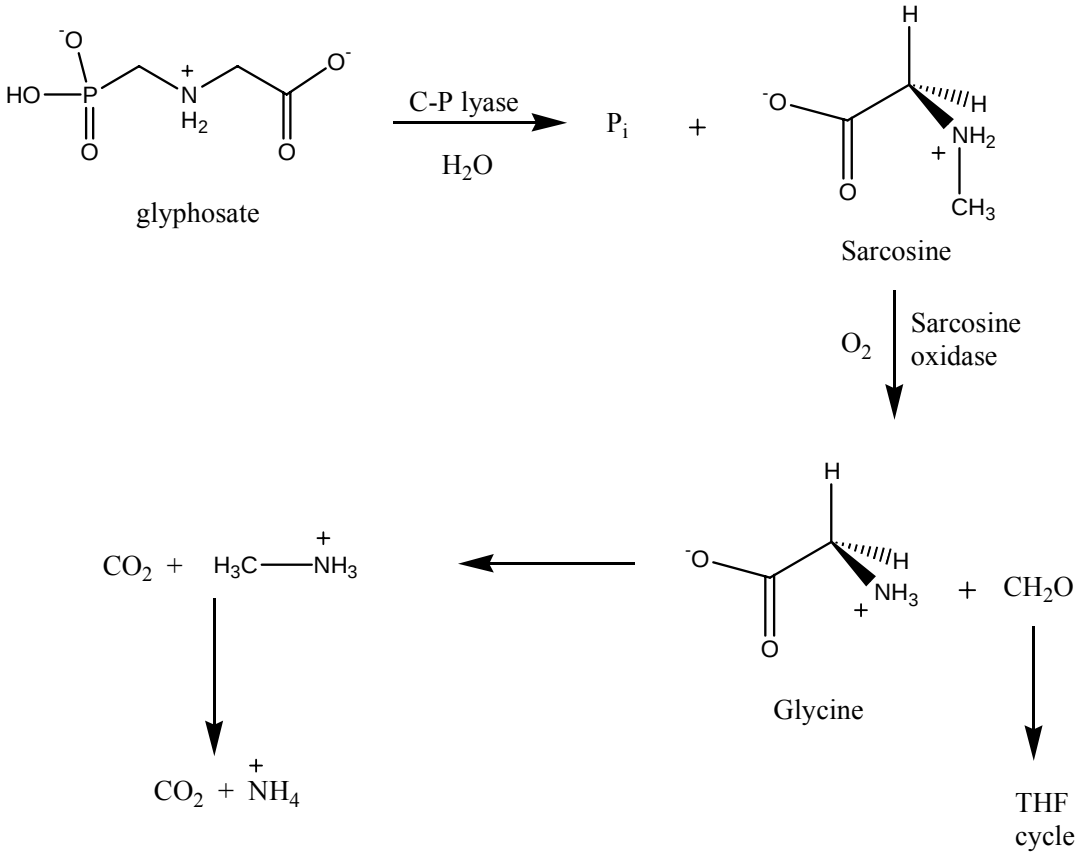

Figure 1.19: The sarcosine pathway of glyphosate degradation.

In contrast, the results of studies into the degradation of 1-^{14}C-glyphosate in sterile, detached tobacco leaves and sugar beet[6] show that the herbicide undergoes decarboxylation to yield a small percentage of $^{14}CO_2$. The remainder of the herbicide was either extracted in its original form or as AMPA. When the same researchers tested 3-^{14}C-glyphosate, only 1 % of the labelled compound was evolved as $^{14}CO_2$. In this experiment the P-C bond appeared to be stable. This is contrary to both the pathways depicted in Figure 1.18 and Figure 1.19, and may suggest that yet another pathway for the biodegradation of glyphosate is in place.

It is also possible that glyphosate can degrade in soils *via* a photolytic pathway, although the results of early work suggest that this plays a minor role in the decomposition process due to the considerably faster degradation by microbes.[14] Later work concluded that glyphosate might be photolabile in water, after photolysis of a 1 ppm solution of glyphosate resulted in a significant transformation to AMPA over 14 days.[14] Meanwhile, testing of control glyphosate solutions kept in dark storage for two weeks showed the

herbicide to be stable. This is supported by more recent research by Mallat and Barcelo,[12] whose studies on groundwater and river water have shown that glyphosate can be photolytically decomposed to AMPA in aqueous systems. Their research found that the presence of humic, or organic, substances can enhance the degradation of glyphosate. It was suggested that this is due to humic substances acting as a photosensitiser. The authors[12] claimed that for compounds that do not absorb sunlight, such as glyphosate, indirect photolysis through a photosensitiser is necessary for any photochemical transformation to take place. This would account for the increase in degradation of glyphosate in water when high levels of humic substances are present.[12] However, there may also be larger microbe populations under such humic conditions, and this too might lead to acceleration of the decomposition of glyphosate. Furthermore, the authors did not consider the effect of transition metal ions that may have been present in the water samples. It is possible that the existence of such metal ions could promote adsorption of the herbicide – the metal could then act as a photosensitiser, possibly aiding in the photochemical degradation of glyphosate. Such an effect could be significant since transition metal ions are known for their involvement in photo-redox processes.[30]

As an aside, the research carried out for the purposes of this thesis has shown an inconsistency regarding the UV absorption of glyphosate. The authors above[12] claim that glyphosate does not absorb UV light. Our own studies into this have shown that dilute glyphosate solution exhibits strong absorption in the UV range between 200 and 400 nm. From a biological standpoint, in natural systems only UV radiation in the range of 300-400 nm reaches the earth, as shorter wavelengths are absorbed by the ozone layer and other atmospheric gases. It is possible that the researchers mentioned above[12] were referring to this biological UV range. According to our data, absorption of UV by glyphosate solution between 300-400 nm is weaker than from 200-300 nm, but not so weak as to brand glyphosate as being unable to absorb UV radiation.

1.2.4 Effects of glyphosate on soil fertility

There has been some debate on the effects of glyphosate on the ability of soil-microbes to flourish, and since microbial activity is an important factor in determining soil fertility, research into the effects of glyphosate on the populations of soil-microbes has taken place.

Marsh *et al*[31] stated that CO_2 is produced by both micro- and macroorganisms in the soil, so the measurement of the evolved CO_2 from glyphosate-treated soils is inconclusive evidence that microbes are flourishing from their metabolism of glyphosate. Also, changes in microbial species are difficult to detect, so the glyphosate could be eliminating an important species of microbe while stimulating another. However, it was concluded that activity in the soil was definitely stimulated, as the total amount of CO_2 evolved was greater than the contribution could have been from the complete breakdown of the herbicide.[31] Nitrogen mineralisation was also stimulated by the glyphosate treatment, and this observation could have two explanations: (1) the glyphosate could have stimulated the activity of nitrifying organisms (a beneficial effect for soil fertility in that these organisms increase the availability of nitrogen to plants), and/or (2) the glyphosate molecules could have completely broken down, releasing nitrogen.

A later study on the effects of soil microbial activity[27] concluded that the addition of glyphosate to soils has a favourable effect on microbe populations. It was found that glyphosate application rapidly stimulated the activity of soil microorganisms, as measured by carbon and nitrogen mineralisation. The highly linear relationship between the amount of glyphosate added and the amount of carbon and nitrogen mineralised suggests that glyphosate was directly responsible for the increase in microbial activity. They concluded that even at excessive application rates, glyphosate should be quickly degraded by soil microbes without having an adverse effect on the organisms.

1.2.5 Persistence and mobility of glyphosate in soils

Persistence in the soil is not a fixed property of any herbicide since its adsorption and degradation rates are dependent on several factors including the soil type and its properties, the microbes present in the soil, and the cultivation methods used.[6] Glyphosate tends to be moderately persistent in soils and there are several half-lives documented for the herbicide, ranging from 3 days when applied to a silt loam, to 270 years when applied to a clay loam.[6]

These results can be explained by the constitution of the individual soils. As the names suggest, silt loam has a lower clay content compared to clay loam (Table 1.3).

Soil type	Clay content (%)	Silt content (%)	Sand content (%)
Silt loam	12 - 27	> 50	N/A
Clay loam	27 - 40	N/A	20 - 45

Table 1.3: The percentage of clay, silt and sand present in silt and clay loams.[32]

Clay is described as an alimino silicate, with magnesium and/or iron substituting for all or part of the aluminium.[32] Clay particles have the ability to hold water, perhaps due to the association between the water molecules and the metal ions that comprise the clay. It is not unfeasible then, considering this apparent affinity of clay for oxygen donors, that clay particles are also capable of adsorbing free glyphosate. Sand and silt, on the other hand, comprise SiO_2, and may not have the ability to adsorb glyphosate.

The difference in soil type may also be responsible for discrepancies in the literature regarding the leaching of glyphosate. A study undertaken by Veiga *et al*[3] of forest soils in northern Spain found that glyphosate and its main metabolite, AMPA, could be detected 20-35 cm below the surface of the treated soil despite adsorption onto soil components. This has raised concern, since at this depth glyphosate degradation occurs slowly due to a smaller microbial population than at more elevated soil levels. This result of the leaching of glyphosate into deeper soils contrasts to some reports referred to by Franz *et al*[6] where it is claimed that glyphosate has low mobility in soils and is essentially non-leachable. Again, soil type and the exact constitution of it are possible reasons for the discrepancy.

1.2.6 Glyphosate-tolerant plants

Although there have been several reports of plant species in the field becoming resistant to some potent herbicides, the natural development of glyphosate resistance among weeds has not been observed despite the extensive global use of the herbicide for many years.[6] Some species such as bermudagrass and conifers do have a resistance to foliage-applied glyphosate when in their dormant state but this is attributed to limitations in uptake or translocation problems as opposed to a natural resistance to the compound. It is thought

that the absence of glyphosate-resistant weeds is due to the herbicide's short life-span once soil contact is made, and the fact that the herbicide usually does not reside, in its free form, in the soil from one year to the next.
Generally, there are four methods by which a plant can gain herbicide-tolerance:[6]

1. The overproduction of a target enzyme, such as EPSP synthase, leading to higher tolerance toward the herbicide.
2. The target enzyme is altered in such a way that the herbicidal compound cannot bind so efficiently, whilst allowing the normal function of the enzyme to continue.
3. The phytotoxic compound is metabolised to less toxic substances after adsorption by the plant.
4. The alteration of non-target entities, which minimises the toxic effect of the herbicide. Examples include decreased permeability or translocation of the herbicide, and compartmentalisation of the herbicide in locations far from the active site of the target enzyme.

Since glyphosate is a broad-spectrum herbicide it does not discriminate between desirable and weed plant species. However, the employment of biotechnology has led to the advent of "Roundup® Ready" crops. Such crops, developed *via* genetic modification, now enable farmers to apply herbicides without the concern of wind-blown herbicide solution affecting crop species. Since 1996, transgenic plants that have glyphosate-tolerance, including soybean, canola, cotton, and corn, have been developed and commercialised. Such plants can be engineered either by the over-production of wild-type EPSP synthase (method 1 above) or by the production of an EPSP synthase that has a decreased affinity for glyphosate (method 2 above).[33] However, only the latter method (method 2) gives a plant with a level of glyphosate-tolerance that is commercially acceptable.

In the development of glyphosate-tolerant corn, two gene cassettes from the *Agrobacterium* species (strain CP4 EPSP) genome were inserted into the DNA of corn. The gene cassettes express EPSP synthase that is functionally similar to the EPSP synthase enzymes found in plants but exhibits a much reduced affinity for glyphosate.[34] This reduced affinity is due to the presence of, in the glyphosate-tolerant EPSP synthase, an alanine instead of a glycine at amino acid residue 96.[32]

1.3 Structures of Metal-Glyphosate Complexes

Our knowledge of the high degree of adsorption of glyphosate to soil-residing metals has led to considerable interest in the synthesis and characterisation of metal-glyphosate complexes. Until 1988, no X-ray crystal structure determination of a metal-glyphosate complex had been published, although the structure of free glyphosate had long been solved.[22] It has been suggested[35] that this lack of crystal structure determinations of metal-glyphosate complexes is due to the variability of water solubility between the complexes. However, the syntheses of some monomeric and polymeric structures have been successful, and stability constants for divalent and trivalent metal complexes, IR spectroscopy data and X-ray powder diffraction results have been obtained.[36]

1.3.1 The Ca(glyphosate) complex

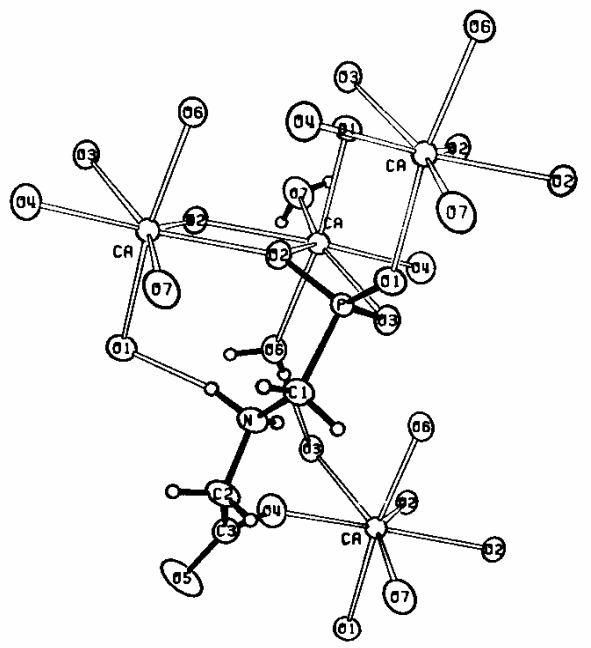

Figure 1.20: A Ca(glyphosate) polymeric complex.

Smith and Raymond published the first crystal structure of a metal-glyphosate complex in 1987 (Figure 1.20).[22] Each calcium ion is seven-coordinate and is bonded to four different glyphosate units. Four phosphonate oxygen atoms from three different glyphosate molecules, one carboxylate oxygen atom from a fourth glyphosate molecule, and two oxygen atoms from water molecules complete the coordination sphere of the calcium ion.

The donation of electrons from two phosphonate oxygen atoms of the same glyphosate unit results in the formation of a four-membered chelate ring. Only the oxygen atoms of the glyphosate molecules donate to the metal centre – the nitrogen atom is not coordinated.

Hard-Soft-Acid-Base (HSAB) theory helps to explain why Ca(II) prefers the oxygen donors of glyphosate, and not the nitrogen donor. The Ca(II) ion is hard and prefers to accept from a hard donor such as oxygen, rather than a softer donor such as a secondary amine. No five-membered chelate rings are present. The formation of such a chelate ring would necessitate the donation from the soft secondary amine donor to a hard Ca(II) centre.

Each glyphosate unit donates to four different calcium ions. A hydrogen-bonding network is present and connects each glyphosate unit to a neighbouring glyphosate unit, and connects each water molecule to a glyphosate unit. The conformation of the coordinated glyphosate is very different from that of the free acid, given that the torsion angle of C1-N-C2-C3 is 143.0^{o} in the calcium-glyphosate complex, but is 74.6^{o} in free glyphosate. C1 and C3 are more or less in an *anti* conformation in the complex, whereas they are *gauche* relative to each other in free glyphosate.

1.3.2 The Cu(glyphosate) complex

Glyphosate is very capable of coordinating through its nitrogen atom, as seen in the first transition metal-glyphosate complex to be characterised by X-ray crystallography (Figure 1.21).[37]

The glyphosate in this polymeric Cu-glyphosate complex is chelated to the copper ion in a tridentate fashion and forms a distorted square pyramid about the Cu(II) ion. Four donors coordinate to the basal plane of the square pyramid: the amine nitrogen atom, the carboxylate oxygen atom, one phosphonate oxygen atom of the same glyphosate unit, and a phosphonate oxygen atom of one adjacent glyphosate ligand. It is notable that in this complex, the Cu(II) accepts from a nitrogen donor. The reason behind this becomes clear when one considers the softness and size of the Cu(II). This metal ion is relatively soft

and small, and accepts electrons from the soft nitrogen donor. The small size of the Cu(II) perhaps facilitates the formation of the five-membered chelate rings by enforcing a certain bite angle upon the chelate rings. It is possible that such a bite angle leads to their stability and, therefore, their formation is favourable. A phosphonate oxygen atom of a second adjacent glyphosate ligand caps the square pyramid. Each copper ion is bonded to three glyphosate units. The sixth possible coordination site is vacant, but if occupied would yield an octahedral complex. The polymer exists as a chain of copper ions and glyphosate units in a zigzag conformation.

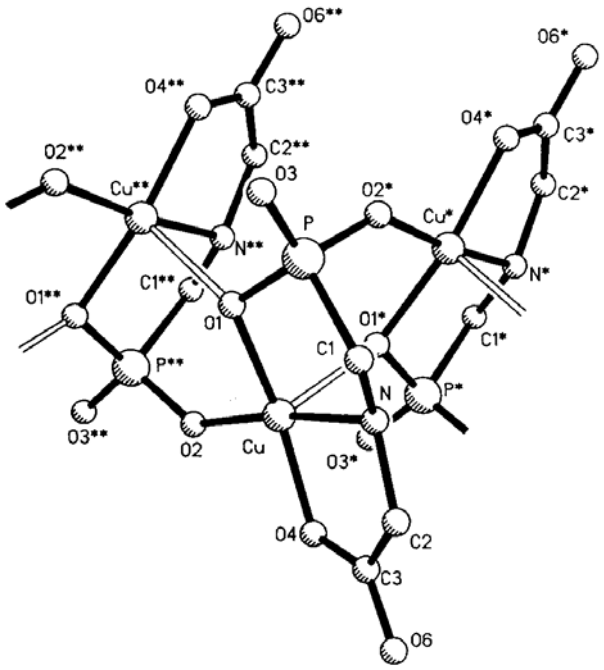

Figure 1.21: A Cu(glyphosate) polymeric complex.

1.3.3 The Ba(glyphosate) complex

Figure 1.22 shows the crystal structure of one $\{[Ba(glyphosate)(H_2O)_2]_2\}$ unit of the infinite polymeric structure of this substance.[35] The primary interactions between the barium ion and the glyphosate are through a carboxylate oxygen atom (O(2)) and a phosphonate oxygen atom (O(4)), leading to an eight-membered ring. The nitrogen atom is protonated and does not donate to the metal centre. Ba(II) is quite hard and prefers to accept from a hard oxygen donor, as exhibited in the obtained crystal structure.

The O(2) atom forms part of a bidentate carboxylate interaction with the barium ion of an adjacent complex, and the second carboxylate oxygen atom (O(1)) is linked to yet another barium ion. The two coordinated water molecules (O(6) and O(7)) are involved in intermolecular hydrogen-bonding interactions with O(4) and O(5), respectively. The proton on the nitrogen (N(1)) hydrogen bonds to O(3). Geometrically, the coordinated glyphosate shares a similar conformation to that of the free acid.

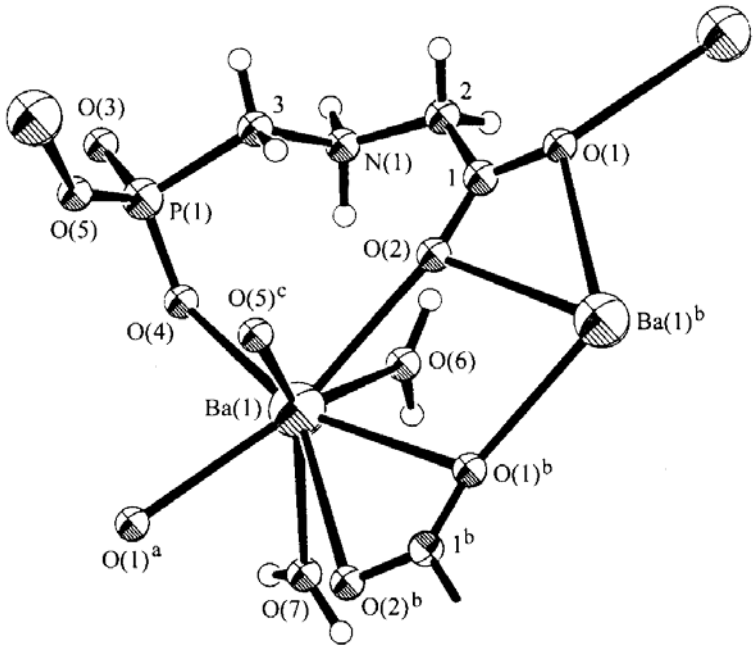

Figure 1.22: A Ba(glyphosate) polymeric complex.

1.3.4 The Pt(glyphosate) complex

A monomeric platinum(IV)-glyphosate complex, $[Pt(glyphosate)Me_2(H_2O)]^{2+}$ with an octahedral geometry is shown in Figure 1.23.[36] This was the first metal-glyphosate complex to be characterised where the glyphosate exhibits a facial, tridentate coordination mode. Two chelate rings are formed from the coordination of glyphosate to the platinum centre. Pt(IV) is relatively soft compared with Ca(II) and Ba(II), and likes to accept electron density from the softer nitrogen atom of the glyphosate. The additional donation from two oxygen atoms assists the formation of two chelate rings. Pt(IV) is small enough such that the formation of the chelate rings is favourable, *i.e.* the bite angles brought on by the size of the metal ion stabilise the rings.

Two *cis* methyl groups and one water molecule take up the remaining three facial coordination sites on the platinum. The amine nitrogen atom and one phosphonate oxygen atom are *trans* to the methyl groups. The glyphosate is coordinated *via* its nitrogen atom, a phosphonate oxygen atom, and a carboxylate oxygen atom. The crystal structure is stabilised by hydrogen bonding involving the coordinated water molecule. The structure shown is one of two enantiomers present in equal quantities in the unit cell.

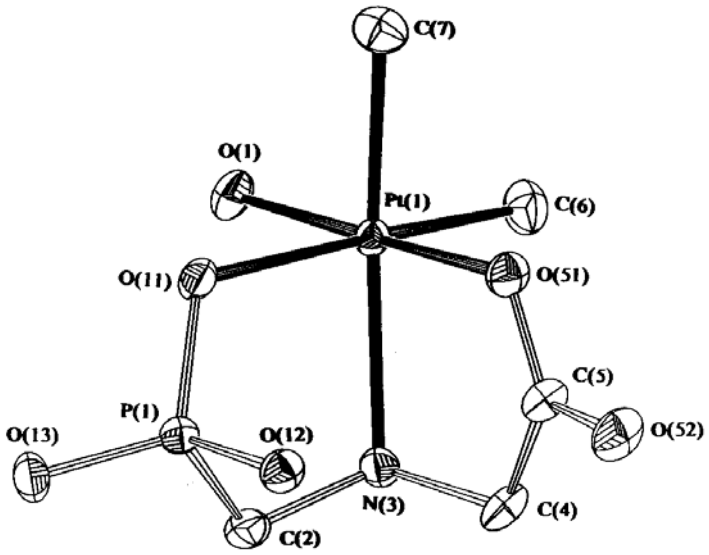

Figure 1.23: A Pt(glyphosate) monomeric complex.

1.3.5 The $[Co(glyphosate)]_2]^{3-}$ complex

The $[Co(glyphosate)_2]^{3-}$ complex was synthesised by Heineke *et al* in 1994 (Figure 1.24).[38]

The NMR spectra of the product showed it to be a mixture of isomers. However, the crystals obtained from the isomer mixture underwent X-ray crystal structure determination, and the resulting crystal structure was found to be the *fac-RS-all-trans* isomer (Figure 1.24). ^{1}H and ^{31}P NMR spectra of a solution of the crystals immediately after dissolution showed only the peaks for the *fac-RS-all-trans* isomer. However, after standing overnight a mixture of isomers in the sample was evident. The process of isomerisation was found to reach equilibrium after two hours of dissolution at room temperature.

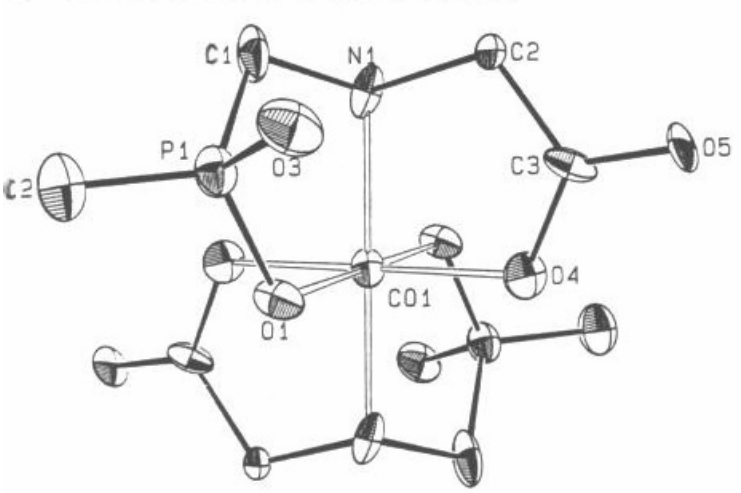

Figure 1.24: The crystal structure of $[Co(glyphosate]_2]^{3-}$.

The 15 possible stereoisomers, including seven sets of enantiomers, of $[Co(glyphosate)_2]^{3-}$ are shown in Figure 1.25.[38] The facile interconversion between stereoisomers is an unusual observation for Co(III) systems, which, with their d^6 configurations, are usually kinetically inert.

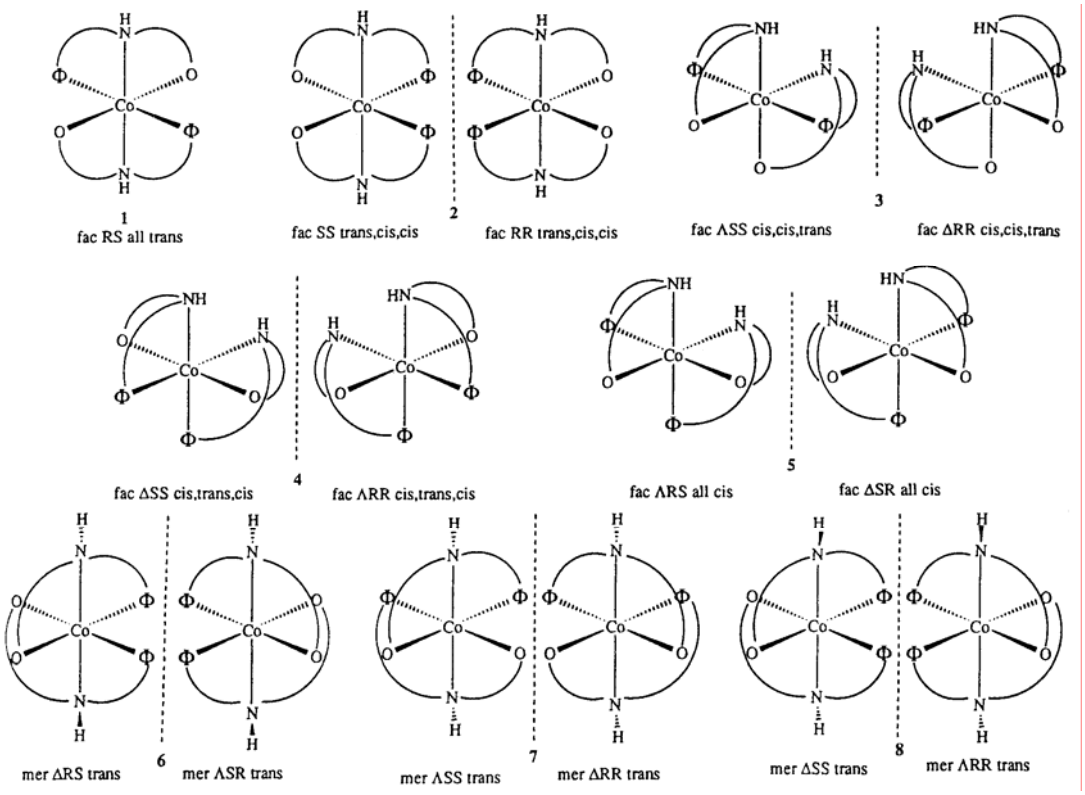

Figure 1.25: Possible $[Co(glyphosate)_2]^{3-}$ isomers. Key: $\Phi = CH_2PO_3^{2-}$; $O = CH_2CO_2^-$.

1.4 Reactivity of Metal-Glyphosate Complexes and Related Compounds

Due to the high degree of metal complexation that glyphosate undergoes in soils, an area of significant interest in the laboratory is the synthesis of metal-glyphosate complexes. Although the degradation of glyphosate in soils is mainly due to microbial activity, a significant amount of the herbicide is bound to metal ions in the soil (Section 1.2). It is entirely possible that these metal-glyphosate adducts in soils can undergo chemical or photochemical reactions which lead to the degradation of glyphosate. As reported by Marsh *et al*,[31] glyphosate in soils may be degraded *via* chemical rather than biochemical means, while in aqueous systems the herbicide may be photochemically degraded.[6,7,12,14] Another interesting detail to consider when regarding the possible chemical degradation of glyphosate was first broached in section 1.1.3.2. Figure 1.12 shows the synthesis of glyphosate, and quite notable is the synthetic step from the dicarboxymethyl species to the monocarboxymethyl species.[6] This step is a dioxygen-induced elimination of one carboxymethyl group, and yields the desired molecule, glyphosate. It is possible that a second elimination could take place in the presence of O_2 to yield a decomposed glyphosate species.

Keeping in mind the essential role that metal ions play in the inactivation of glyphosate in soils,[16] it is of interest to determine if glyphosate can be degraded by chemical or photochemical means when it is coordinated to a metal ion. Studies in the laboratory into the reactivities of metal-glyphosate complexes should endeavour to explore the reaction conditions that such complexes might be susceptible to, such as changes in pH and irradiation with UV light. The products of these reactions may provide a hint as to the mechanisms at hand when metal-bound glyphosate is degraded in natural situations.

Thus far, and in spite of the ready availability of metal-glyphosate complexes, little research has been undertaken in the field of coordinated glyphosate reactivity.

1.4.1 The reactivity of cobalt-glyphosate complexes under basic conditions

While there has been little work undertaken in the area of coordinated glyphosate reactivity, complexes of a closely related ligand, iminodiacetate (IDA) have been studied.[39] IDA has two carboxymethyl groups adjacent to its central amine group (Figure 1.26), rather than one carboxymethyl and one phosphonomethyl group (as exhibited in the glyphosate molecule).

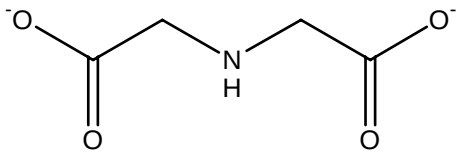

Figure 1.26: The structure of dianionic IDA. The protonation state can vary between cationic and dianionic species.

In the context of the reactivity of glyphosate when bound to metal cations, one result from the literature regarding metal-IDA complex reactivity can be considered particularly significant.[39] Initial attempts to synthesise a Co(III) complex containing tris(2-aminoethylamine) (tren) and IDA as ligands resulted in a low yield of $[Co(tren)(IDAH)]^{2+}$, the desired product, and a large amount of a by-product, identified as $[Co(tren)(gly)]^{2+}$ (Figure 1.27).

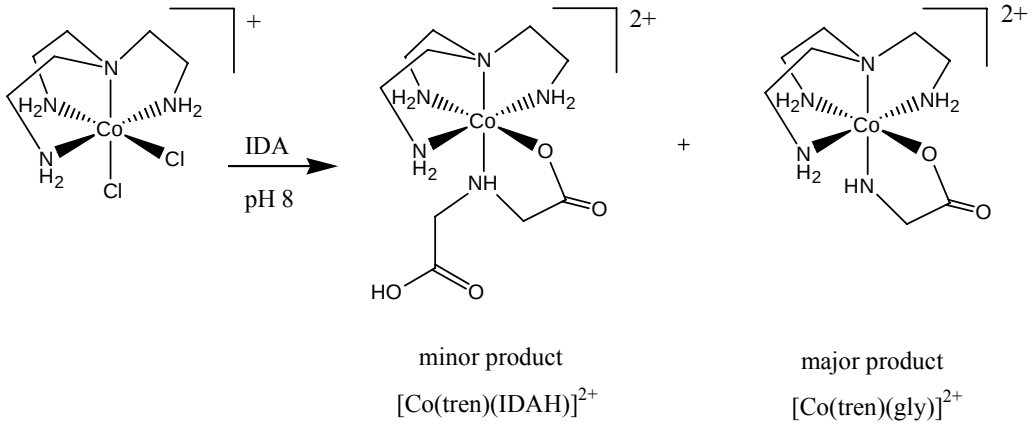

Figure 1.27: Products of the reaction of $[Co(tren)Cl_2]^+$ and IDA at pH 8.

Realising the reaction was possibly pH-sensitive, the researchers[39] repeated the synthesis at a pH of 7, resulting in a good yield of the desired complex (Figure 1.28). When a

solution of this complex was raised to a pH greater than 8, $[Co(tren)(gly)]^{2+}$ and Co(II) were obtained. The presence of Co(II) indicated that the dealkylation was occurring *via* an oxidative pathway – the IDA ligand was most likely being oxidised to a coordinated imine with concomitant reduction of Co(III). This theory was reinforced when the addition of sacrificial metal complexes to the reaction mixture saw a marked increase in the yield of $[Co(tren)(gly)]^{2+}$.

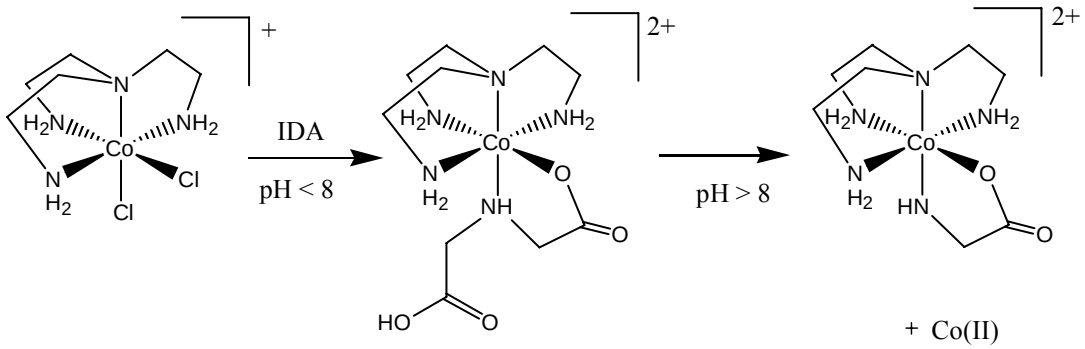

Figure 1.28: Synthesis of $[Co(tren)(IDAH)]^{2+}$ at pH less than 8, and subsequent conversion to $[Co(tren)(gly)]^{2+}$ under basic conditions.

The oxidation of the coordinated IDA ligand is a two-electron process: the metal centre of the $[Co(tren)(IDAH)]^{2+}$ complex accepts one electron to become Co(II), and the metal centre of the sacrificial metal complex accepts the second electron of the oxidation process. This would account for the increase in $[Co(tren)(gly)]^{2+}$ when sacrificial metal complexes were added to the reaction mixture.

It was proposed that the base-induced oxidation of the coordinated IDA ligand led to an imine complex, according to Figure 1.29.[39] The imine can then undergo ligand loss or decarboxylation to yield the $[Co(tren)(gly)]^{2+}$.

Initially, it was not possible for the researchers[39] to ascertain which pathway, A or B as shown in Figure 1.29, was followed in the base-induced dealkylation of $[Co(tren)(IDAH)]^{2+}$. In an attempt to clarify this, a related complex (Figure 1.30) with a pendant methyl group on the chelate ring which can act as a label in the reaction, was prepared.

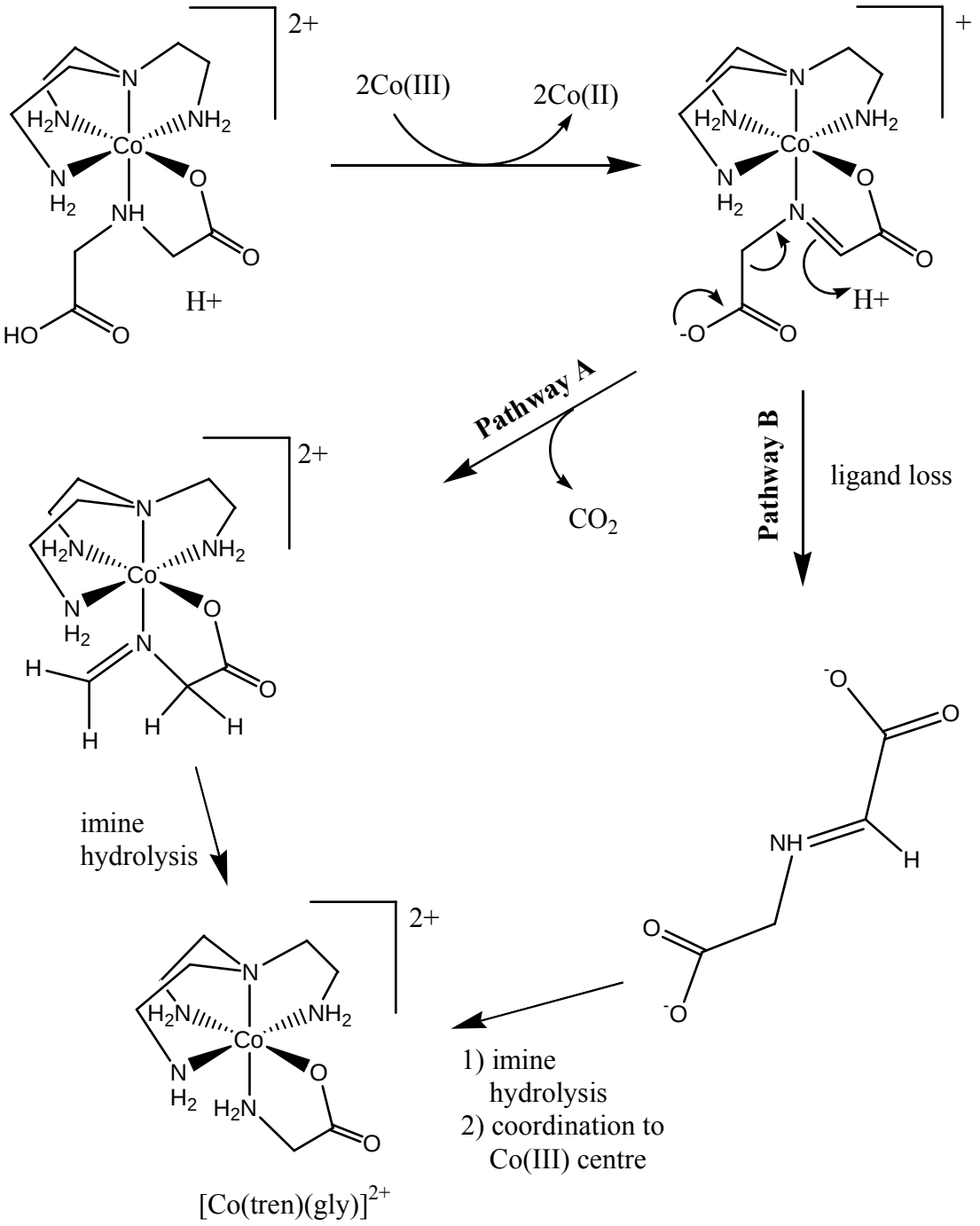

Figure 1.29: Two possible pathways for the formation of $[Co(tren)(gly)]^{2+}$ from $[Co(tren)(IDAH)]^{2+}$.

It was thought that treatment of the *p*-$[Co(tren)(cmi)]^{2+}$ complex to basic conditions would provide an insight into which pathway, A or B, would be followed. Pathway A would result in an alaninato complex, while pathway B would result in a glycinato complex (Figure 1.31).[39]

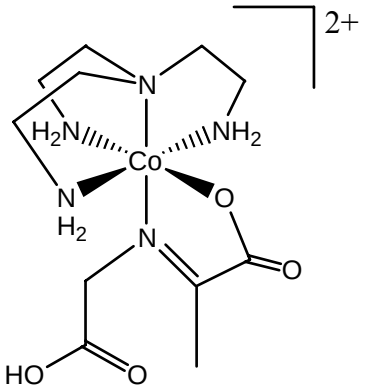

Figure 1.30: *p*-[Co(tren)(cmi)]$^{2+}$

However, analysis of the reaction mixture showed both *p*-[Co(tren)(ala)] $^{2+}$ and *p*-[Co(tren)(gly)]$^{2+}$ were present, suggesting that both pathways A and B (Figure 1.29) occur in the dealkylation of *p*-[Co(tren)(cmi)]$^{2+}$, and possibly also of [Co(tren)(IDAH)]$^{2+}$.[39]

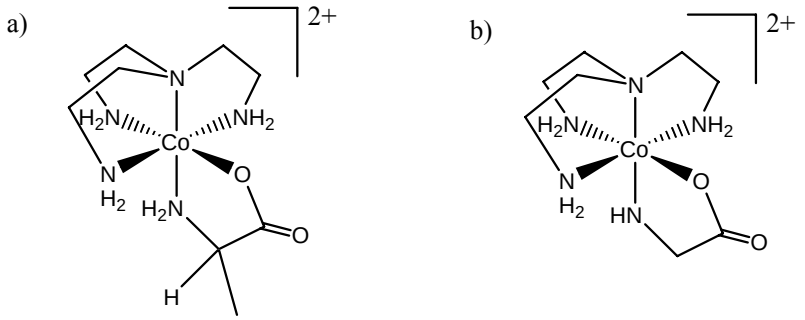

Figure 1.31: a) the complex formed via pathway A, *p*-[Co(tren)(ala)]$^{2+}$ and b) the complex formed via pathway B, *p*-[Co(tren)(gly)]$^{2+}$.

The observed base-induced dealkylation of [Co(tren)(IDAH)]$^{2+}$ is an important result in the context of the reactivity of its related compounds. Glyphosate is structurally related to IDA and it may be feasible that it can undergo similar transformations when exposed to basic conditions. It is possible that in natural systems, if suitable conditions, such as elevated pH levels, occur, that glyphosate may undergo similar reactivity. If this is the case, glyphosate could be decomposed to inert substances including CO_2 and glycine, as observed by Hartshorn[39] when [Co(tren)(IDAH)]$^{2+}$ was treated to basic conditions.

The result of the base-induced dealkylation of [Co(tren)(IDAH)]$^{2+}$ may be considered significant in terms of another member of the Co-tren system. [Co(tren)(PMGH)]$^{2+}$

(Figure 1.32) is an example of a metal-glyphosate complex that has been synthesised,[40] and is strictly analogous to the $[Co(tren)(IDAH)]^{2+}$ complex. $[Co(tren)(PMGH)]^{2+}$ consists of a tren ligand coordinated in a tetradentate fashion to a Co(III) centre. The amine nitrogen atom and the carboxylate oxygen atom of PMG occupy the two remaining *cis* sites. The enantiomer shown in Figure 1.32 with the PMG amine group *trans* to the tertiary amine group of the tren ligand is obtained when the synthesis is carried out. The alternative isomer that would arise if the amine nitrogen atom of the PMG was to coordinate *cis* to the tertiary amine on the tren ligand is not observed. Donation to the metal centre from the comparatively large phosphonate group does not occur, possibly due to steric effects. Such coordination to the Co(III) through the oxygen atoms of the phosphonate group would lead to a sterically more hindered structure, due to the larger number of atoms joined to the phosphorus centre.

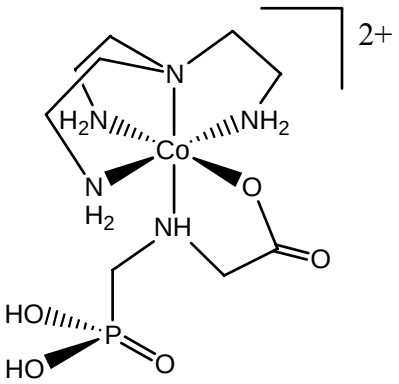

Figure 1.32: $[Co(tren)(PMGH)]^{2+}$

$[Co(tren)(PMGH)]^{2+}$ was subjected to basic conditions[40] but did not react to form the glycinato complex, contrary to the results that were observed when $[Co(tren)(IDAH)]^{2+}$ was reacted under similar conditions.

The difference in reactivity between the $[Co(tren)(IDAH)]^{2+}$ and $[Co(tren)(PMGH)]^{2+}$ complexes provokes the study of other systems where amine-containing ligands, rather than tren, are used in conjunction with glyphosate and Co(III), or IDA and Co(III). It is thought that the comparisons of the reactivities between metal-glyphosate complexes and metal-IDA complexes may prove useful in determining the mechanisms occurring when glyphosate is subjected to basic conditions in natural systems.

It is one of the objectives of this research to repeat the reaction of $[Co(tren)(PMGH)]^{2+}$ under basic conditions to check for reproducibility.

1.4.2 Photochemistry of coordinated amino acids

With its central amine group and an adjacent carboxylate group, glyphosate is structurally related to the common amino acids. Simple amino acids such as glycine contain two good donor groups (the amine and the carboxylate), and substituted amino acids may contain more. It is well established in the literature that these donor groups can coordinate to metal centres to form metal-amino acid complexes, and the photochemical reactivity of these species is well known.[30] It is plausible that the reactivity of amino acid complexes could serve as a model for the reactivity of metal-glyphosate complexes when they are subjected to similar conditions.

To comprehend how photolytic reactions may occur it is important to appreciate the processes that can occur when matter is exposed to light. Absorption of a photon by a molecule in its "ground state" can lead to a change in the electronic energy level within that molecule.[41] Molecules in a photon-induced excited state are able to undergo reactions that the ground state is not capable of, such as redox reactions, ligand substitution, bond cleavage, elimination and addition reactions, and isomerisation.

Until around 20 years ago, it was thought that irradiation with UV or visible light of transition metal complexes in solution could lead to one of just three outcomes:[30]

- Change of oxidation of the central metal atom and possible release of the ligands.
- Substitution of one of the ligands for a solvent molecule.
- Isomerisation of the complex or its ligands.

However, a fourth kind of photo-induced reaction was postulated by Poznyak and Pavlovski.[30] In the literature were numerous examples of the photochemical reactivity of the ligands of transition metal complexes. The reactions included photodecarboxylation of

coordinated aminocarboxylato ligands, elimination of molecular nitrogen from coordinated azido ligands, and the elimination of ligand fragments in the photolysis of ethylenediamine complexes, among others. These reactions formed the fourth category of the photochemistry of transition metal complexes that Poznyak and Pavlovski[30] put forward. The first reaction mentioned above, the photodecarboxylation of coordinated aminocarboxylato ligands, is of great interest of us in terms of the decomposition of glyphosate when bound to metal ions in the soils. It is important here to note the difference between an amino acid and an aminocarboxylato ligand. An amino acid is defined as a species that has an amine group and a carboxylate group adjacent to the same carbon atom (the α-carbon atom). An aminocarboxylato ligand is a species that has an amine group and a carboxylate group within the structure, but not necessarily to the same carbon atom.

Past studies have revealed that amino acids bound in a bidentate fashion to a Co(III) centre can undergo photo-induced decarboxylation when treated with light.[30] Complexes of the type $[Co(L_4)aa]^{2+}$ have been tested in this manner, resulting in the contraction of the chelate ring to yield a Co-$(CH_2)_n$-N organocobalt fragment (Figure 1.33). The stability of the products depends both on the nature of L_4 and on the magnitude of n.[30] For example, if $L_4 = (en)_2$, the stability of the intermediates depends on the size of the resulting chelate ring – a three-membered ring will be less stable than a four- or five-membered ring. On the other hand, if $L_4 = (bpy)_2$, the stability of the photolysis product is dependent on the extent of the π-acceptor orbitals on the bipyridine ligands. Such π-acceptor orbitals are known to stabilise metal-carbon σ bonds.[30] Generally speaking, the complexes eventually break down to give ammonia and a carbonyl-containing compound.

Photolysis of polydentate amino acids with five-membered chelate rings, *e.g.* $EDTA^{4-}$ in the complex $[Co(EDTA)]^-$, have shown that multiply chelated complexes can also undergo decarboxylation to yield a three-membered chelate ring as observed for some bidentate amino acids (Figure 1.34).[41] This implies that glyphosate complexes, which may have up to two five-membered chelate rings, could too undergo similar photochemical decomposition. Another point of interest to mention, as Poznyak and Pavlovski[30] noted, is that, contrary to popular belief, these photodecarboxylation reactions can be carried out in aqueous medium in the presence of air. It was previously believed that such reactions had

to be carried out using organolithium compounds in a dry environment. This ability of coordinated aminocarboxylato ligands to decarboxylate in the presence of water is interesting in terms of the degradation of coordinated glyphosate. It is entirely possible, then, that metal-glyphosate complexes in solution might be photolytically active and undergo decarboxylation when exposed to UV light.

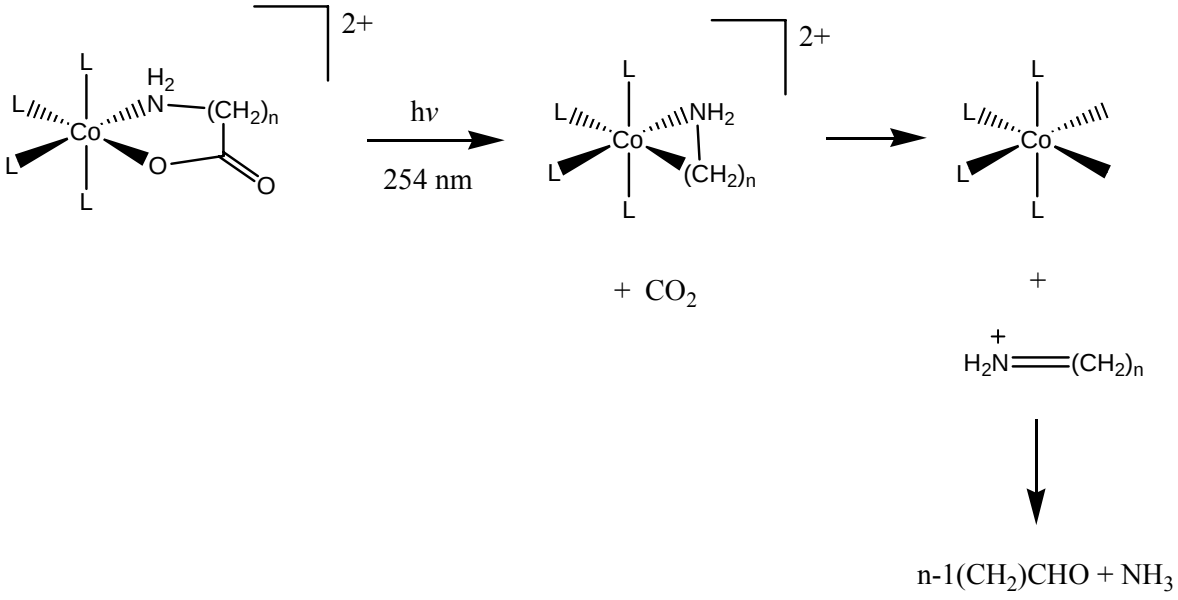

Figure 1.33: Photodecarboxylation of [Co(L4)aa] (n=1,2,3).[30]

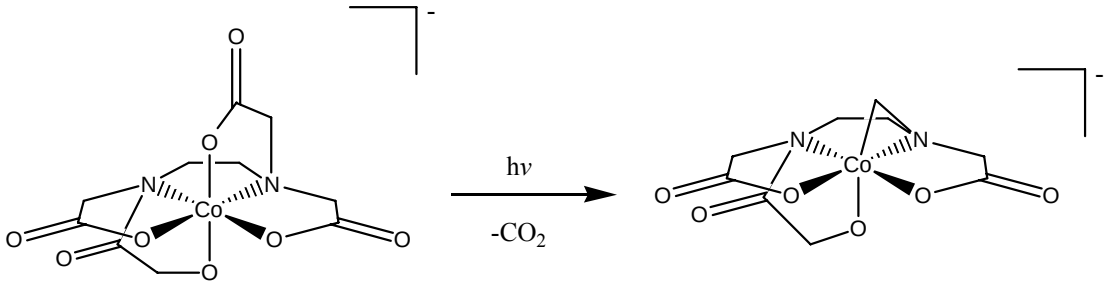

Figure 1.34: The photolysis of $[Co(EDTA)]^-$.

Given that glyphosate is an amino acid derivative, the decarboxylation reactions of coordinated amino acids, as described above, are a significant result in terms of what may happen to metal-bound glyphosate when photolysed. In this case, it is also possible that decarboxylation can occur, resulting in the (at least partial) degradation of glyphosate.

Hence, with the aim of determining the photolytic decomposition pathways that coordinated glyphosate may undergo, the study of metal-glyphosate complexes in the lab is necessary.

1.5 Summary and Objectives of the Work Described in this Thesis

Glyphosate acts as a potent, fast-acting herbicide, and its development in the late 1960s fulfilled the need of a broad spectrum, systemic weedkiller.[6] The widespread use of glyphosate has promoted much interest in the fate of the compound in natural environments. The majority of studies point towards microbial degradation being the main route of glyphosate degradation in soils, although in soils and water photochemical degradation may take place.

Once soil contact is made, glyphosate is quickly inactivated by adsorption onto metal ions that reside in the soil.[16] This adsorption appears to render the herbicide unavailable to microbial metabolism. However, it is possible that glyphosate that is bound to a metal ion in the soil can undergo chemical or photochemical degradation.

The objective of this research has been to synthesise and characterise new Co-glyphosate complexes, where the coordination of glyphosate is not unlike that which may exist in nature. Chapter 2 includes a description of the synthesis and characterisation of the complexes.

A number of complexes that are described in Chapter 2 were subjected to photolysis and base treatment so that their behaviour under these conditions could be explored. The propensity of the complexes to undergo oxidation and subsequent degradation of the glyphosate ligand is discussed in Chapter 3. It is hoped that the results of the reactivity studies of these complexes may give us an indication as to the mechanisms at work when metal-glyphosate complexes decompose in the lab, and indeed, *in vivo*.

Chapter 2 - Synthesis and Characterisation of $[Co(L)(PMG)]^{n+}$ Complexes

2.1 Introduction

The aim of the research presented in this thesis was to synthesise and characterise novel cobalt-PMG and cobalt–IDA complexes and study their reactivity under certain conditions. Co(III) was chosen as a suitable metal, since, with its d^6 electron configuration, it is diamagnetic. This d^6 configuration leads to Co(III) having no unpaired electrons, which makes the metal ideal for NMR studies. Co(III) is also inert to ligand substitution, so complexes of the metal are ideal for X-ray crystal structure analysis and other characterisation techniques, where a stable, inert species is needed.

Since cobalt (III) was the metal ion of choice for our research it was crucial to overcome the problem of isomer interconversion observed in the $[Co(PMG)_2]^{3-}$ complex, as reported by Heineke *et al*[38] and referred to in Section 1.3. During the research of Heineke *et al*[38] only one of the fifteen possible stereoisomers was isolated and characterised by X-ray crystal structure determination. When the complex was in solution, up to ten of the stereoisomers were believed to be present, although the exact number of isomers was difficult to determine from the NMR data due to the extensive overlapping of the peaks.

If one wishes to examine the reactivity of Co-PMG complexes it is necessary, then, to prevent the interconversion between possible isomers. If this is not achieved, and reactivity trials take place, the results would be considered inconclusive, as it could not be ascertained exactly how each isomer reacts to the given conditions, or, indeed, which isomer(s) are reactive. The reactivity of coordinated PMG may depend on its coordination mode – thus, to reach any conclusions in this research, it is important that the isomer interconversion problem is resolved.

One feasible method of ensuring that the interconversion between isomers does not occur is by limiting the available coordination sites available to the PMG. This limiting of

available sites can be achieved by coordinating an ancillary ligand to the metal centre prior to the coordination of the PMG ligand.

It was decided to use several nitrogen-containing ancillary ligands during the course of this research, given the stability of cobalt complexes with such donors. The ligands employed consist of various donor atoms, denticities and geometries, and were coordinated to Co(III) prior to the addition of PMG. Thus, the coordination sites available to the PMG were limited and controlled.

The ancillary ligands that were employed in this research are depicted in Figure 2.1 and include 1,4,7-triazacyclononane (tacn), a facially coordinating tridentate amine donor ligand; diethylene triamine (dien), a tridentate amine donor ligand that can coordinate facially or meridionally; 2,6-bis(aminomethyl)pyridine (bamp), a tridentate ligand that coordinates meridionally with its one pyridine donor and two amine donors; tris(2-aminoethylamine) (tren), a tetradentate amine donor ligand that coordinates in a tripodal fashion, leaving two *cis* sites on the metal vacant; and tris(2-picolyl)amine (tpa), a ligand similar to tren in that it is tetradentate and displays tripodal coordination, but has one amine donor and three pyridine nitrogen donors.

The coordination modes of these ligands are depicted in Figure 2.2. The unoccupied coordination sites, available for an additional ligand, such as PMG, to donate to are shown.

The PMG ligand can display different coordination modes depending on the sites available to it. It can act as a bidentate ligand, where it can bind through the carboxylate oxygen atom and the amine nitrogen atom. When coordinating in this mode, it is likely to preferentially bind through the carboxylate group rather than the phosphonate group. This could be due to steric effects caused by the large phosphorus atom. PMG can also act as a tridentate ligand, where it may bind to a metal through the phosphonate group, the amine nitrogen atom, and the carboxylate group.

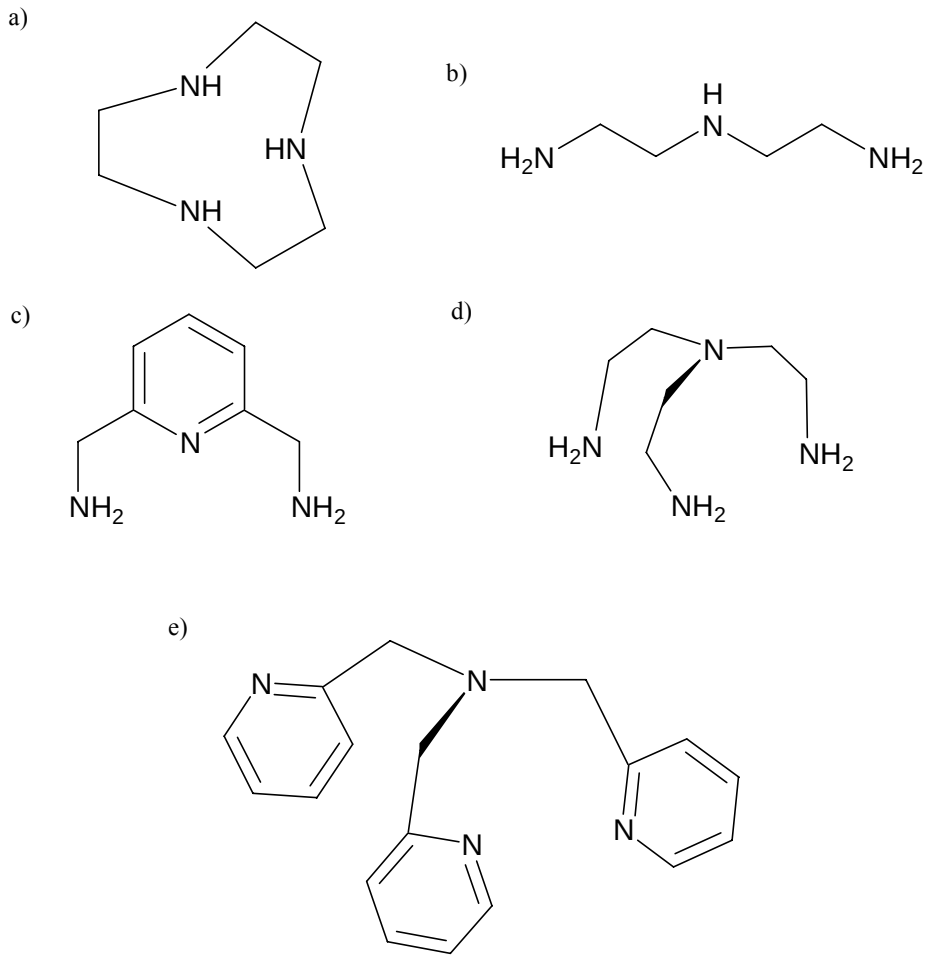

Figure 2.1: Ligands used in this research: a) tacn; b) dien; c) bamp; d) tren; and e) tpa.

The first PMG complex to be prepared by this research group[40] was $[Co(tren)(PMGH)]Cl_2 \cdot 0.5CH_3OH$, and was first introduced in Section 1.4.1. The tren ligand occupies four coordination sites on the Co(III), leaving two *cis* sites free for the coordination of PMG. Figure 2.3 depicts one enantiomer of this system, and shows that the PMG coordinates to the central cobalt atom through the carboxylate oxygen atom and the amine nitrogen atom. It is possible to produce another stereoisomer of this system, where the PMG coordinates *via* the amine nitrogen atom and a phosphonate hydroxyl oxygen atom. In this case, the carboxymethyl group would form a pendant arm. Such a stereoisomer is not formed under normal reaction conditions, possibly due to the steric clash that would be caused by coordination of the relatively large phosphonate group.

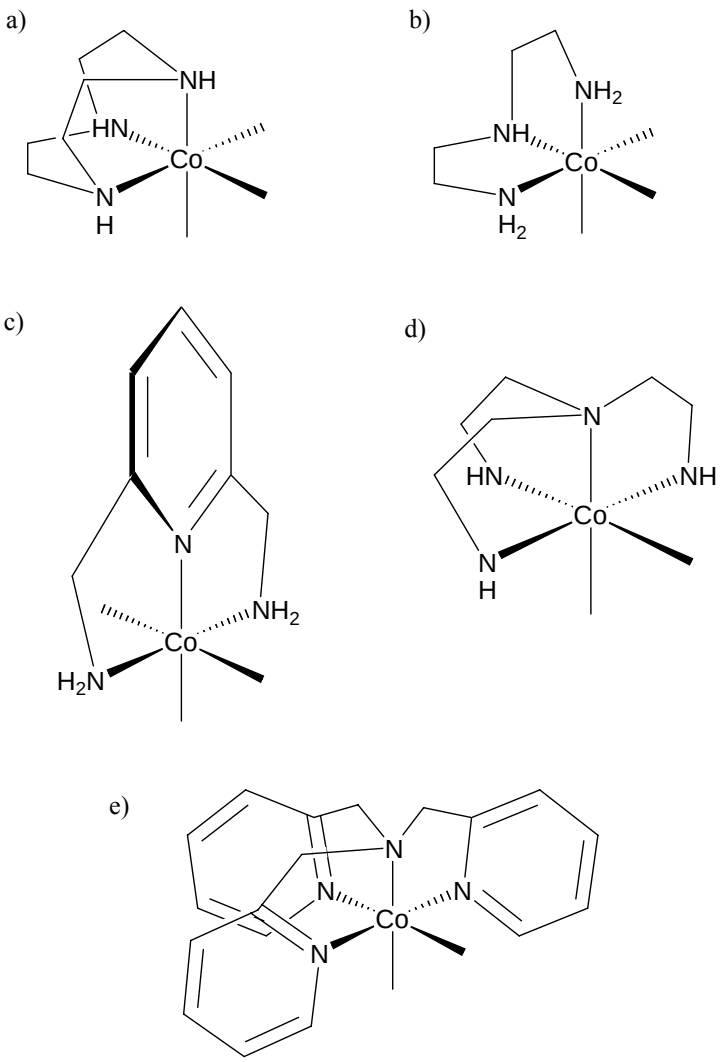

Figure 2.2: The binding modes of a) tacn; b) dien (facial coordination shown here, but can also coordinate meridionally); c) bamp; d) tren; and d) tpa.

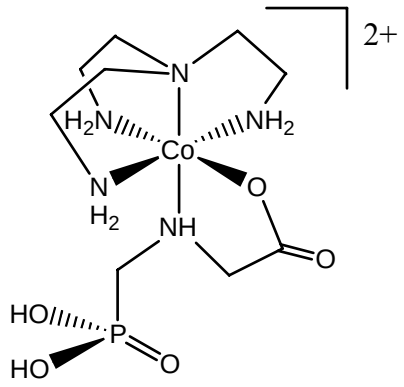

Figure 2.3: $[Co(tren)(PMGH)]^{2+}$

The following section describes the synthesis and characterisation of a variety of new $[Co(L)(PMG)]^{n+}$ and $[Co(L)(IDA)]^{n+}$ complexes. The characterisation techniques used include NMR spectroscopy, elemental analysis and mass spectrometry. In most cases, the discussions of the NMR spectra for each complex appear in the order of ^{1}H, ^{13}C, then ^{31}P. The assignment of the peaks corresponding to the PMG or IDA ligands are discussed before the assignment of the signals given by the ancillary ligand.

2.2 Results and Discussion

2.2.1 [Co(tacn)(PMG)]Cl·HCl·2.5H$_2$O

2.2.1.1 Synthesis

The first step in this synthesis involved the preparation of the tacn ligand.

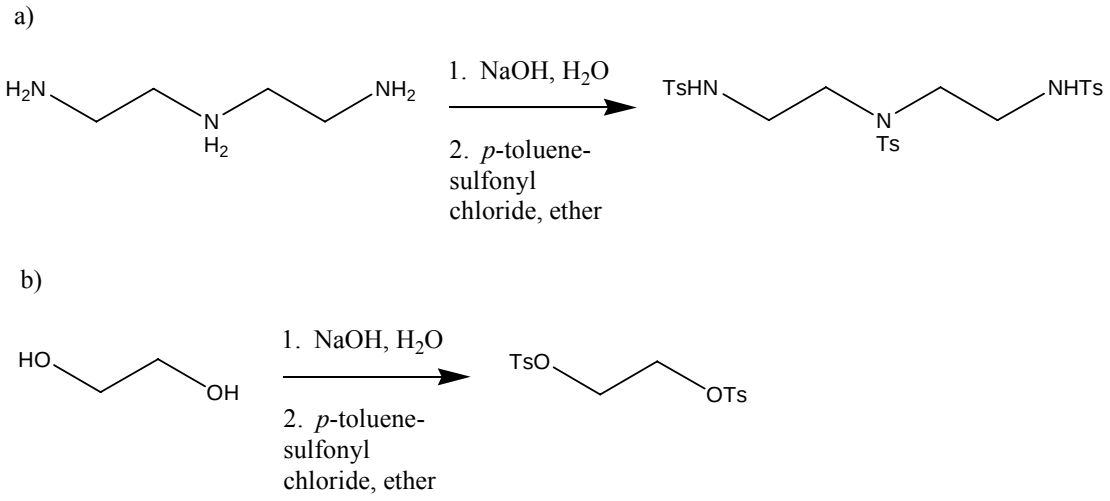

Figure 2.4: The synthesis of the precursors to tacn: a) tri-tosylated diethylene triamine,[42] and b) di-tosylated ethylene glycol.[43]

The synthesis of tacn required that the starting materials be protected *via* tosylation. Thus, tri-tosylated diethylene triamine[42] and ditosylated ethylene glycol[43] were prepared following published methods (Figure 2.4). Cyclisation of tosylated ethylene glycol and tri-tosylated diethylene triamine was achieved *via* a literature method[42] under anhydrous

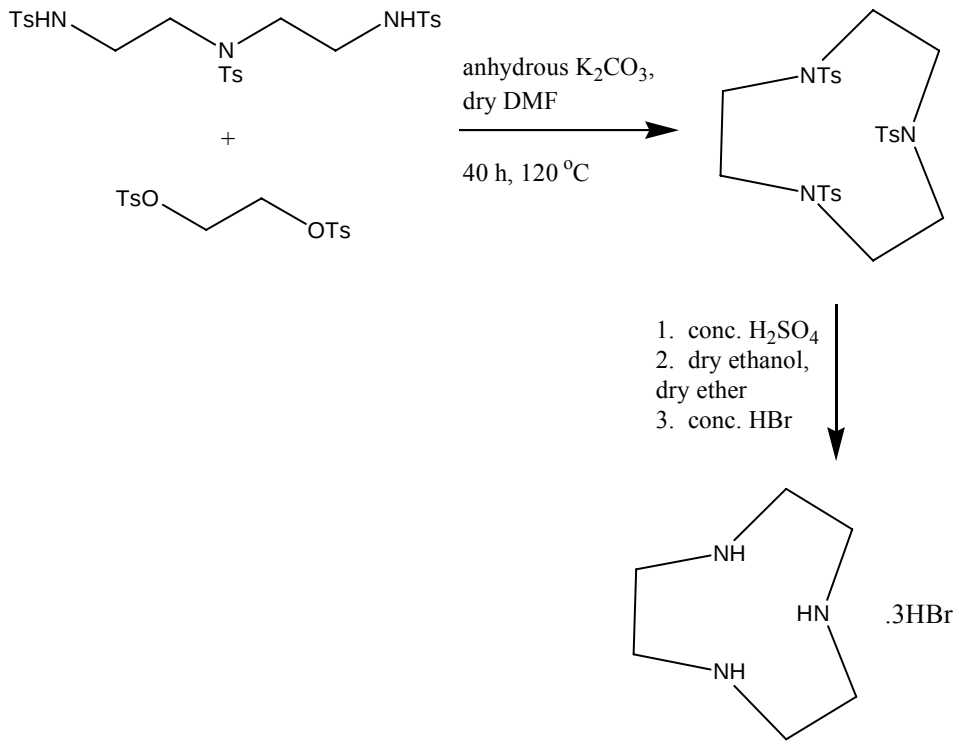

Figure 2.5: The synthesis of tacn.3HBr from its precursors.[42,45]

conditions (Figure 2.5). Contrary to the procedure denoted in the literature,[42] dichloromethane was used to extract the product, since it has a lower toxicity than benzene. Likewise, the crude product was recrystallised from ethanol, not ethanolic benzene, to give a mass of white needles. Attempts to deprotect the needles, according to a published procedure,[44] involved a lengthy workup that resulted in a low yield, so it was decided that another method was needed. Consequently, successful deprotection with a reasonable yield was achieved following a method recorded in a PhD thesis,[45] yielding the tacn.3HBr salt.

$[Co(tacn)(NO_2)_3]$ and $[Co(tacn)Cl_3]$ were then synthesised *via* literature methods (Figure 2.6).[46] $[Co(tacn)(PMG)]Cl{\cdot}HCl{\cdot}2.5H_2O$ was then prepared following a standard procedure for coordination of amino acids to metal complexes (Figure 2.6),[40] at neutral pH.

The reaction mixture was chromatographed on a Dowex cation exchange column, using HCl as an eluent. This separated the components of the mixture into different coloured bands.

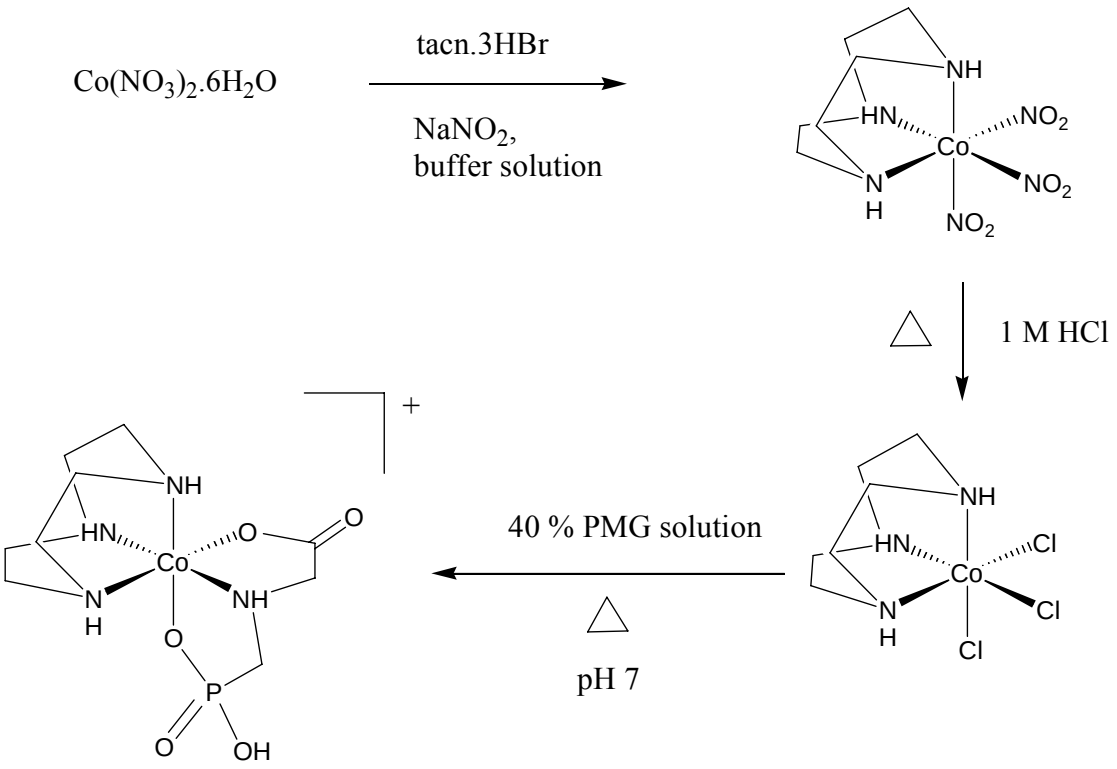

Figure 2.6: Synthesis of [Co(tacn)(PMG)]Cl·HCl·2.5H_2O.[39,45]

The use of acid as an eluent increases the likelihood of the non-coordinated oxygen atom on the phosphonate group being protonated, giving the desired complex an overall charge of 1+. A complex with a 1+ charge can be expected to travel down a Dowex column with reasonable speed: neutral species should elute very quickly, while highly charged species will have considerable affinity for the resin and will require greater concentrations of eluent to facilitate band migration. With this in mind, it was expected that the desired product would migrate rapidly down the column.

The desired complex has four nitrogen donors and two oxygen donors donating to a Co(III) centre. This suggests that the complex would be pink in colour. Indeed, a band of this colour that moved rapidly down the column was isolated, removed from the column and dried down on a rotary evaporator to yield a bright pink solid.

2.2.1.2 NMR spectroscopy

The ^{1}H NMR spectrum consists of several distinct peaks, plus a large multiplet between 3.5 and 2.8 ppm. A doublet at 7.2 ppm has been assigned to the amine proton on the

PMG. This signal is split due to the protons on the neighbouring carbon atoms. Two signals, at 8 ppm and 6.6 ppm and of single and double intensity, respectively, possibly represent the protons on the tacn amine nitrogen atoms. A quartet at 4.4 ppm has been assigned to one proton on the carboxymethylene carbon atom of the PMG. The COSY NMR spectrum shows a correlation between the quartet at 4.4 ppm and the signal at 3.4 ppm. This peak at 3.4 ppm has therefore been assigned to the remaining proton of the carboxymethylene carbon atom. A multiplet at 3.6 ppm possibly corresponds to a proton on the phosphonomethylene carbon atom of the PMG. The COSY NMR spectrum of the complex shows a correlation between the peak at 3.6 ppm and a signal at 3.0 ppm. Therefore, we have assigned the peak at 3.0 ppm to the second proton on the phosphonomethyl carbon atom of the PMG ligand.

The remaining peaks in the multiplet between 3.5 and 2.8 ppm have been assigned to the tacn methylene protons.

The ^{13}C NMR spectrum shows a peak at 187.0 ppm, most likely representing the carbonyl carbon atom of the PMG ligand. A signal at 60.6 ppm corresponds to the carbon atom on the carboxymethylene arm. The doublet assigned to the methylene carbon atom on the phosphonomethylene arm is seen at 52.8 and 50.9 ppm. We expect two, half-height signals from this single carbon atom, since it has a neighbouring phosphorus atom with a spin of ½ which splits the signal from the carbon into two.

Five peaks appearing between 54.5 and 51.5 ppm in the ^{13}C NMR spectrum correspond to the six ethylene carbon atoms on the tacn. Four of these signals are of single intensity, and one is of double intensity. The ^{13}C NMR spectrum of free tacn exhibits just one peak since all of the carbon atoms are in equivalent environments. However, when the tacn is coordinated to a metal centre that has other inequivalent donor atoms attached, the environments of the tacn carbon atoms become non-equivalent, leading to the multiple peaks.

Due to the complex containing only one phosphorus atom, the ^{31}P NMR spectrum exhibits one peak, the chemical shift of which is 38.4 ppm.

2.2.1.3 X-ray crystallography

Attempts were made to grow crystals of the $[Co(tacn)(PMG)]^+$ complex that were suitable for X-ray crystal structure determination. These included the application of two methods: vapour diffusion and slow evaporation. The vapour diffusion of various solvents that are miscible in water, including methanol, ethanol, and acetone, into aqueous solutions of the complex was initiated. The complex had a propensity to crystallise when acetone was used as the water-miscible solvent. Solid material formed within 24 hours to yield bright pink blocks or heavily twinned needles.

Unfortunately, the crystals that were deemed suitable for X-ray crystal structure determination proved to be extensively disordered, even though the X-ray data obtained was very good.

As a means of understanding the occurrence of disorder within solid-state structures it is necessary to appreciate that a crystal structure is not solved from the reflections created by just one molecule of a species in its solid state, but from the average of the sum of all reflections created by all the atoms and molecules in a unit cell, across all unit cells within a crystal. Figure 2.7 shows how the trigonal planar carboxylate carbon atom and the tetrahedral phosphonate phosphorus atom of the $[Co(tacn)(PMG)]^+$ complex can "map" onto each other to give the observed model structure.

Figure 2.8 shows the disordered crystal structure obtained for the $[Co(tacn)(PMG)]^+$ complex, modelled in the Pna2/1 space group.

The geometry of the complex is octahedral around the Co(III) centre. The bond between O3 and O4 is an artifact of the model used to describe the disorder. The disorder in the complex also creates the illusion of the PMG ligand containing two phosphonate arms, rather than one phosphonate arm and one carboxylate arm.

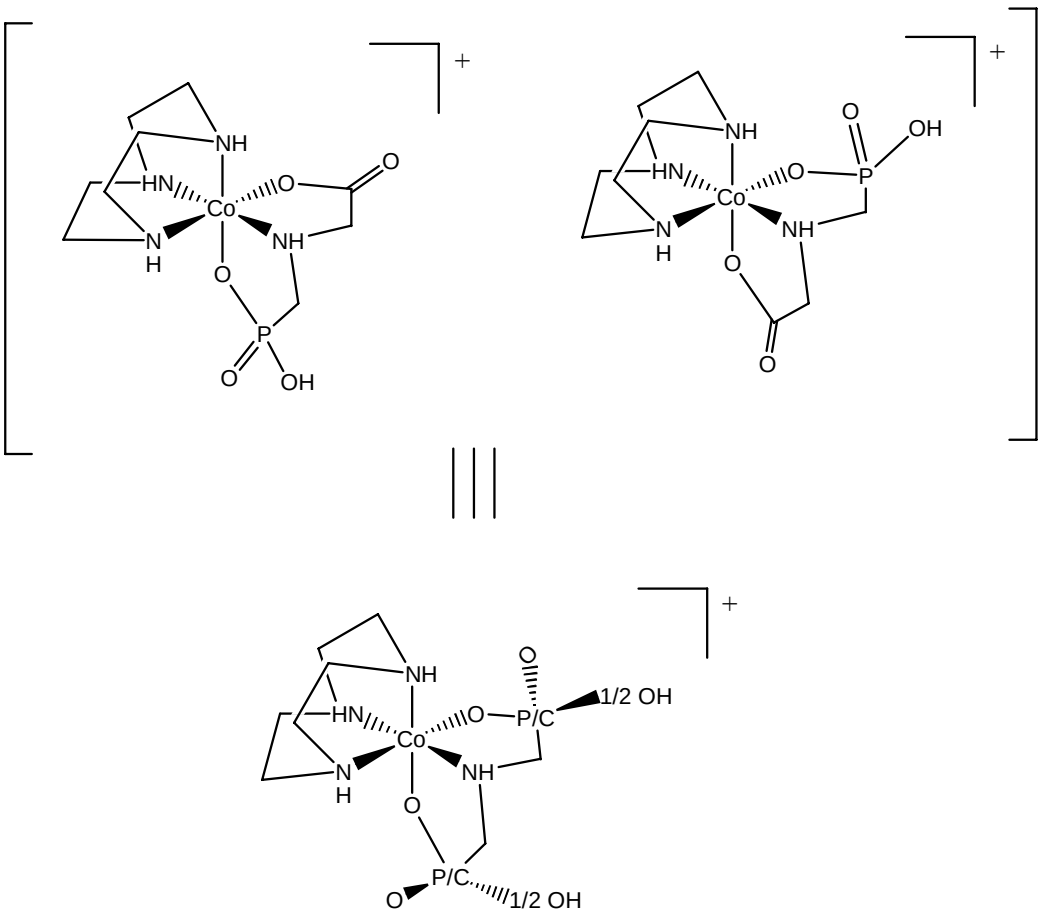

Figure 2.7: Diagram of the possible cause of the disorder observed in the X-ray crystal structure of $[Co(tacn)(PMG)]^{+}$.

In reality, the PMG would be most likely be coordinated through a carboxylate oxygen atom, the amine nitrogen atom, and a phosphonate oxygen atom.

A chloride counterion is present in the unit cell, as well as two oxygen atoms. These oxygen atoms most likely arise from two water molecules. However, the crystallographic data obtained did not refine sufficiently well to ascertain the positions of the protons on the water molecules.

2.2.1.4 Elemental analysis and mass spectrometry

The elemental analysis results of the complex agree well with the proposed structure, and gives us the exact chemical formula of the complex, $[Co(tacn)(PMG)]Cl{\cdot}HCl{\cdot}2.5H_2O$.

Mass spectrometry of the complex shows a major peak at 355.1185. This corresponds very well with the expected relative molecular mass of the cationic complex that has lost its counterions and associated water molecules.

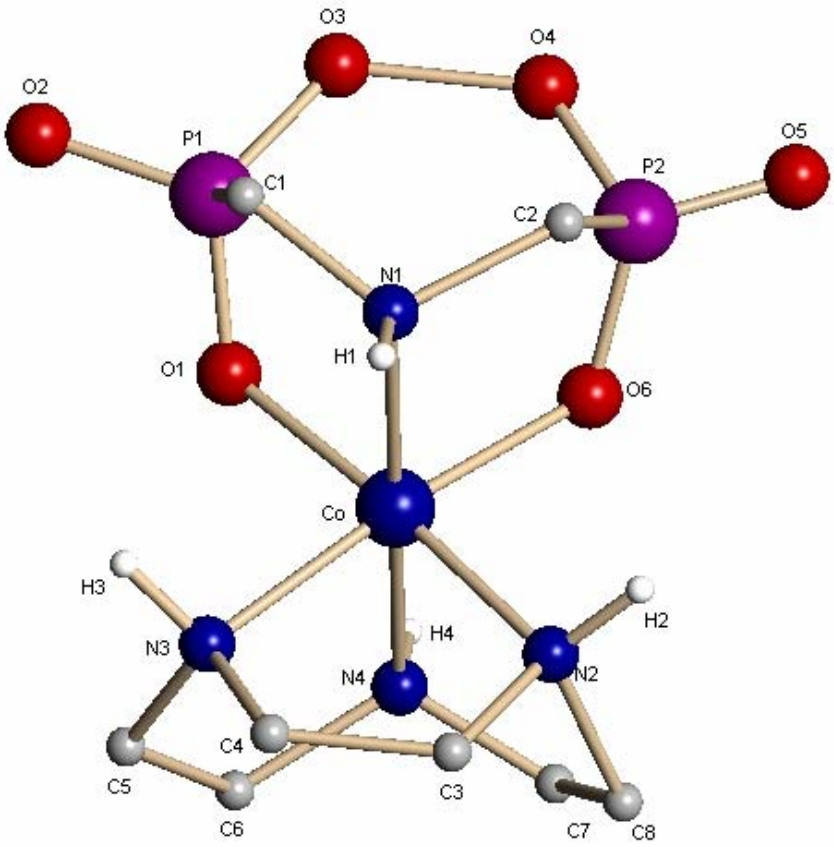

Figure 2.8: Disordered X-ray crystal structure of the [Co(tacn)(PMG)]Cl·2O complex. Methylene protons, the chloride counterion and water molecules have been omitted for clarity. Selected bond lengths (Å): Co-N1 1.99, Co-N2 1.93, Co-N3 1.96, Co-N4 1.94, Co-O1 1.94, Co-O6 1.93, P1-O1 1.42, P1-O2 1.40, P1-O3 1.54, P2-O4 1.50, P2-O5 1.31, P2-O6 1.45. R_1 = 9.6%.

2.2.1.5 X-ray crystallography of [Co(tacn)(PMG)ZnCl$_3$]·H$_2$O

Due to the propensity of tetrachlorozincate salts of Co(III) complexes towards crystallisation, it was decided to attempt to grow X-ray quality crystals of

$[Co(tacn)(PMG)]^{+}$, using $[ZnCl_4]^{2-}$ as a counterion. This was undertaken in the hope that the crystals would not exhibit disorder as observed for the crystal structure of [Co(tacn)(PMG)]Cl·2O.

The result of these crystallisation attempts (depicted in Figure 2.9) was the production of $[Co(tacn)(PMG)ZnCl_3]\cdot H_2O$.

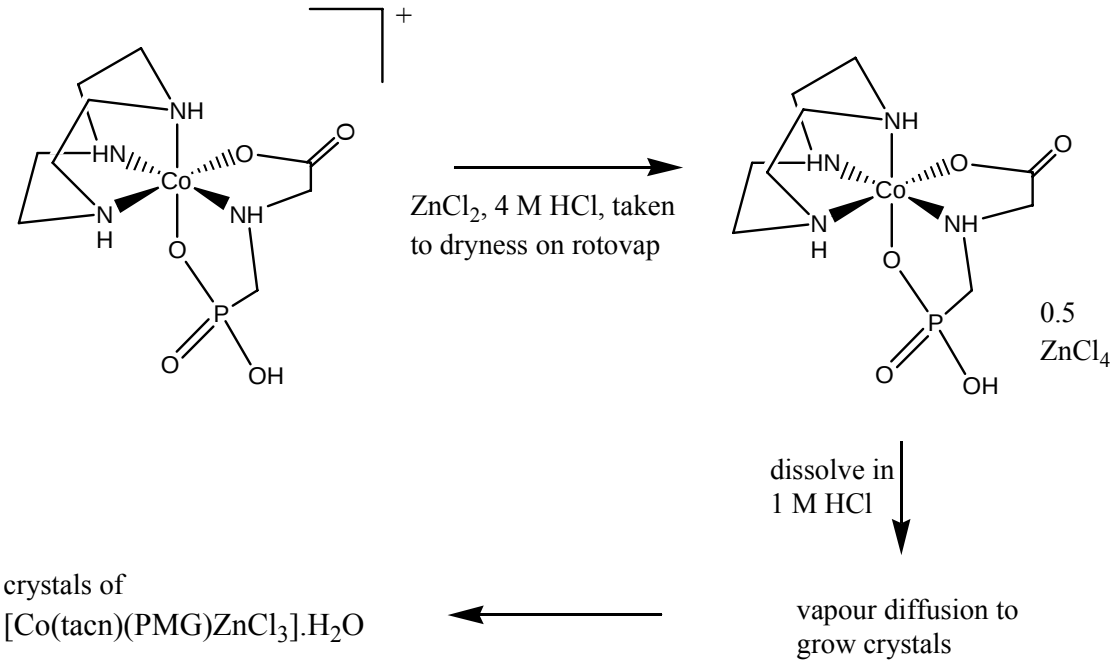

Figure 2.9: The procedure used to grow $[Co(tacn)(PMG)ZnCl_3]\cdot H_2O$ crystals.[47]

Vapour diffusion of acetone into an aqueous solution of the complex successfully promoted crystal growth, the morphology of the crystals being block-like.

Suitable crystals of $[Co(tacn)(PMG)ZnCl_3]\cdot H_2O$ were isolated and an X-ray crystal structure was obtained (Figure 2.10).

The result of this crystal structure is much more satisfactory than for the [Co(tacn)(PMG)]Cl·2O example. The space group of the crystal structure is the very unusual Fdd2.

An octahedral coordination sphere surrounds the central Co(III) ion. The tacn is coordinated facially to the Co(III) centre *via* the amine nitrogen atoms. The PMG ligand

occupies the remaining three sites, and donates through a carboxylate oxygen atom, the amine nitrogen atom, and the phosphonate oxygen atom.

O4 is protonated, and this is reflected in the P-O4 bond length, which is 1.58 Å. Interestingly, the distances between P and O3 and O5 are similar – 1.47 Å and 1.48 Å, respectively. We would expect P-O3 to be longer if it is a single bond, and P-O5 to be shorter if it is a double bond. Therefore, we cannot speculate which atom, O3 or O5, belongs to the phosphonyl group. It is apparent, then, that both P-O3 and P-O5 exhibit some double bond character. This is expected given that both O3 and O5 are coordinated to metal atoms.

A strong hydrogen bonding interaction is observed between C1 and O4 (2.8 Å). This possibly causes the geometric distortion of C1 (it appears tetrahedral rather than the expected trigonal planar). A strong hydrogen bonding interaction of 2.5 Å is also seen between O6 and O4.

It is of interest to note that the zinc of the $ZnCl_3$ component has coordinated to a phosphonate oxygen atom on the PMG molecule.

This is not the first time that this kind of phenomenon has been observed. Hartshorn and Otter[47] subjected an aqueous sample of $[Co(HL^{1a})_2][ZnCl_4]Cl$ (HL^{1a} = a protonated tridentate oxime ligand, as depicted in Figure 2.11) to photolytic conditions and allowed crystals to grow from the photolysate.

The X-ray crystal structure that was elucidated showed that a $ZnCl_3$ fragment had coordinated *via* the zinc atom to the oxygen atom of one oxime ligand (Figure 2.12).

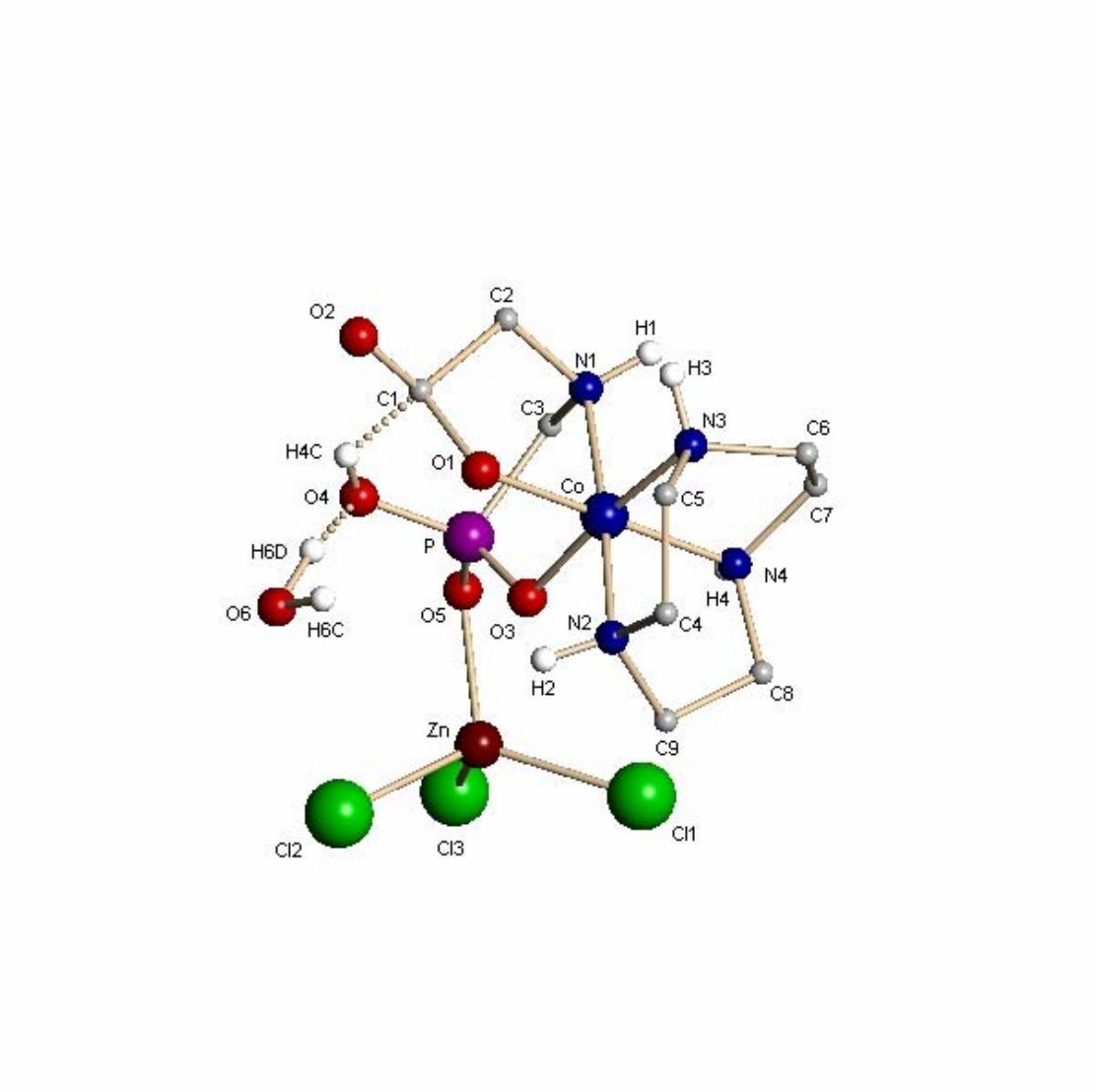

Figure 2.10: X-ray crystal structure of the $[Co(tacn)(PMG)ZnCl_3]\cdot H_2O$ complex. Methylene protons have been omitted for clarity. Note the hydrogen bonding interaction between O6 and O4. Selected bond lengths (Å): Co-N1 2.03, Co-N2 1.91, Co-N3 1.94, Co-O1 1.91, Co-O3 1.91, Zn-O5 1.98, C1-O1 1.44, C1-O2 1.31, P-O3 1.47, P-O4 1.58, P-O5 1.49. $R_1 = 4.2\%$.

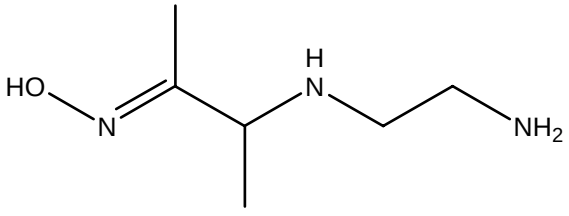

Figure 2.11: The tridentate ligand "1a" as used by Otter and Hartshorn.

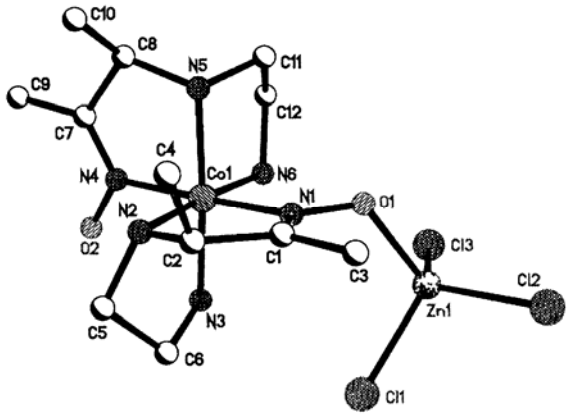

Figure 2.12: Crystal structure of $[Co(L^{1a})(L^{1a}ZnCl_3]$.

2.2.1.6 NMR spectroscopy of [Co(tacn)(PMG)ZnCl$_3$]·3H$_2$O

NMR studies were carried out on the $[Co(tacn)(PMG)ZnCl_3]\cdot 3H_2O$ species. The results of the ^{13}C, ^{1}H and ^{31}P NMR spectra were identical to those obtained for the $[Co(tacn)(PMG)]Cl\cdot HCl\cdot 2.5H_2O$ complex. The coordinated $ZnCl_3$ fragment has not altered the NMR data at all. This is probably because of the lability of the Zn^{2+} ion – when the complex is dissolved in water the $ZnCl_3^-$ arm falls off the phosphonyl oxygen atom. This yields an aqueous complex of $[Co(tacn)(PMG)]^+$. Thus, when in solution, $[Co(tacn)(PMG)]Cl\cdot HCl\cdot 2.5H_2O$ and $[Co(tacn)(PMG)ZnCl_3]\cdot 3H_2O$ are identical species.

2.2.1.7 Elemental analysis and mass spectrometry

The elemental analysis result agrees well with the proposed structure, and tells us that the exact formula for the complex when in its solid state is $[Co(tacn)(PMG)ZnCl_3]\cdot 3H_2O$.

The mass spectrometry result for the $[Co(tacn)(PMG)ZnCl_3]\cdot 3H_2O$ complex is identical to that of $[Co(tacn)(PMG)]Cl\cdot HCl\cdot 2.5H_2O$, with a peak at 355.1185.

2.2.2 [Co(dien)(PMG)]Cl

2.2.2.1 Synthesis

To prepare the starting material for this complex, commercially available dien was coordinated to the Co(III) to give $[Co(dien)(NO_2)_3]$, followed by HCl-induced anation to give $[Co(dien)Cl_3]$ (Figure 2.13).[48]

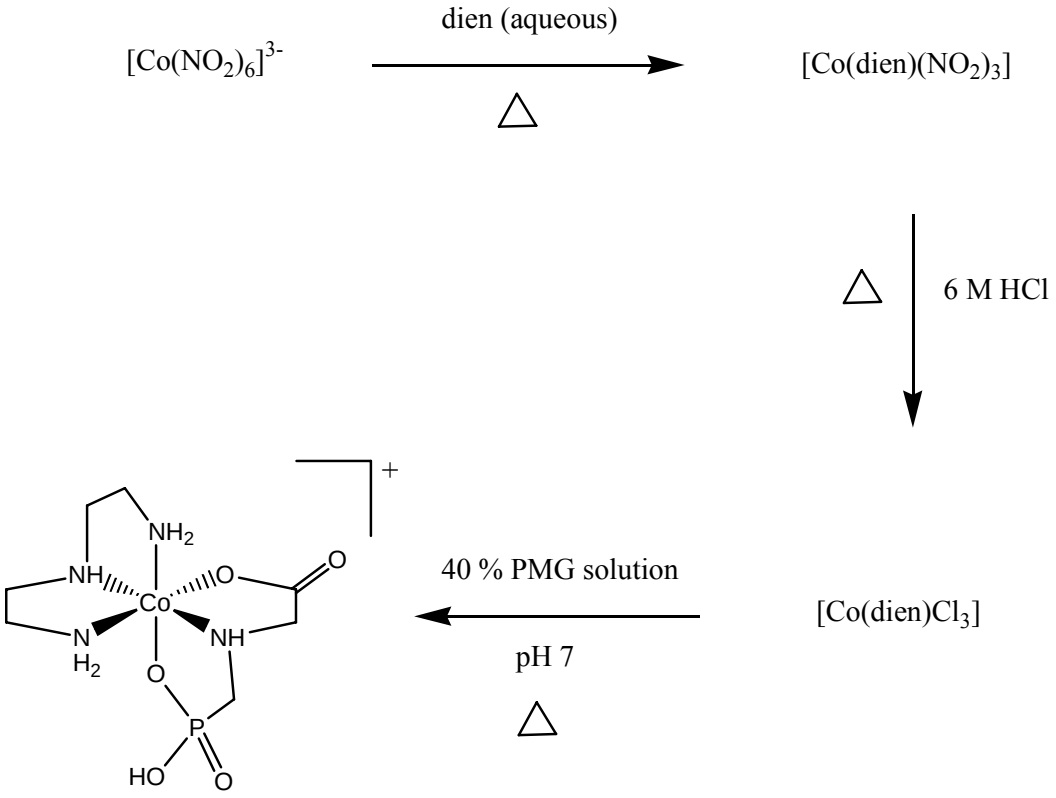

Figure 2.13: Synthesis of *fac*-[Co(dien)(PMG)]Cl. The synthesis of the meridional isomer can occur under the same reaction conditions, but for simplicity only the facial isomer is shown.

PMG was then coordinated to the $[Co(dien)Cl_3]$, following a similar method as for the synthesis of $[Co(tacn)(PMG)]Cl{\cdot}HCl{\cdot}2.5H_2O$.[40] The components of the resulting reaction mixture were then separated on a column using ion exchange chromatography. As in the $[Co(tacn)(PMG)]Cl{\cdot}HCl{\cdot}2.5H_2O$ species, the [Co(dien)(PMG)]Cl complex has four nitrogen donors and two oxygen donors donating to the Co(III) centre. Hence, the expected colour of the product was pink. Indeed, the main band to elute from the

chromatography column was bright pink. The band was removed and dried on a rotary evaporator.

2.2.2.2 NMR spectroscopy

The ^{13}C NMR spectrum of the pink solid exhibited two signals in the carbonyl region of the spectrum, suggesting that the band was a mixture of two different [Co(dien)(PMG)]Cl diasteroeisomers. Since dien is a linear, flexible ligand, it is able to coordinate in a facial or meridional fashion (Figure 2.14).

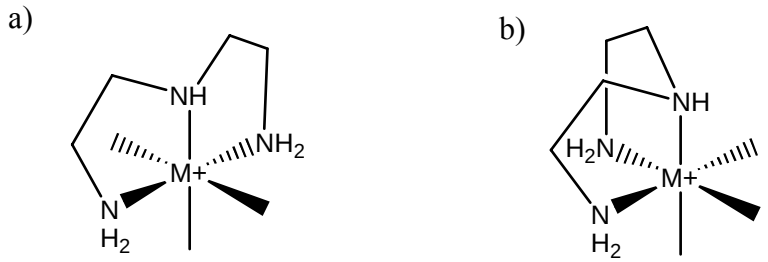

Figure 2.14: The possible wrapping modes of dien around a metal centre: a) meridional, and b) facial.

If the PMG ligand was to coordinate meridionally to 'a' in Figure 2.14, two possible isomers could exist: one where the proton on the secondary amine of the dien is *syn* with respect to the carbonyl group of the PMG ligand, and one where the proton is *anti*. Both isomers would likely exist as a set of enantiomers (Figure 2.15). In the meridional system, the amine nitrogen atom of the PMG is always *trans* to the secondary amine of the dien ligand.

If the PMG were to bond facially to 'b' in Figure 2.14, the amine of the PMG ligand could exist in a *trans* or *cis* position with respect to the secondary amine of the dien ligand. These *trans* and *cis* isomers could each exist as a pair of enantiomers (Figure 2.16). In the facial system, the amine nitrogen atom of the PMG ligand can be *cis* or *trans* to the secondary nitrogen atom of the coordinated dien ligand.

Several attempts to separate the isomers involved the employment of various chromatographic methods, but all were unsuccessful.

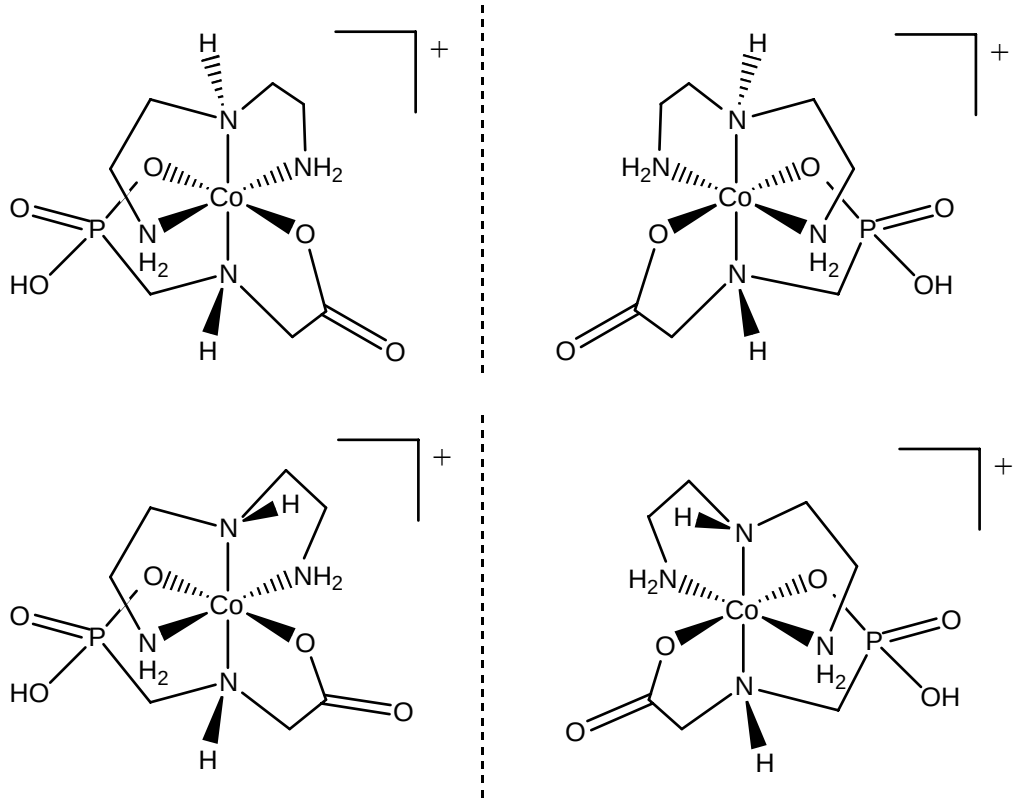

Figure 2.15: The four possible stereoisomers of *mer*-[Co(dien)(PMG)]$^{+}$.

2.2.2.3 Mass spectrometry

The mass spectrometry results of [Co(dien)(PMG)]$^{+}$ are supportive of the proposed mixture. The spectrum shows one large peak at 329.1016, representative of a [Co(dien)(PMG)]$^{+}$ ion.

2.2.3 Co(tren)(PMGH)]Cl_2·0.5CH_3OH

This complex has been synthesized, partially characterised, and its reactivity under basic conditions tested in the past,[40] but more of the complex was required so that ongoing characterization studies could be undertaken, specifically elemental analysis, and full assignment of the peaks appearing in the ^{1}H and ^{13}C NMR spectra.

We also required more material to check the reproducibility of the reaction chemistry that was observed when subjected to basic conditions.[40] It was also important to this project to

examine the reaction of this complex under photolytic conditions.

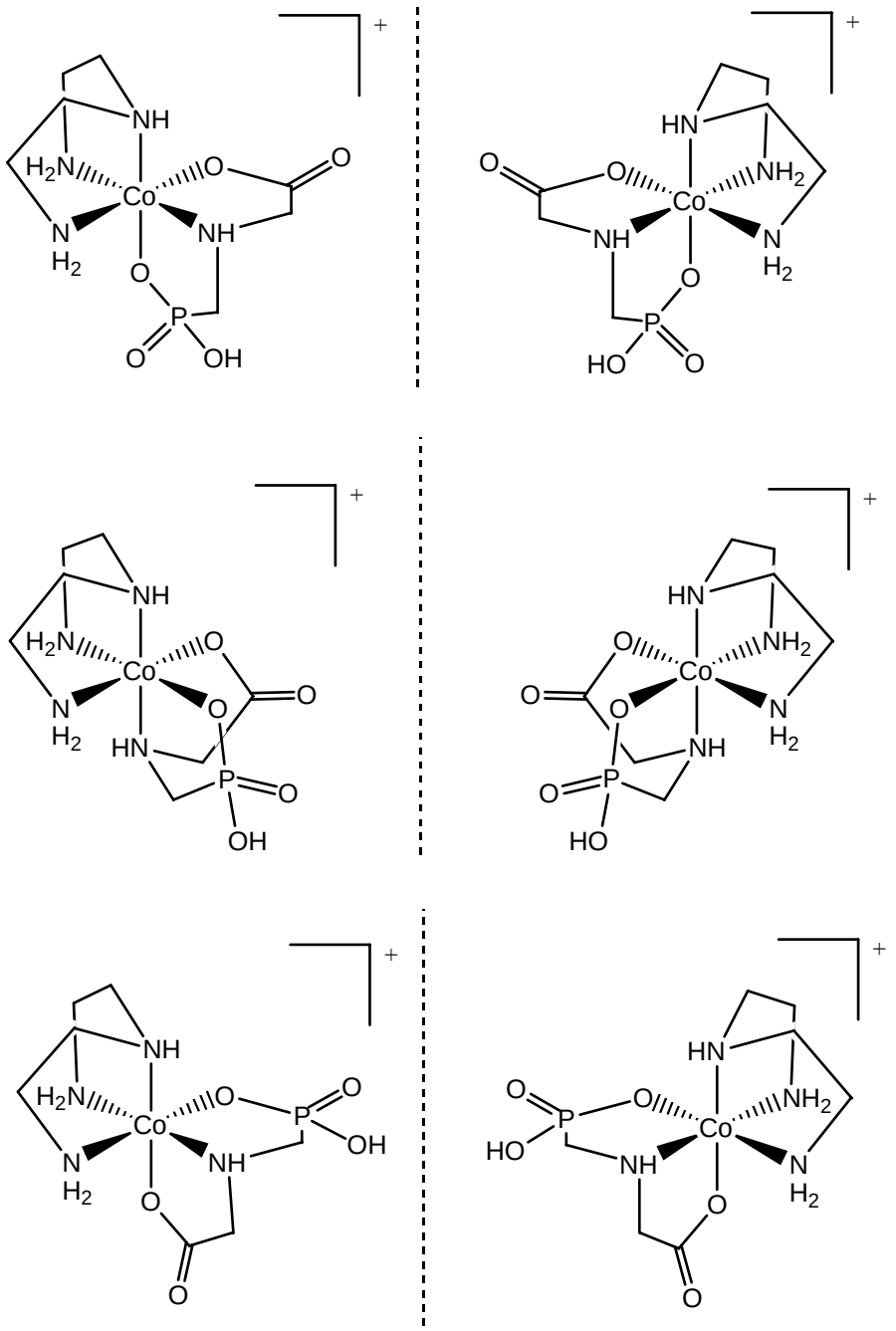

Figure 2.16: The six possible stereoisomers of *fac*-[Co(dien)(PMG)]$^{+}$.

2.2.3.1 Synthesis

[Co(tren)$(NO_2)_2$]Cl and then [Co(tren)Cl_2]Cl.H_2O were prepared following a published procedure.[50] [Co(tren)(PMGH)]$^{2+}$ was then synthesised, using a standard method for

coordinating amino acids to metal centres (Figure 2.17).[40]

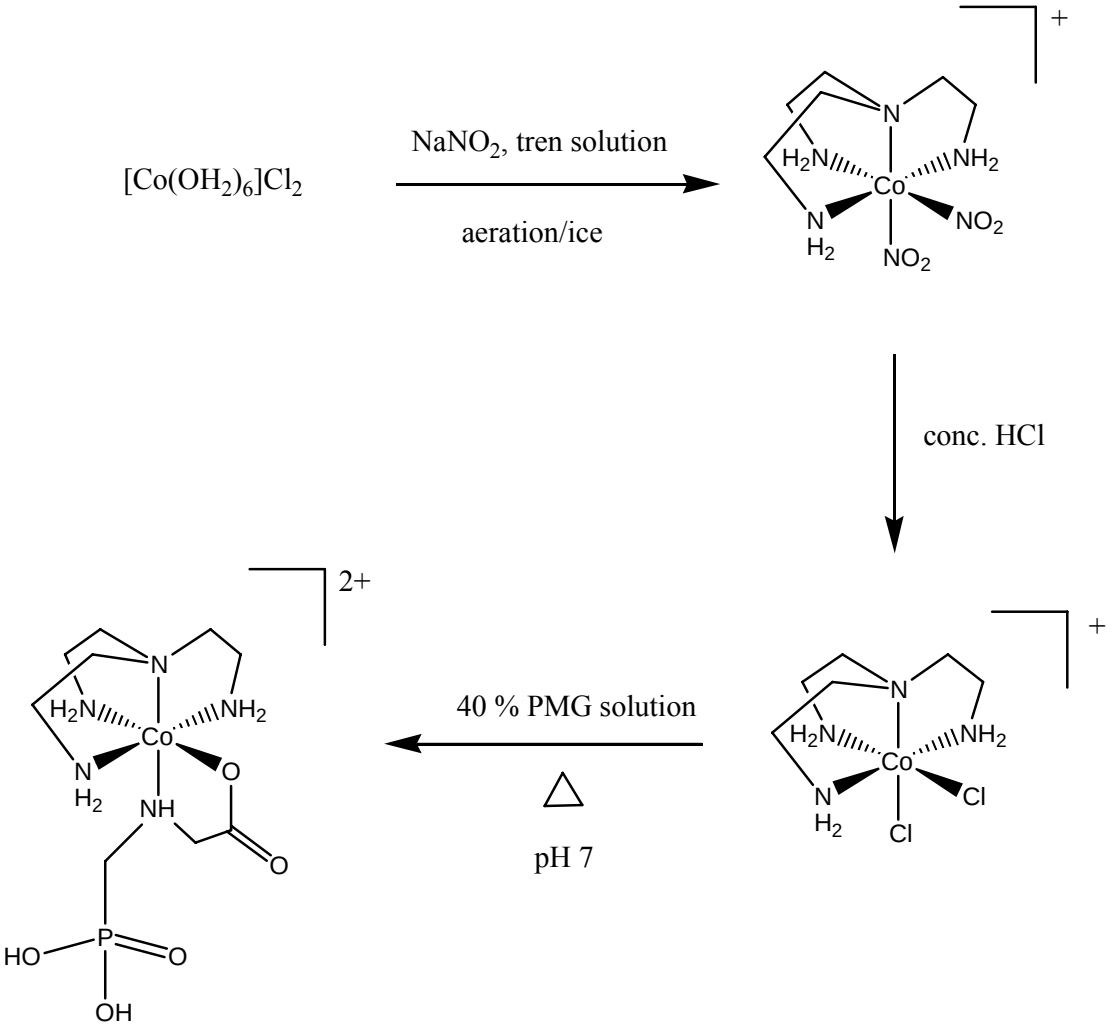

Figure 2.17: Synthesis of $[Co(tren)(PMGH)]Cl_2 \cdot 0.5CH_3OH$.

The reaction was carried out at pH 7, and the resulting solution was chromatographed on a Dowex column. Two distinct bands developed, both a shade of orange. The first band was removed from the column and dried down to an oil that soon solidified. This band was found to be the desired product, $[Co(tren)(PMGH)]^{2+}$. NMR spectroscopy of the second band found it to be starting material ($[Co(tren)Cl_2]^{+}$. Solid material of the first band was grown following this established procedure:[49] A small amount of water was added to the oil, then methanol was added until the point of turbidity was reached. The mixture was placed in the freezer to allow crystals to grow, then the solid material was collected and washed with methanol and ether.

2.2.3.2 NMR spectroscopy

A HETCOR NMR experiment of the $[Co(tren)(PMGH)]Cl_2 \cdot 0.5CH_3OH$ complex was obtained to aid in the assignment of the peaks in the ^1H NMR spectrum. A signal at 6.3 ppm has been assigned to the amine proton of the PMG ligand. Two quartets, at 3.9 and 3.7 ppm, possibly represent the protons on the methylene group of the carboxymethyl arm of the PMG. The chemical shift of the protons on the methylene group of the phosphonomethyl arm of the PMG cannot be ascertained, as the HETCOR NMR spectrum does not show sufficient data. It is likely that the signals representing these protons lie within the multiplet than is observed between 3.7 and 2.8 ppm.

The peaks that arise at 5.4, 5.2, and 5.0 ppm have been assigned to the protons on the amine groups of the tren ligand. The protons on the ethylene groups of the tren ligand probably contribute to the multiplet that lies between 3.7 and 2.8 ppm.

A peak at 185.1 ppm in the ^{13}C NMR spectrum has been assigned to the carbonyl carbon atom of the PMG ligand. The carbon atom of the methylene group of the carboxymethyl arm of the PMG probably gives rise to a slightly split peak at 59.8 ppm. This signal is split due to the nearby phosphorus atom. The carbon atom of the methylene group of the phosphonomethyl arm of PMG may give rise to a split signal, centred at 53.6 ppm.

Three peaks between 64.7 and 62.2 ppm most likely represent the carbon atoms adjacent to the tertiary amine of the tren ligand. Further upfield, between 48.2 and 47.0 ppm, three peaks are observed that have been assigned to the carbon atoms neighbouring the primary amines of the tren ligand.

The ^{31}P NMR spectrum of this complex exhibits one signal at 12.1 ppm.

2.2.3.3 Elemental analysis

A sample of the complex was submitted for elemental analysis. The results give us the formula of the complex, the $[Co(tren)(PMGH)]Cl_2 \cdot 0.5CH_3OH$.

2.2.4 [Co(tpa)(PMGH)]Cl_2

2.2.4.1 Synthesis

The first requirement in the synthesis of this complex was to prepare the tpa ligand, and this was carried out according to Figure 2.18. Many attempts were made to synthesise the solid tpa ligand *via* this route, but most resulted in the formation of a viscous, brown oil, rather than a tan precipitate of the perchlorate salt as expected from the reported procedure.[51]

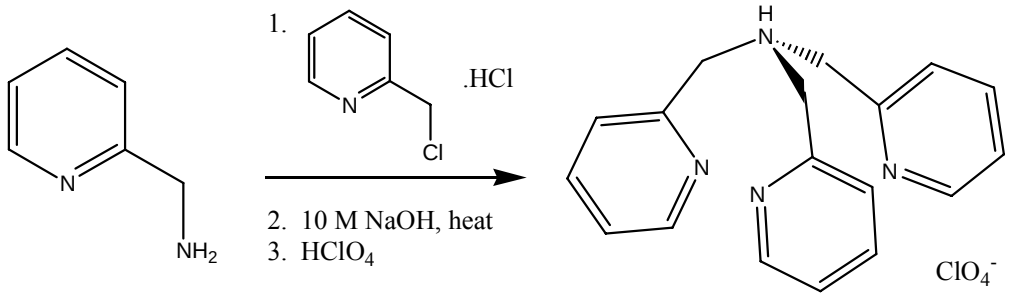

Figure 2.18: The synthesis of tpa·$HClO_4$.

However, the components of the crude brown mixture were successfully coordinated to sodium cobaltinitrite to give a bright orange powder, $[Co(tpa)(NO_2)_2]^+$, in high yield (Figure 2.19).[51] The ^{13}C NMR spectrum of the powder was consistent with it being the desired dinitro complex.

The next step was to convert the $[Co(tpa)(NO_2)_2]ClO_4$ to the chloro species. The first attempt followed a literature method[51] that resulted in the complex $[Co(tpa)(H_2O)Cl](ClO_4)_2 \cdot 3.5H_2O$ in an unsatisfactorily low yield. This method involved the heating of the $[Co(tpa)(NO_2)_2]ClO_4$ in dilute HCl solution with the eventual addition of a small quantity of perchloric acid. Rotary evaporation of the reaction solution yielded a poor amount of the required product.

Another method was attempted[52] which resulted in a reasonable yield of $[Co(tpa)Cl_2]ClO_4$. This method involved the heating of a suspension of

$[Co(tpa)(NO_2)_2]ClO_4$ in 6 M HCl solution, and then the freezing of the reaction mixture overnight to give a good quantity of purple crystals (Figure 2.19).

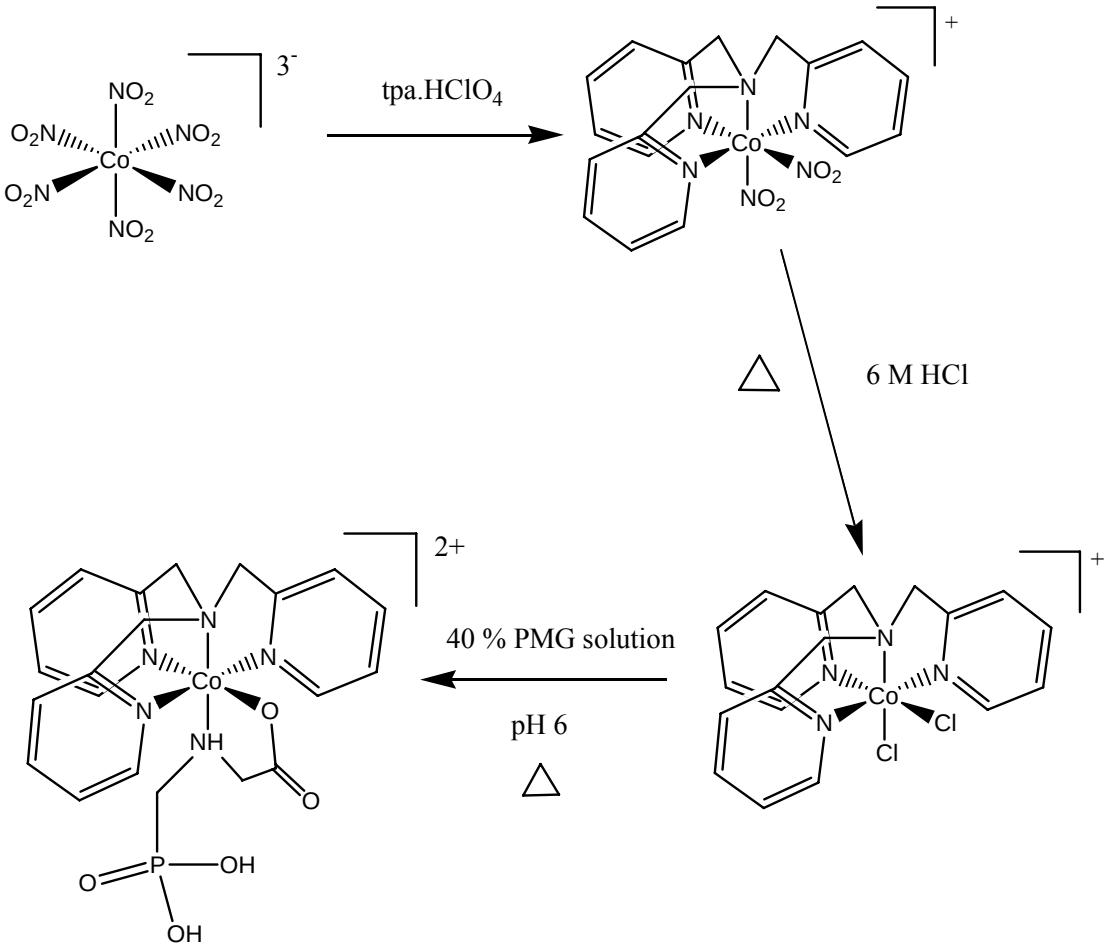

Figure 2.19: Synthesis of $[Co(tpa)(PMGH)]Cl_2$.

The synthesis of $[Co(tpa)(PMGH)]Cl_2$ followed a similar method as for the synthesis of $[Co(tacn)(PMG)]Cl{\cdot}HCl{\cdot}2.5H_2O$,[40] and was first attempted at a pH of 7. When the procedure was carried out at this pH a significant amount of decomposition of the reaction mixture components resulted. This decomposition became evident when column chromatography was initiated, from the development of a large, brown, stationary band at the top of the Dowex column. The bands that eluted were a minor pink band and a medium orange band. The pink band was shown, *via* ^{13}C NMR spectroscopy, to be the $[Co(tpa)Cl_2]^+$ starting material.

The orange band was also taken to dryness so that NMR studies of it could be undertaken. Orange is the expected colour of the desired complex, due to its five nitrogen donors and single oxygen donor. However, once dry it became green-yellow in colour, suggesting the presence of some Co(II). The ^{13}C NMR spectrum of this band resembled that which would be expected of free tpa. On the basis of these NMR results, the attempted synthesis of the $[Co(tpa)(PMGH)]Cl_2$ complex at pH 7 had not been successful. It was concluded that this reaction may be pH sensitive, and that repeating the synthesis at a lower pH would be necessary.

The synthesis was repeated using the same method as described above, but was carried out at a pH of 6. When the reaction mixture was loaded onto a Dowex column it was immediately obvious that less brown decomposition material was present than when the reaction was carried out at pH 7. A medium orange band was relatively quick to elute, and dried down to an orange-peach oil, but in poor yield.

2.2.4.2 NMR spectroscopy

Without having collected a HETCOR NMR experiment, it is difficult to assign the peaks appearing in the ^{1}H NMR spectrum to the protons on the PMG ligand.

However, the ^{1}H NMR spectrum exhibits eight signals in the aromatic region, between 9.2 and 7.5 ppm. The integration of these peaks tells us that 12 protons contribute to these signals. These peaks can therefore be assigned to the aromatic protons on the tpa ligand, of which there are 12.

^{13}C NMR studies of the product imply that the desired product has been synthesised. A signal, possibly corresponding to the carbonyl carbon atom of the PMG ligand, is present at 184.4 ppm. A signal of full intensity at 59.3 ppm has been assigned to the methylene carbon atom of the carboxymethyl portion of the PMG ligand. A split signal of half intensity, centred at 57.7 ppm, possibly represents the carbon atom of the phosphonomethyl arm of the PMG ligand.

Five groups of three signals, between 164.8 and 124.4 ppm, in the ^{13}C NMR spectrum have been assigned to the aromatic carbon atoms of the tpa ligand. The methylene carbon atoms of the tpa ligand possibly give rise to the three peaks between 74.6 and 71.5 ppm.

The $[Co(tpa)(PMGH)]Cl_2$ complex was successfully synthesised on two occasions, but the result of the ^{31}P NMR spectra of the two samples do not agree. One sample shows a peak at 14.8 ppm, while a sample prepared later shows a peak at 11.9 ppm.

The variation in the phosphorus NMR peaks can possibly be attributed to the apparent instability of the complex. It became evident, *via* visual observations and ^{13}C NMR studies, that when exposed to the air the complex decomposed. It was observed that the colour of the complex became purple-blue over a short timeframe. Storage of the complex under an inert atmosphere, such as argon gas, also resulted in a decomposed product. Possibly due to the instability of the complex, efforts to grow crystals *via* vapour diffusion and slow evaporation for X-ray crystal structure determination were fruitless. The complex, when subjected to either method of crystal growing, changed from an orange-peach colour to purple-blue.

It was thought possible that the complex had undergone some decomposition, perhaps ligand exchange to yield the $[Co(tpa)(H_2O)_2]^{3+}$ or $[Co(tpa)Cl_2]^{+}$ species. The ^{13}C NMR spectrum of the decomposition product exhibits five pairs of signals between 166.6 and 124.5 ppm. These signals have been assigned to the aromatic carbon atoms of the tpa ligand. Each pair consists of one tall peak and one peak of half height, and it is this pattern of signals that is indicative of a complex containing an internal mirror plane. Two other peaks, at 72.9 and 71.4 ppm, also exhibit this 2:1 intensity ratio and probably correspond to the methylene carbon atoms of the coordinated tpa ligand.

A signal at 183.7 ppm is present in the ^{13}C NMR spectrum of the decomposed product. It is possible that this peak represents the carbonyl peak of the coordinated PMG ligand. This peak is normally seen at 184.4 ppm in the $[Co(tpa)(PMGH)]Cl_2$ complex. Exposing the decomposition product to air for longer led to the disappearance of the carbonyl peak at 183.7 ppm in the ^{13}C spectrum.

The phosphorus NMR result for the decomposition product shows one peak at 9 ppm. It is likely that this peak represents free PMG, whose phosphorus atom peak appears at 9.0 ppm in its ^{31}P NMR spectrum. Although the ^{13}C NMR of the decomposed product exhibits little evidence of free PMG, it is possible that this free ligand is present. Phosphorus NMR is more sensitive than carbon NMR, and this factor may explain the discrepancy. The observation of a single peak at 9.0 ppm in the ^{31}P NMR spectrum is strong evidence of the presence of free PMG.

2.2.4.3 Mass spectrometry

Mass spectrometry of the $[Co(tpa)(PMGH)]Cl_2$ complex shows a good result, with a peak at 516.1371, representative of the $[Co(tpa)(PMGH)]^{2+}$ complex free of counterions. However, the peak is small in comparison with the two major signals at 384.0871 and 195.1004. It is possible that the peak at 384.0871 represents $[Co(tpa)(H_2O)_2]^{3+}$, which has a calculated molecular mass of 384.8 g mol^{-1}. This result would agree with the ^{13}C NMR spectrum of the decomposed product that suggested the presence of a symmetrical species such as $[Co(tpa)(H_2O)_2]^{3+}$.

2.2.5 [Co(bamp)(PMG)]Cl·2.5H$_2$O

2.2.5.1 Synthesis

The ancillary ligand, bamp, for this complex was prepared *via* literature methods, according to Figure 2.20. Synthesis of 2,6-dichloromethylpyridine from 2,6-pyridinedimethanol took place following a literature method.[53] The 2,6-dichloromethylpyridine was then converted to 2,6-bis(aminomethyl)pyridine dihydrochloride (bamp·2HCl)[54] *via* the intermediate 2,6-bisphthalimide pyridine.

The bamp was coordinated to Co(III) by dropwise addition of an aqueous solution of the ligand into an aerating solution of sodium cobaltinitrite.[55] The yellow powder that resulted underwent a ligand exchange reaction in concentrated HCl to yield $[Co(bamp)Cl_3]$ (Figure 2.21).[55]

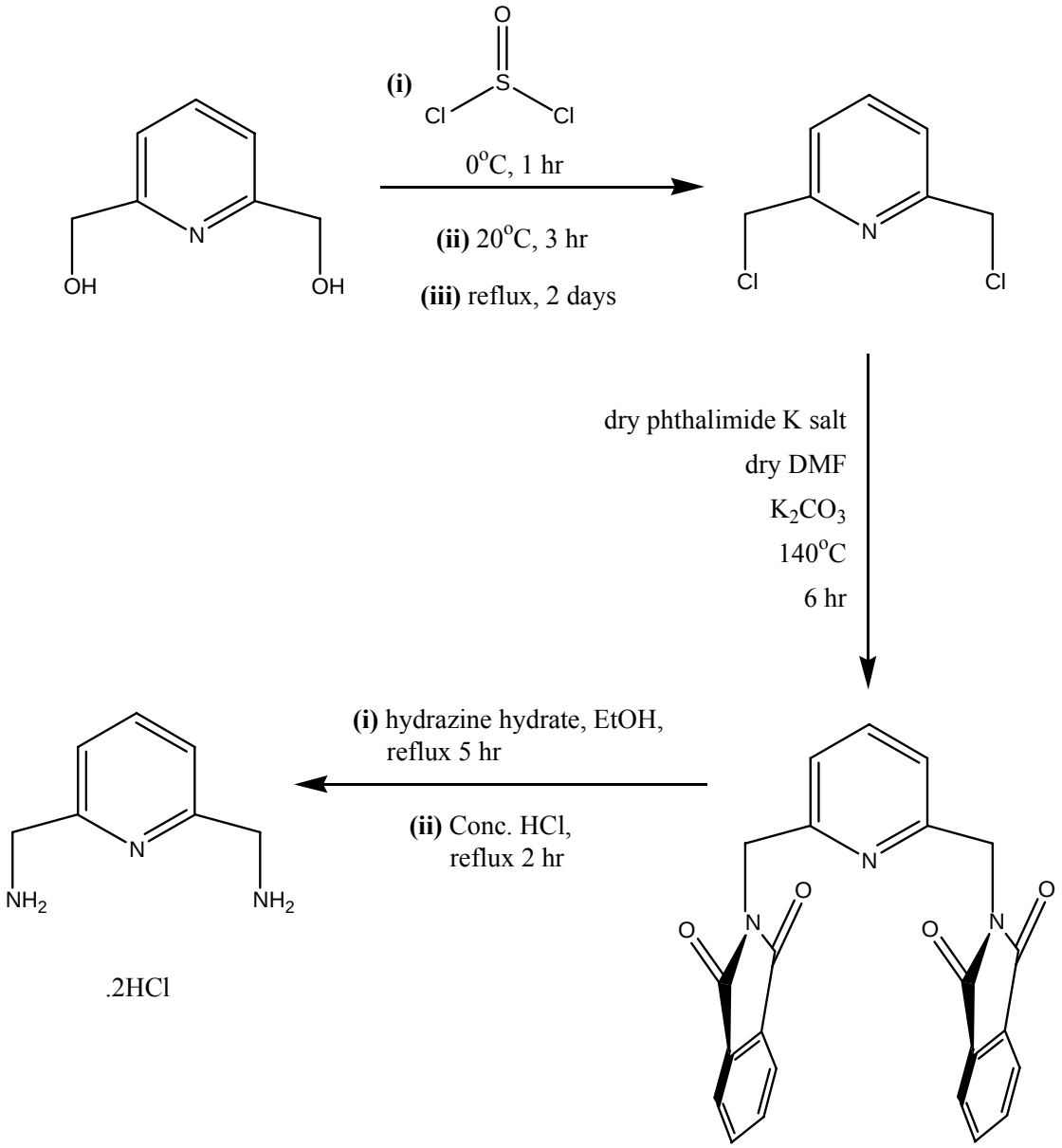

Figure 2.20: Synthesis of bamp·2HCl.

$[Co(bamp)(PMG)]Cl{\cdot}2.5H_2O$ was synthesised following a similar method as for the synthesis of $[Co(tacn)(PMG)]Cl{\cdot}HCl{\cdot}2.5H_2O$.[40] The procedure was successfully carried out at pH 7. After the synthesis, the reaction mixture was chromatographed on a Dowex column with increasing concentrations of HCl, leading to one major red band that moved rapidly down the column. As for the $[Co(tacn)(PMG)]^+$ and $[Co(dien)(PMG)]^+$ complexes, the expected colour is red due to the atoms that donate to the octahedral Co(III) centre: two oxygen atom donors and four nitrogen atom donors. The band was dried to give a red solid. The ^{13}C NMR spectrum that followed showed the red band to be the desired product, although it was contaminated with isopropyl ammonium ion. The

band underwent various chromatographic procedures to free it of the isopropyl ammonium contaminant. The clean product was dried down and crystallised rapidly in the round-bottomed flask. This material was ideal for solid-state analyses such as elemental and UV/vis.

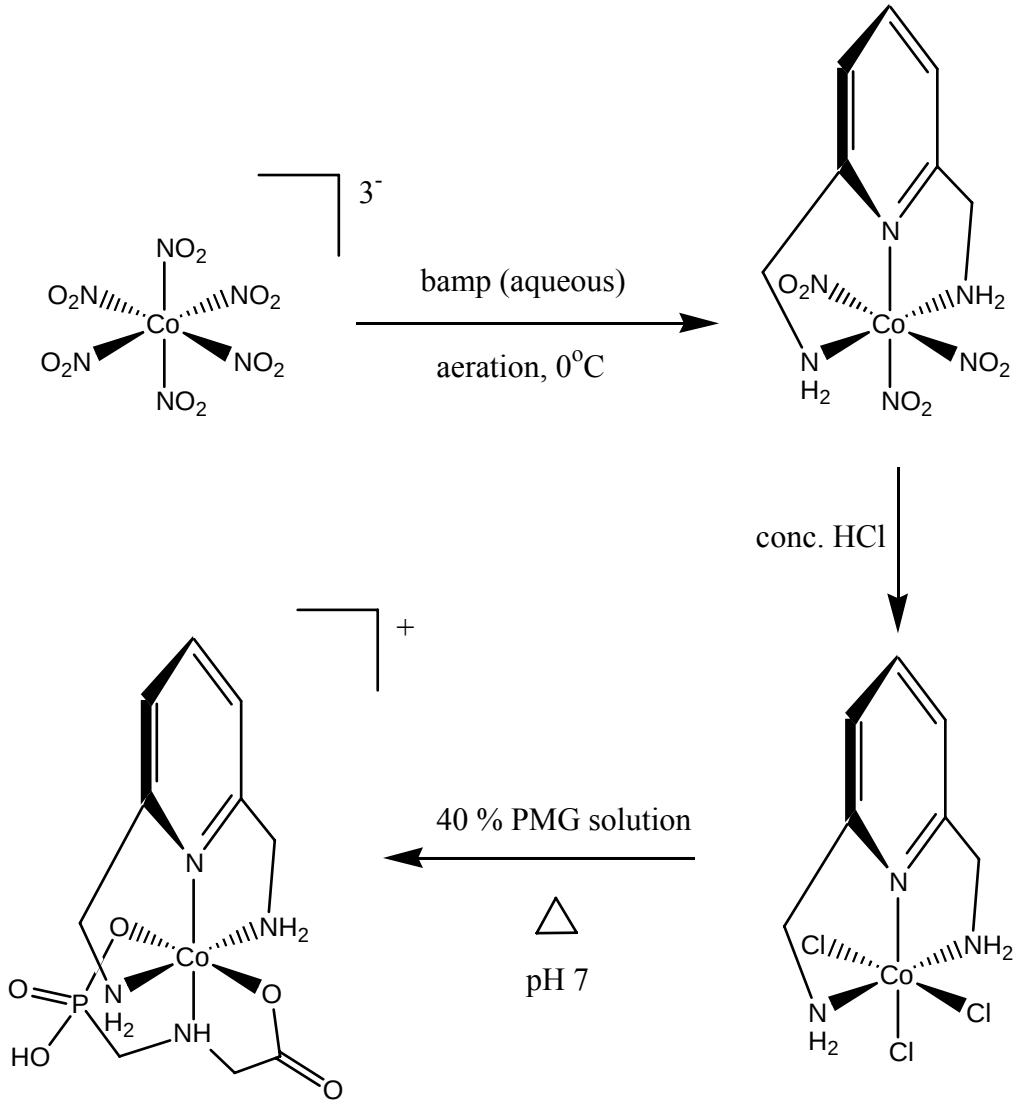

Figure 2.21: Synthesis of [Co(bamp)Cl_3] and the subsequent synthesis of [Co(bamp)(PMG)]Cl·2.5H_2O.

2.2.5.2 NMR spectroscopy

Four multiplets can be seen between 4.5 and 3.0 ppm in the ^{1}H NMR spectrum of the [Co(bamp)(PMG)]Cl·2.5H_2O complex. However, without the aid of a HETCOR NMR

spectrum, the assignment of these peaks to particular protons in the PMG ligand is difficult.

The ^{1}H NMR spectrum shows two signals in the aromatic region that perhaps represent the three protons on the pyridine ring of the bamp ligand. The triplet at 8.2 ppm possibly represents the proton that resides on the carbon *para* to the nitrogen atom. This signal is split by the protons on the two neighbouring carbon atoms. Another signal appears at 7.8 ppm and is a doublet. This signal most likely represents the two protons attached to the *meta* carbon atoms, relative to the nitrogen atom, and is split by the proton on the *para* carbon atom. The signal at 7.8 ppm has double the integration of the peak at 8.2 ppm, since it represent two protons. It is interesting to note that although these two *meta* protons are in non-identical environments, they share the same chemical shift.

The ^{13}C NMR spectrum of the complex shows a peak at 184.8 ppm, probably corresponding to the carbonyl carbon atom of the PMG ligand. The signal that most likely represents the methylene carbon atom adjacent to the carbonyl group of the PMG is slightly split, by the nearby phosphorus atom, into two peaks which are each of half intensity. The chemical shift of the split peaks is centred at 59.3 ppm. The signal that possibly corresponds to the methylene carbon atom adjacent to the phosphorous atom of the PMG is split into two signals which are also of half intensity, their chemical shift being centred at 50.1 ppm.

Two small peaks between 165.7 and 165.8 ppm have been assigned to the two quaternary carbon atoms on the bamp ligand. A full-intensity peak at 144.4 ppm is likely to represent the carbon atom in the *para* position relative to the nitrogen atom of the bamp pyridine ring, while the carbon atoms in the *meta* positions are possibly represented by two peaks, also of full intensity, at 124.0 and 123.9 ppm. The two methylene carbon atoms on the bamp ligand are most likely represented by two full intensity peaks at 55.0 and 54.4 ppm.

The ^{31}P NMR spectrum for the complex shows a single peak at 36.0 ppm.

2.2.5.3 Elemental analysis and mass spectrometry

The elemental analysis of the solid material obtained gives us the exact molecular formula of the complex, $[Co(bamp)(PMG)]Cl \cdot 2.5H_2O$.

The mass spectrometry result of this complex is consistent with the proposed structure, exhibiting a major peak at 363.0033. This peak represents the $[Co(bamp)(PMG)]^+$ skeleton.

2.2.5.4 X-ray crystallography

X-ray quality crystals were grown by vapour diffusion of a variety of solvents into an aqueous solution of the complex, with acetone yielding the best result. The crystals were red and block-like in morphology.

Figure 2.22 shows the resulting X-ray crystal structure. The space group of the crystal structure is $P2_1/c$. It can be seen that the bamp ligand coordinates in a meridional manner to the Co(III) centre. This is an obligatory coordination mode for the bamp ligand – its geometry is planar due to the rigid pyridine ring. The geometry of the complex deviates from a perfect octahedron, possibly due to the bite angles of the ligands.

The PMG ligand is coordinated meridionally *via* a carboxylate oxygen atom, the amine nitrogen atom, and a phosphonate oxygen atom. The P-O3 bond is longer than the P-O4 and P-O5 bonds. Therefore, P-O3 is most likely a single bond. Neither O4 or O5 are protonated, and their bond lengths to P are the same. This is probably due to resonance between the $P\text{-}O^-$ oxygen atom and the phosphonyl oxygen atom. No chloride counterion is present in the unit cell, and this is consistent with the P-O4/P-O5 fragment being deprotonated. The lack of a proton on O4 or O5, and the consequent lack of a chloride counterion, is an unusual result. The elemental analysis of the freshly prepared complex showed full protonation and the presence of one chloride counterion. Apparently, when crystals of this complex are grown under the conditions stated above, deprotonation of the phosphonate group occurs.

Five solvated water molecules are associated with the complex but have been omitted from Figure 2.2. Two of the water molecules are not complete: one incomplete water molecule has one proton missing, while the other is lacking both protons. An unidentified, solvated three-carbon chain is present in the unit cell and is possibly an acetone unit.

The C1 atom appears to be trigonal planar, as expected for a carbonyl carbon atom. A carboxylate carbon atom is coordinated to the metal centre.

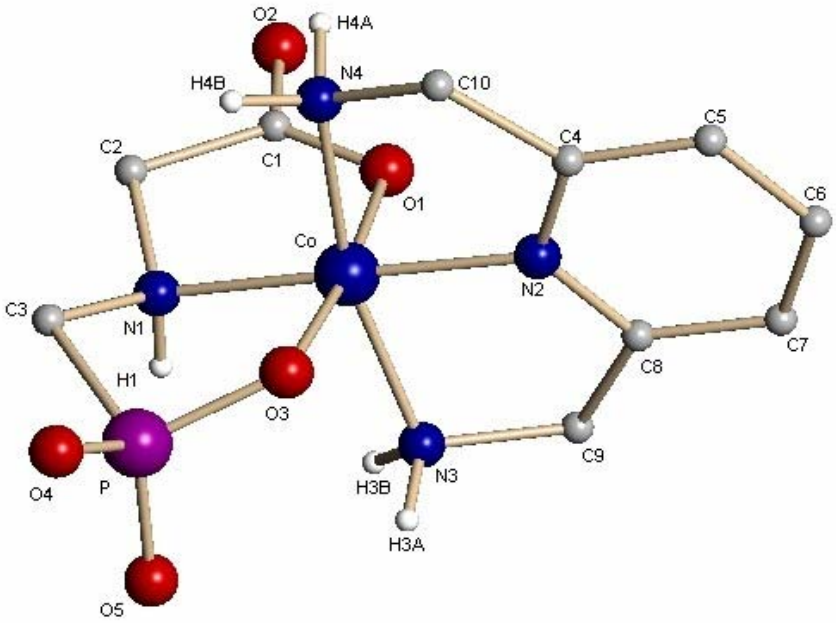

Figure 2.22: The X-ray crystal structure of the [Co(bamp)(PMG)]·3H_2O·OH·O·C_2·C complex. Methylene protons and associated water/solvent molecules have been omitted for clarity. Selected bond lengths (Å): Co-N1 1.93, Co-N2 1.86, Co-N3 1.94, Co-N4 1.95, Co-O1 1.89, Co-O3 1.91, C1-O2 1.23, C1-O1 1.28, P-O3 1.55, P-O4 1.50, P-O5 1.50. R_1 = 4.4%.

2.2.6 [Co(tpa)(IDAH)]Cl_2

It was desirable to synthesise this species so that its reactivity could be compared with that of [Co(tpa)(PMGH)]Cl_2.

2.2.6.1 Synthesis

An attempt to prepare the [Co(tpa)(IDAH)]Cl_2 complex was made according to Figure 2.23. The tpa ligand[51] was synthesised then complexed to Co(III) to give [Co(tpa)$(NO_2)_2$]ClO_4.[51] Ligand exchange then took place to yield [Co(tpa)Cl_2]ClO_4.[52]

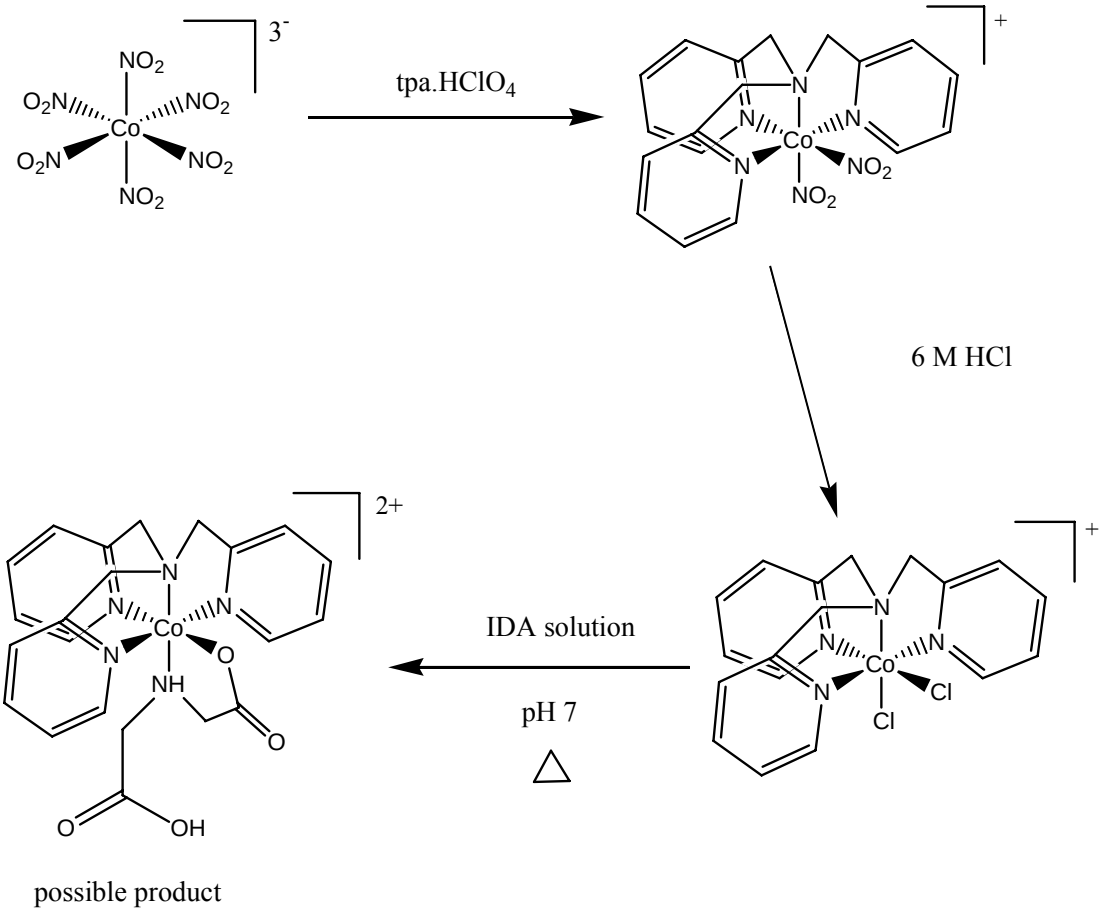

Figure 2.23: Attempted synthesis of [Co(tpa)(IDAH)]Cl_2.

[Co(tpa)Cl_2]ClO_4 was then reacted with IDA at a pH of 7.[40] The final solution was loaded onto a Dowex column and elution began. A large brown decomposition band, similar to that observed in the synthesis of [Co(tpa)(PMGH)]Cl_2, was evident at the top of the column. Elution with HCl saw the migration of a medium, slow-moving orange band, the

expected colour of the complex due to the five nitrogen donors and the single oxygen donor it possesses. However, the band was removed from the column and the ^{13}C NMR proved it to be free tpa ligand.

It was concluded that this reaction was also pH sensitive, as observed before for the synthesis of the $[Co(tpa)(PMGH)]Cl_2$ complex.

The reaction was repeated with the pH of the reaction solution maintained at 6. When chromatographed down a Dowex column and eluted with HCl, two bands developed, both a shade of pink. The bands were removed and dried down so that NMR spectra could be collected.

2.2.6.2 NMR spectroscopy

The first, and major band was found to be $[Co(bpa)(IDA)]^+$ (bpa = bis(2-picolyl)amine) (Figure 2.24).

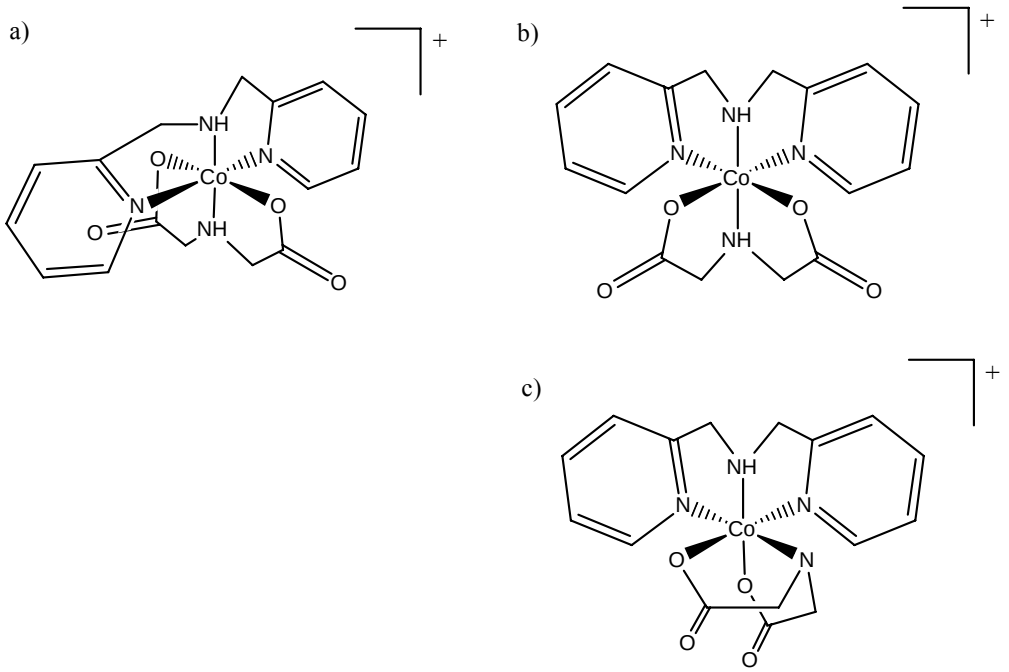

Figure 2.24: a) *mer*-$[Co(bpa)(IDA)]^+$; b) and c) two diastereoisomeric forms of *fac*-$[Co(bpa)(IDA)]^+$.

The ^{1}H NMR spectrum of the isolated band shows several signals, none of which can easily be assigned without the aid of a two-dimensional NMR experiment.

The peaks in the ^{13}C NMR spectrum were somewhat easier to assign. There are 16 signals in the spectrum, so the species present in the product are most likely to be 'a' or 'c' in Figure 2.24. Both of these complexes would lead to 16 peaks in the ^{13}C NMR spectrum, but we are unable to ascertain exactly which complex is present. There is no evidence of species 'b' in the spectrum. This would give rise to just eight peaks due to the large degree of symmetry in the complex.

Two peaks at 187.3 and 186.4 ppm in the ^{13}C NMR spectrum have been assigned to the carbon atoms of the carbonyl groups of the IDA ligand. Between 64.3 and 61.4 ppm lie four signals of approximately equal intensity. These probably represent the four methylene carbon atoms of the complex, but it is difficult to determine which carbon atom gives rise to which peak.

Five sets of two peaks between 166.8 and 125.7 ppm can be assigned to the ten aromatic carbon atoms of the bpa ligand.

The isolation of $[Co(bpa)(IDA)]^{+}$ when using $[Co(tpa)Cl_2]ClO_4$ as a starting material is an interesting result as it implies that decomposition of the tpa ligand is taking place. It was verified, *via* ^{13}C NMR, that the starting material was in fact $[Co(tpa)Cl_2]ClO_4$, and not $[Co(bpa)Cl_3]$. It was concluded that the reaction of the tpa ligand to bpa was most likely to be occurring during the attempted synthesis of $[Co(tpa)(IDAH)]^{2+}$.

A similar phenomenon was observed recently by Lonnon *et al.*[56] These researchers attempted to coordinate a heptadentate ligand, bpa-tpa (Figure 2.25) to a Co(III) metal centre. The X-ray crystal structure (Figure 2.26) obtained for the complex showed that a $tpaCO_2^{-}$ unit had in fact coordinated to the cobalt. By some means, during the synthesis of the complex, a bpa fragment had been oxidatively cleaved from the bpa-tpa, leaving a $tpaCO_2^{-}$ ligand. Either bond 1 or bond 2 (Figure 2.25) had been broken. Oxidative decomposition was proposed to be the cause of the cleavage, and was initiated by either atmospheric oxygen or the perchlorate ion ($Co(ClO_4)_2{\cdot}6H_2O$ was the starting material in

the synthesis). The researchers[56] emphasised that pyridylmethylamine species are susceptible to oxidative cleavage when Co(III) is present, as similar reactivity was not observed when other metal ions, such as Mn(II), Fe(II), and Ni(II) were used.

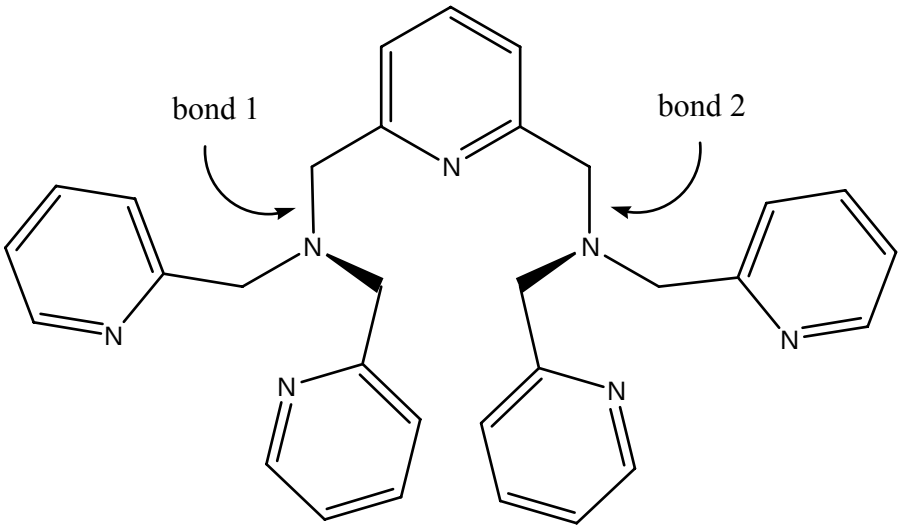

Figure 2.25: The bpa-tpa ligand.

This theory of Co(III) inducing the oxidative cleavage of pyridylmethylamine ligands might help explain the production of $[Co(bpa)(IDA)]^{+}$ when attempting to synthesise $[Co(tpa)(IDAH)]^{2+}$.

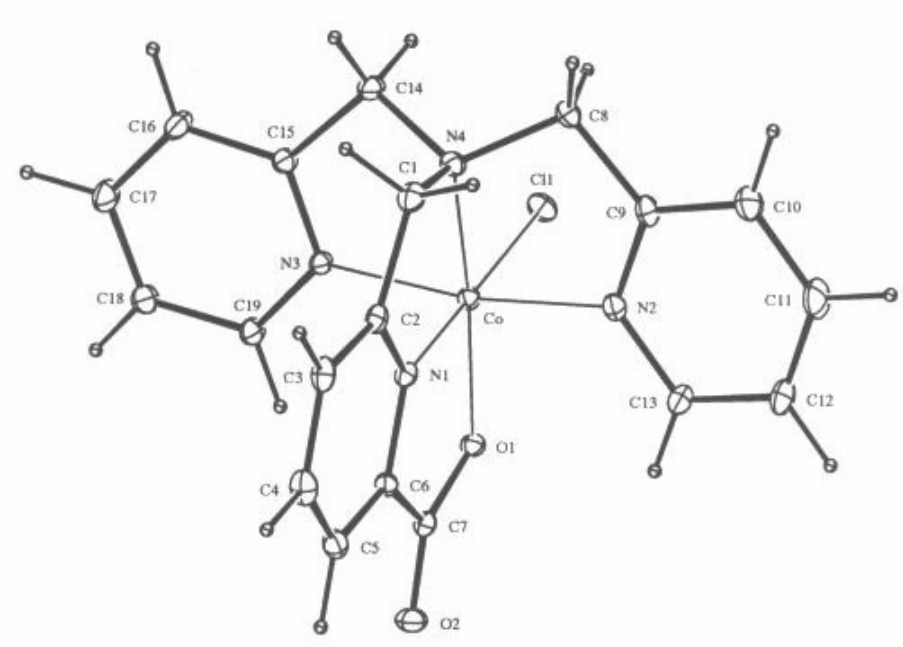

Figure 2.26: The crystal structure of $[Co(tpaCO_2)Cl]^{+}$.[56]

However, in our research, some of the desired complex (the synthesis of which is shown in Figure 2.23) may have in fact been synthesised. The second band to migrate down the column was minor in volume and was dried down to a pink-orange oil. Interpretation of the NMR spectra of the band suggest that the desired $[Co(tpa)(IDAH)]^{2+}$ complex had been synthesised.

The ^{1}H NMR spectrum of the band shows several multiplets in the 9.1 to 7.4 ppm range, that most likely represent the protons on the tpa ligand. The 5.3 to 3.1 region also exhibits numerous peaks, which probably correspond to the amine and methylene protons. Without the aid of a HETCOR NMR spectrum it is difficult to assign these peaks.

Two signals at 186.9 and 185.1 ppm in the ^{13}C NMR spectrum has been assigned to the carbon atoms of the carbonyl groups of the IDA ligand. The two methylene carbon atoms of the IDA ligand possibly give rise to signals at 58.7 ppm and 59.5 ppm.

Five sets of three signals appear in the 165.1 to 124.3 ppm region. It is thought that these signals represent the 15 carbon atoms on the pyridine rings of the tpa ligand. A group of three signals between 71 ppm and 74 ppm possibly correspond to the methylene carbon atoms of the tpa ligand.

The observed grouping of the signals into sets of three can be expected due to the protonated amine on the IDA ligand. This proton destroys the mirror plane that would otherwise run through the molecule.

2.2.6.3 Mass spectroscopy

The mass spectrum of the $[Co(bpa)(IDA)]^{+}$ complex is supportive of the proposed structure. The main peak observed appears at 389.0194, which agrees well with the calculated formula mass of the $[Co(bpa)(IDA)]^{+}$ structure.

Contrary to the results of the ^{13}C NMR spectrum, the mass spectrum of the second band is not supportive of the presence of $[Co(tpa)(IDAH)]^{2+}$. The mass spectrum exhibits peaks at 170.0780, 200.1534, 293.0495, and 389.1002 – the $[Co(tpa)(IDAH)]^{2+}$ fragment would lead to a peak at 479.9.

2.2.7 [Co(bamp)(IDA)]Cl

2.2.7.1 Synthesis

The starting material for this complex, $[Co(bamp)Cl_3]$, was synthesised according to the procedure shown in Figure 2.21.

The synthesis of the [Co(bamp)(IDA)]Cl complex was then carried out according to the procedure for the synthesis of $[Co(tacn)(PMG)]Cl{\cdot}HCl{\cdot}2.5H_2O$.[40] During the first attempt the pH was maintained at 7. When the reaction mixture was loaded onto a Dowex column and elution with HCl began, a large, brown decomposition band remained at the top of the Dowex while an orange band migrated down the column. When this band was removed from the column and dried, it turned blue, evidence of Co(II) being present in the band.

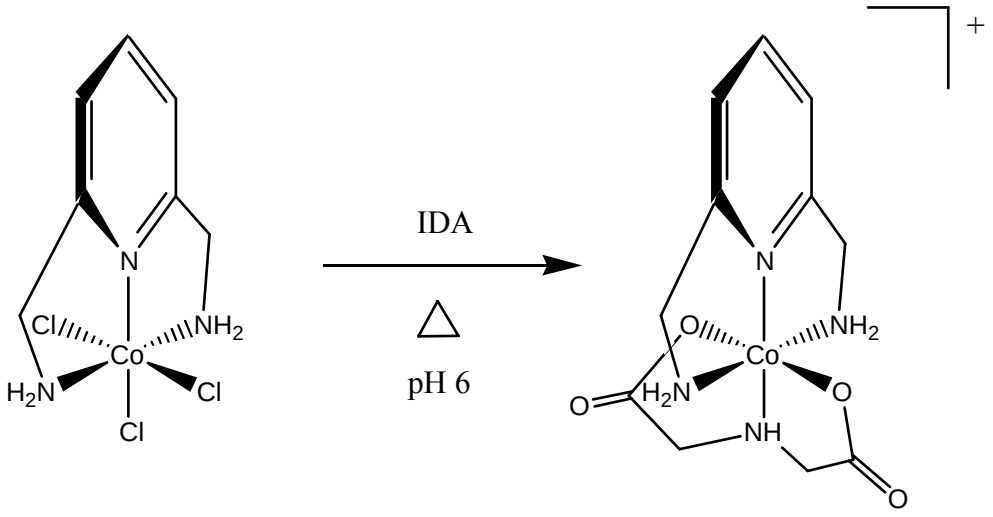

Figure 2.27: Synthesis of [Co(bamp)(IDA)]Cl.

The synthesis was repeated, more successfully, at a pH of 6 (Figure 2.27). After the reaction mixture was loaded onto a Dowex column, elution with HCl began which saw the development of one major red-orange band. After being removed from the column the band was dried to a red solid. NMR studies on the band showed it to be the desired complex.

2.2.7.2 NMR spectroscopy

The ^{1}H NMR spectrum of the product shows three multiplets in the aromatic region, which can most likely be assigned to the three protons on the pyridine ring of the bamp ligand. Comparison with the ^{1}H NMR spectrum of the $[Co(bamp)(PMG)]^{+}$ complex helps us with the assignment of these peaks. The multiplet at 8.2 ppm possibly represents the proton on the carbon atom *para* to the nitrogen atom of the pyridine ring. The multiplet at 7.7 ppm perhaps can be assigned to the protons on the carbon atoms *meta* to the nitrogen atom of the pyridine ring. It is possible that the small multiplet at 8.0 ppm is an impurity of some kind. Three multiplets are also present in the 5.6 to 4.0 ppm range. These probably correspond to the methylene protons of the IDA and bamp ligands, although without a HETCOR NMR spectrum it is difficult to assign these peaks.

The ^{13}C NMR spectrum exhibits a peak at 185.2 ppm which has been assigned to the two carbonyl carbons atoms of the IDA ligand. The carbonyl groups of the IDA are equivalent due to the mirror plane that runs through the complex, and give rise to one. A DEPT NMR spectrum was obtained to assist in the assignment of the remainder of the peaks. In this experiment, the signals corresponding to carbon atoms with no or two protons attached point downwards, while the carbon atoms with one proton attached point upwards. A downwards peak of double intensity at 58.4 ppm has been assigned to the two methylene carbon atoms on the IDA ligand. Two neighbouring peaks of single intensity are present at 165.8 and 164.4 ppm. These peaks have been assigned to the quaternary carbon atoms on the bamp ligand, and they point downwards in the DEPT spectrum, as do the carbonyl carbon atom signals. An upwards peak at 144.3 ppm possibly represents the carbon atom in the *para* position relative to the nitrogen atom of the bamp pyridine ring. Although the two carbon atoms that lie in the *meta* position on the same pyridine ring are in non-equivalent environments, they are most likely represented by the single, upwards peak of double intensity at 123.8 ppm. These two carbon atoms are in non-equivalent environments due to the proton on the PMG amine being *syn* or *anti* with respect to the coordinated PMG ligand. Two downward peaks of single intensity at 54.8 and 54.3 ppm probably represent the methylene group carbon atoms on the bamp ligand.

2.2.7.3 Mass spectrometry

The mass spectroscopy result is supportive of the proposed structure. A major peak at 327.0805 is clearly representative of the $[Co(bamp)(IDA)]^+$ cation, which has a calculated mass of 326.75 g mol^{-1}.

2.3 UV/vis Spectroscopy

The UV/vis results obtained for the new complexes were as expected for octahedral transition metal compounds, and are presented in Table 2.1. In some cases, where it was not possible to use solid material in preparing the analysis solutions, we have been unable to calculate the variable ε.

Complex	absorbance	λ_{max} (nm)	ε_{max} (M^{-1} cm^{-1})
$[Co(tacn)(PMG)]Cl{\cdot}HCl{\cdot}2.5H_2O$	0.207, 0.111	355, 500	68, 37
$[Co(tacn)(PMG)ZnCl_3]{\cdot}3H_20$	0.286, 0.178	355, 500	98, 61
[Co(dien)(PMG)]Cl	0.899, 0.178	365, 525	N/A
$[Co(bamp)(PMG)]Cl{\cdot}2.5H_2O$	0.475, 0.313, 0.366	360, 460, 520	182, 120, 129
[Co(bpa)(IDA)]Cl	1.007, 0.658	342, 474	N/A
[Co(bamp)(IDA)]Cl	0.941, 0.812	360, 495	N/A

Table 2.1: The UV/vis absorption data for the complexes tested. For those complexes where a solid sample was unavailable for analysis, the extinction coefficient, ε, is unable to be calculated (signified by N/A). Note also, that contrary to expectation, ε_{max} for $[Co(tacn)(PMG)]Cl{\cdot}HCl{\cdot}2.5H_2O$ and $[Co(tacn)(PMG)ZnCl_3]{\cdot}3H_20$ are not the same.

2.4 Summary

This chapter has outlined the synthesis and characterisation of several new cobalt-PMG and cobalt-IDA complexes.

Several organic, amine-containing ancillary ligands have been used during the preparation of the complexes. The ligands tren and dien were commercially available, but the remaining ligands (tacn, bamp, and tpa) needed to be synthesised following documented

procedures in the literature. Coordination of the ancillary ligands to Co(III) prior to the addition of PMG or IDA has led to an array of new complexes. Characterisation of the complexes has taken place *via* NMR spectroscopy and mass spectrometry, and in some cases elemental analysis and X-ray crystal structure determination. The latter two analytical processes proved to be elusive for some of the complexes prepared. This is mainly due to the failure of the complexes concerned to crystallise, or the instability of the compounds when exposed to air.

These complexes have been prepared so that they can undergo reactivity studies, as presented in Chapter 3.

Chapter 3 - Reactivity of $[Co(L)(PMG)]^{n+}$ Complexes

3.1 Introduction

It can be assumed, from the number of research groups studying the degradation of glyphosate worldwide, that there is great interest in this subject. When one considers the degree of adsorption to metal ions that glyphosate undergoes in the soil, it is surprising that until now little study of the reactivity of metal-glyphosate complexes in the laboratory has been undertaken. Accordingly, one possible area of research in the lab is how metal-glyphosate complexes might behave when subjected to various reaction conditions. With this in mind, we have subjected a number of complexes, described in Chapter 2, to UV radiation and base treatment. This chapter documents the current state of our investigations into the reactivity of these metal-glyphosate complexes.

There are two reactions of particular interest to us: the photolysis of metal-glyphosate complexes, and the reaction of deprotonated glyphosate. It is thought that the results of these areas of research may give us some insight as to how glyphosate reacts in natural situations, and what reactions it is chemically capable of.

The photolysis of metal-bound glyphosate is an important arena to explore, given that in natural environments glyphosate binds to metal ions residing in the soil: the resulting metal-glyphosate complexes might then be irradiated with UV light from the sun. Recall from Section 1.4.2 that coordinated amino acids can undergo decarboxylation when irradiated with UV light, and that glyphosate is in fact an amino acid and might be prone to similar reactivity. It is possible that such irradiation can induce reactions in the metal-glyphosate complexes and, indeed, within the ligand itself, leading to some level of decomposition in the glyphosate species.

Another field of interest is the reactivity that C-deprotonated glyphosate may undergo. This area of study is explored to learn more about what reactions might occur within such a molecule, since the loss of a proton is often the first step in a chemical reaction. It is

possible that the deprotonation of the herbicide can occur when positioned in the active site of an enzyme within a microbe. It is well established that microbes are central in the degradation of glyphosate in soils, but, as covered in Chapter 1, the mechanisms behind this process are not entirely clear. What if, during the metabolism of glyphosate by a microbe, the herbicide is held near a basic residue in the active site of an enzyme? It is possible that deprotonation occurs, and that this step contributes to the subsequent degradation of glyphosate.

It is also possible that the elevations in soil pH can bring about deprotonation of coordinated glyphosate. It is generally easier to deprotonate a coordinated ligand than the free species. Therefore, a glyphosate molecule that is coordinated to a metal ion in the soil may be susceptible to an increase in pH, while the free ligand may not be.

To assess how coordinated glyphosate might react under the aforementioned conditions, a number of the complexes described in Chapter 2 were irradiated with UV light, and subjected to base treatment. It is anticipated that the results of such studies will give us an indication of the reactions that glyphosate, either metal- or enzyme-bound, may undergo in natural environments, and perhaps the mechanisms behind its reactivity.

3.2 Photolysis Reactions

To understand exactly why we are interested in undertaking photolysis reactions on the prepared Co-glyphosate complexes, it is necessary to explore the documented photolytic reactivity of related compounds. It is now well accepted that the UV irradiation of metal-aminocarboxylato complexes can result in the reactivity of the aminocarboxylato ligand. The photolysis of aminocarboxylato ligands coordinated to Co(III) centres was described in Section 1.4.2, and it was shown that decarboxylation can occur. This is an important outcome in terms of the degradation of glyphosate, which is also an aminocarboxylato species. It is difficult to think of a reason why, when coordinated to a metal ion in the soil, glyphosate wouldn't be prone to a similar outcome if exposed to UV light. Hence, it seems viable that the photolysis of metal-glyphosate complexes both in the laboratory and in nature could cause decarboxylation, leading to (at least) partial decomposition of the

herbicide. Of course, in natural situations only the metal-glyphosate adducts on the surface of the soils would be susceptible to UV irradiation.

Photo-induced decarboxylation of a coordinated aminocarboxylato ligand (the category of compound which includes amino acids) begins with the absorption of a photon from the light source.[30] This absorption results in a ligand-to-metal-charge-transfer (LMCT), which is the movement of one electron from a ligand orbital onto an orbital on the metal centre. In effect, the transfer of an electron to the metal cleaves the M-X bond, and this results in a reduced metal ion and a radical X species, according to Figure 3.1.

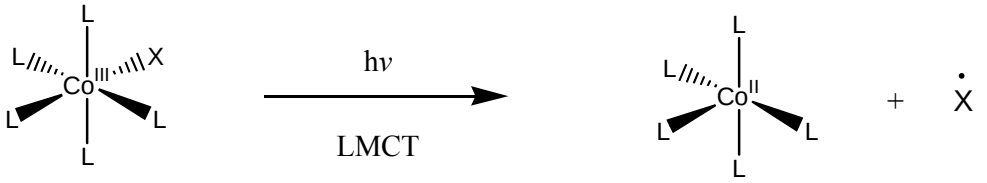

Figure 3.1: The absorption of a photon by a cobalt complex, resulting in the homolysis of the Co-X bond and generation of a radical.

An extension of the idea portrayed in Figure 3.1 is the decarboxylation of aminocarboxylato ligands coordinated to Co(III). The proposed mechanism for this process is shown in Figure 3.2.[30]

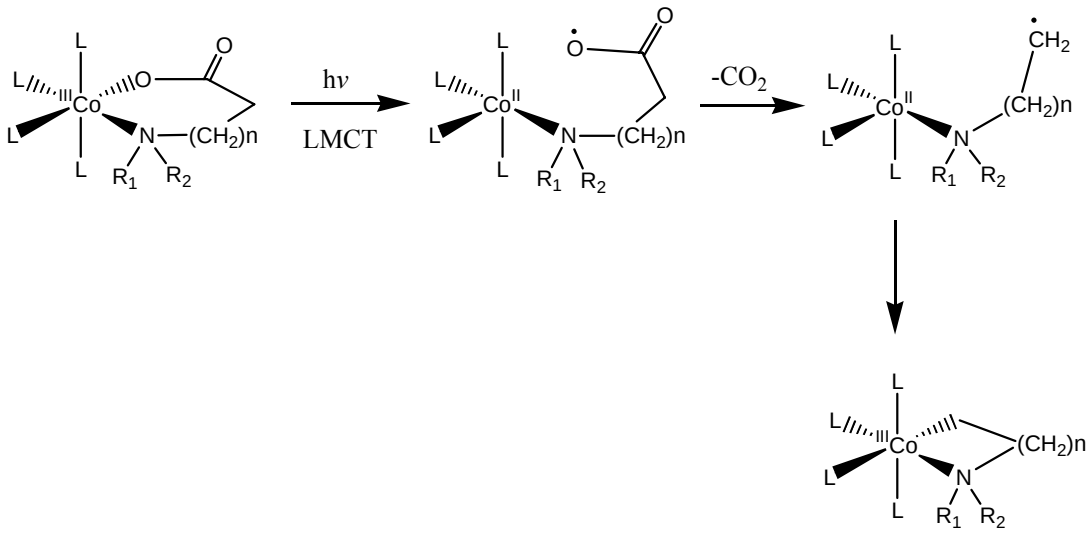

Figure 3.2: The possible mechanism behind the decarboxylation of coordinated aminocarboxylato ligands, as postulated by Poznyak and Pavlovski.[30] n = 0, 1, 2.

A relevant example of a Co-aminocarboxylato complex that has been found to undergo loss of CO_2 upon irradiation with UV light is shown in Figure 3.3.[41] Photolysis of the complex $[Co(dpg)(phen)]^{2+}$ was found to induce decarboxylation of the glycine fragment of the dpg ligand. The result was complex with a stable three-membered chelate ring.

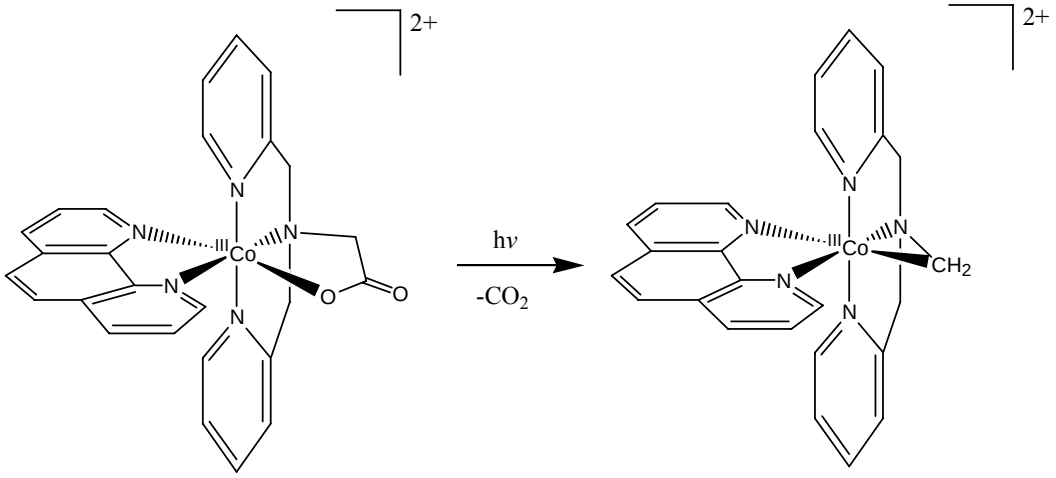

Figure 3.3: The photochemical decarboxylation of $[Co(dpg)(phen)]^{2+}$ to yield a Co-C-N chelate ring.

The resulting Co-C-N ring was sufficiently stable to allow an X-ray crystal structure to be obtained. Other systems that undergo photolysis to yield a Co-C-N ring have also been characterised.[41,57]

Armed with this knowledge of the reactivities that coordinated aminocarboxylato ligands can undergo when exposed to UV light, it is straightforward to see how coordinated glyphosate, also an aminocarboxylato ligand, could be reactive under UV irradiation. As covered in Chapter 1, glyphosate has a propensity to bind to metal ions in soils, forming coordination complexes. Complexes of glyphosate that exist naturally may include iron or aluminium metal centres. The iron complexes may be susceptible to the photochemical route described above when irradiated with UV light from the sun, possibly leading to the decarboxylation of the coordinated glyphosate.

It is less likely that aluminium-glyphosate complexes would be affected in the same way. Aluminium is normally found with oxidation states of 3+ or zero. In order for an aluminium-glyphosate complex to undergo the photochemically induced decarboxylation

process as described above, the Al(III) centre would first have to be reduced to Al(II). The 2+ state is an uncommon and unstable oxidation state for aluminium, and although this dication can be produced from Al(III) *via* anodic oxidation, it is a very short lived species.[58] Thus, such photochemical reactions involving aluminium would not be expected to occur under normal conditions.

With this is mind, iron might seem like the obvious choice of metal to use when preparing metal-glyphosate complexes in the lab. But one has to think of the practicalities involved with the use of such a metal – Fe(III), with its d^5 configuration is paramagnetic and cannot be used for NMR studies, an analytical technique that is central to this research. Co(III) is a better choice, as described in Section 2.1, since it is diamagnetic and therefore ideal for NMR studies, and sufficiently inert to achieve X-ray crystal structure determination. Cobalt is also stable in its 2+ and 3+ oxidations states, rendering it ideal for photochemical studies where one-electron reductions and oxidations may occur. Given that cobalt appears beside iron in the periodic table, it is possible that their chemistries are similar. Therefore, cobalt acts as a good model by which to explore the behaviour of coordinated glyphosate.

UV radiation is the light of choice for these photolysis reactions as it supplies the required amount of energy required to induce electron transitions in the complexes of interest.

A glass quartz cuvette is the chosen vessel in which to carry out the photolysis reactions. Quartz glass is transparent to infrared, visible, and UV light, and it is this property of the material that ensures the most efficient utilisation of the light source during the photolysis experiments. It is possible to carry out photolysis reactions in other vessels such as a 5 mm NMR tube, but such vessels absorb some of the irradiated light, leading to a lengthier experiment duration, *i.e.* less efficient use of the light source.

In summary, the new cobalt-glyphosate complexes that were successfully synthesised and characterised, as outlined in Chapter 2, have been subjected to UV light, so that their reactivities can be assessed. The results of these experiments and the discussion of these can be found below. The discussion of the reactivity of each complex under photolytic

conditions includes an attempt to identify the products of the reactions *via* interpretation of the acquired ^{1}H, ^{13}C, and ^{31}P NMR spectra.

The ^{31}P NMR spectra are not discussed individually. Rather, they are presented as one unit in Section 3.2.2.1, where the signals that occur in the ^{31}P NMR spectra of the photolysates are presented schematically to allow comparisons between them to be made. Phosphorus NMR is a useful technique for this research, since each phosphorus-containing species present in a photolysate gives rise to one peak only in the spectra. ^{31}P NMR is reasonably straightforward to interpret, given that it is proton decoupled. An attempt has been made to identify the species that give rise to the new peaks in the phosphorus NMR.

3.2.1 Results and discussion

All of the photolysis experiments followed the same basic procedure: a sample of the complex being tested was dissolved in D_2O and the solution was placed in a glass quartz cuvette. Photolysis usually began with the lamp power set to 200 W. ^{1}H NMR spectra were obtained at regular intervals, and when a change in the spectrum was detected ^{13}C and ^{31}P (if appropriate for the complex being tested) NMR spectra were collected. If the complex appeared to be reacting sluggishly at 200 W, the lamp power was increased to 500 W, and photolysis and intermittent NMR collection continued. The experiments were terminated when no further changes in the NMR were detected.

A summary of the results from the photolysis experiments is provided in a table in Section 3.2.2, but the details are outlined below.

3.2.1.1 Photolysis of [Co(tacn)(PMG)]Cl·HCl·2.5H$_2$O

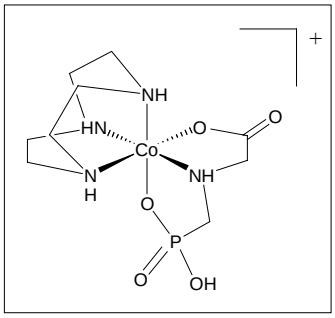

Several observations are notable for this reaction. At the end of the photolysis experiment, it was established that no colour change had taken place.

Gradual broadening of the peaks in the ^{1}H NMR spectra is

evident over time. A signal in the ^{1}H NMR spectrum, which occurs at 7.2 ppm in the non-photolysed complex, has vanished after 2.5 hours of photolysis. One peak, at 3.2 ppm, that contributes to the multiplet between 3.4 and 2.6 ppm in the starting material, has grown considerably in the photolysed sample.

The ^{13}C NMR spectra show that the signal for the carbonyl carbon atom of the PMG ligand, at 187.0 ppm, is no longer detectable after about 12 hours of irradiation. Two new peaks, at 79.1 ppm and 45.2 ppm, appear in the ^{13}C NMR spectra over this time. Broadening and shortening of the signal at 60.4 ppm, corresponding to the methylene carbon atom of the carboxylate portion of the PMG ligand is also observed.

Many new peaks are present in the ^{31}P NMR spectra obtained during the photolysis experiment. The shortening and broadening of the signal corresponding to the [Co(tacn)(PMG)]Cl·HCl·2.5H_2O starting material is also observed. The new peaks that developed are represented schematically in Figure 3.12 as part of the combined discussion of the ^{31}P NMR spectra results.

The observations listed above suggest that this complex is reactive under photochemical conditions. The broadening of the peaks in the ^{1}H NMR spectrum is consistent with Co(II) being produced – this ion is paramagnetic and causes the observed broadening of the NMR peaks. Also notable is the loss of the signal at 7.2 ppm. This signal has been assigned to the amine proton on the PMG ligand through the interpretation of the HETCOR NMR spectrum of the complex, as explained Section 2.2.1.2. Two signals, at 8.0 and 6.5 ppm, which correspond to the amine protons of the coordinated tacn, remain, although somewhat diminished, at the conclusion of the photolysis experiment.

There is evidence of free tacn ligand in the ^{1}H NMR spectrum of the photolysate – it is possible that the new peak at 3.2 ppm represents the methylene protons of the free ligand. This is not surprising as the loss of ligands can be expected upon reduction of Co(III) to Co(II) - this has been observed previously in these kinds of reactions.[59] The loss of ligands is due to the relative reactivity of the metal centres (Co(III) is renowned for being inert, while Co(II) is typically a labile metal centre).

The presence of free tacn in supported by the growth of a signal at 45.2 ppm in the ^{13}C NMR spectra of the photolysate.

Analyses of the ^{13}C NMR spectra conclude that decarboxylation of the PMG ligand may have occurred. This result is suggested by the eventual loss of the carboxylate peak at 187.0 ppm and is possibly linked to the shortening and broadening of the methylene peak at 60.4 ppm (since the carbonyl carbon and the methylene carbon atoms are neighbours it is likely that changes in the complex that affect one nucleus will affect the other).

Since a quantity of the tacn ligand seems to have fallen off the cobalt ion, it is possible that the PMG ligand has too. Non-coordinated amino acids (an example of which might be free PMG) have been known to decarboxylate when irradiated with UV light.[60] Accordingly, it is possible that decarboxylation can occur to free PMG in solution.

If the decarboxylation of the complex was to occur, the methylene carbon atom would undergo a change in environment. This would lead to the decrease in intensity of the original peak for the methylene carbon atom, at 60.4 ppm, and the growth of a new peak corresponding to the new environment of the carbon atom. The reduction in the intensity of the peak at 60.4 ppm is certainly observed. The broadening of this peak could be caused by the presence of Co(II) in solution. A new signal, at 79.1 ppm, grows in intensity as the peaks at 187.0 ppm and 60.4 ppm become shorter. It is possible that the new peak at 79.1 ppm corresponds to the methylene carbon atom in its new environment.

The assignment of the remaining new peak, at 79.1 ppm, may be aided by previous studies into the characterisation of carbinolamines. Browne[60] characterised several new coordinated carbinolamine species, where the amine attached to the Co(III) centre has a $CH_2(OH)$-R group attached. One such species, *ffm*$_x$-$[Co(tetraenol)Cl]^{2+}$ is shown in Figure 3.4.

In Browne's research, the ^{13}C NMR chemical shifts for the methylene carbon atoms of the carbinolamines were in the range of 85 to 90 ppm. With this in mind, a chemical shift of 79.1 ppm is not unreasonable for a carbon atom in a similar environment. This is slightly upfield from Browne's NMR data, but this may be explained by nature of the carbon of

the carbinolamine species. In our research, the possible carbinolamine carbon atom would have two protons attached, while the carbinolamines prepared by Browne were alkyl substituted at the carbon atom.

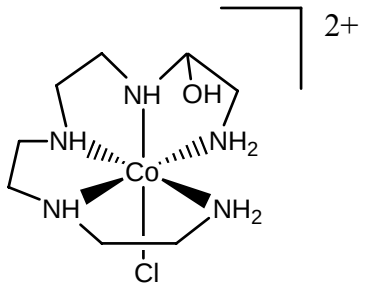

Figure 3.4: One isomer of *ffm*$_x$-[Co(tetraenol)Cl]$^{2+}$

Figure 3.5 illustrates how a carbinolamine species may result from the photolysis of [Co(tacn)(PMG)]Cl·HCl·2.5H_2O. If a carbinolamine has formed, this suggests the presence of an imine intermediate. An imine can develop from the reductive elimination of a Co-C-N ring, which likely to be a very short-lived species. This is possibly why there is no evidence of it in the ^{13}C NMR spectra.

The ^{31}P NMR spectrum of the starting complex exhibits one major peak at 38.4 ppm. Numerous signals were detected in the ^{31}P NMR spectra of the photolysate. This implies that many phosphorus-containing compounds are produced during the experiment, *i.e.* reactivity of some kind has certainly occurred. The peaks that arise in the ^{31}P NMR spectrum during the course of the experiment are displayed in Figure 3.12. The significance of these results, and the outcome from the photolysis of other complexes in this section, is discussed in Section 3.2.2.

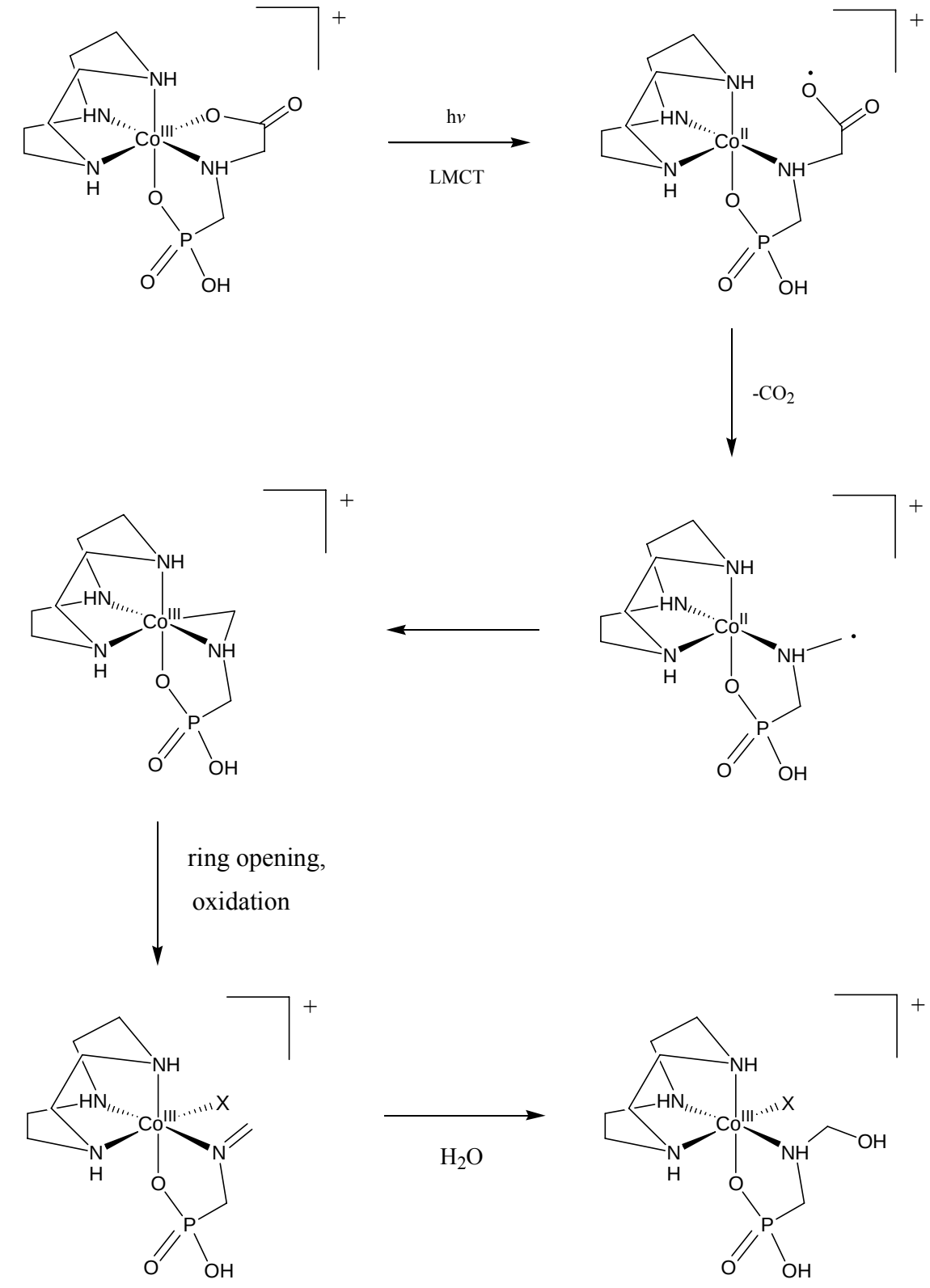

Figure 3.5: The simplified mechanism for the formation of the possible photolysis product of the $[Co(tacn)(PMG)]^{2+}$ complex. X is most likely a solvent molecule.

3.2.1.2 Photolysis of [Co(tacn)(PMG)ZnCl$_3$]·3H$_2$O

The results obtained for the photolysis of this complex are identical for that of the [Co(tacn)(PMG)]Cl·HCl·2.5H$_2$O species. This outcome is rationalised by the lability that would be expected of the zinc ion in the [Co(tacn)(PMG)ZnCl$_3$]·3H$_2$O complex. When this complex is dissolved in water, the zinc ion undergoes rapid exchange, possibly to yield [Zn(Cl$_3$)(H$_2$O)]$^-$, according to Figure 3.6. The [Co(tacn)(PMG)]$^+$ complex is then free in solution.

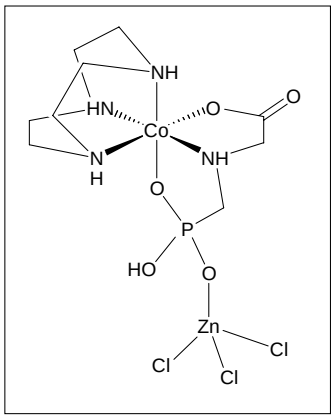

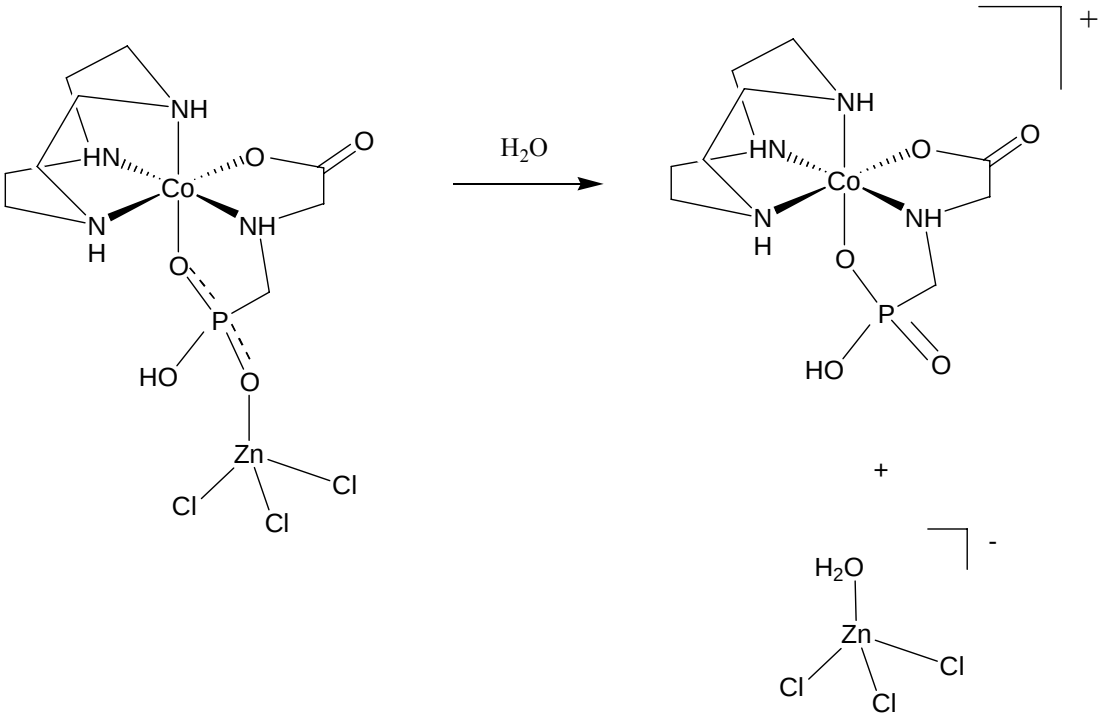

Figure 3.6: The loss of the $ZnCl_3^-$ fragment from [Co(tacn)(PMG)ZnCl$_3$]·3H$_2$O to yield [Co(tacn)(PMG)]$^+$.

The [Co(tacn)(PMG)]$^+$ is then free to react, under photolytic conditions, in the same fashion as its [Co(tacn)(PMG)]Cl·HCl·2.5H$_2$O counterpart, as was described in Section 3.2.1.1.

3.2.1.3 Photolysis of [Co(tren)(PMGH)]Cl_2·0.5CH_3OH

It is observed that the photolysis of this complex at 200 W leads to the rapid loss of the signal representing a proton attached to an amine, at 6.3 ppm, in the ^{1}H NMR spectra. It is also noted that in the same spectrum the multiplet that lies between 4.0 ppm and 3.6 ppm has lost its coupling – what was originally a multiplet consisting of eight peaks has quickly become a multiplet of four peaks.

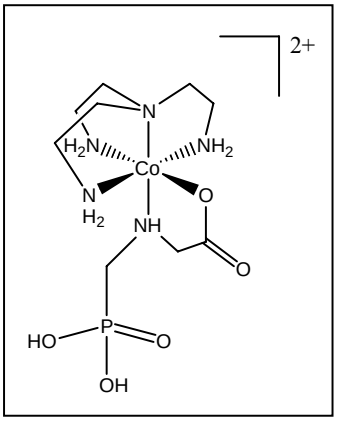

The photolysis reaction at 500 W induced a gradual change of colour from orange to red. Two new, major peaks at 3.2 and 3.0 ppm are evident in the ^{1}H NMR spectra. It is observed that the peaks gradually broaden, and that there is a decrease in the intensities of the peaks corresponding to the starting material.

The ^{13}C NMR spectra show the growth of three new, major peaks at 84.5, 52.9 and 39.5 ppm. After six hours of irradiation there is no evidence of a carbonyl peak, usually observed at 185.1 ppm, in the ^{13}C NMR spectrum.

Numerous new peaks are evident in the ^{13}P NMR spectra that were obtained over the course of the experiment, and these are depicted schematically in Figure 3.14.

The NMR data described above indicate that the complex is photochemically reactive. The broadening of the peaks in the ^{1}H NMR spectra suggest that some of the Co(III) metal centres are being reduced to Co(II). When Co(III) is reduced it is possible that the attached ligands will fall off, due to the lability of the resulting Co(II). This seems to be the case when the $[Co(tren)(PMGH)]^{2+}$ complex is photolysed – it appears that the tren ligand becomes free in solution. The new peaks observed in the ^{1}H NMR spectra, at 3.2 ppm and 3.0 ppm can be assigned to the methylene protons of free tren.

The signals at 52.9 ppm and 39.5 ppm in the ^{13}C NMR spectra are indicative of the loss of tren from the Co(II) centre. These signals correspond to the methylene carbon atoms of free tren. By scrutinising the peak heights of the ^{13}C NMR spectra it can be seen that over

time the amount of free tren increases while the amount of $[Co(tren)(PMGH)]^{2+}$ decreases. It is also noted that, eventually, the ^{13}C NMR spectra shows no carbonyl signal, indicating that decarboxylation of the PMG ligand might have occurred.

Since the tren ligand has probably fallen off the Co(II) centre, it is also possible that PMG has too, yielding the free ligand in the solution. As mentioned earlier non-coordinated amino acids have been known to decarboxylate when irradiated with UV light,[60] so it is possible that the free PMG ligand has decarboxylated.

The ^{31}P NMR spectra show numerous new peaks over the course of the photolysis reaction (Figure 3.14), signifying that several new phosphorus-containing compounds are being produced in the reaction solution. The signal for the starting complex, usually seen at 12.1 ppm, is not observed at the end of the photolysis, supporting the hypothesis that the complex has decomposed. However, at the end of the experiment it is noted that a signal has developed at 8.9 ppm. This is the chemical shift of free PMG. This signal could possibly be assigned to the free ligand – however, there is no evidence of free PMG in the ^{13}C NMR spectrum at this time. This inconsistency is possibly due to the sensitivity of ^{31}P NMR, which is more sensitive than ^{13}C NMR spectroscopy. On account of this, it is likely that free PMG is present in the photolysate.

The appearance of the peak at 84.5 ppm in the ^{13}C NMR spectra may be due to a cyclic carbinolamine species. As covered in Section 3.2.1.1, a chemical shift of around 85 to 90 ppm is reasonable for a carbinolamine carbon atom. If such a species has indeed formed, this implies the presence of an imine precursor, which could develop from the reductive elimination of a Co-C-N ring.

Figure 3.7 illustrates a possible route to a cyclic carbinolamine species, which may give rise to the peak at 84.5 ppm in the ^{13}C NMR spectra. Since the PMG ligand is only bidentate in this complex, once the free imine has formed the likelihood of it re-coordinating to the cobalt centre is low. The ligand is not tethered to the cobalt centre *via* a phosphonate oxygen atom, as seen in other examples, such as the $[Co(tacn)(PMG)]Cl{\cdot}HCl{\cdot}2.5H_2O$ complex. The other possible products of the reaction are

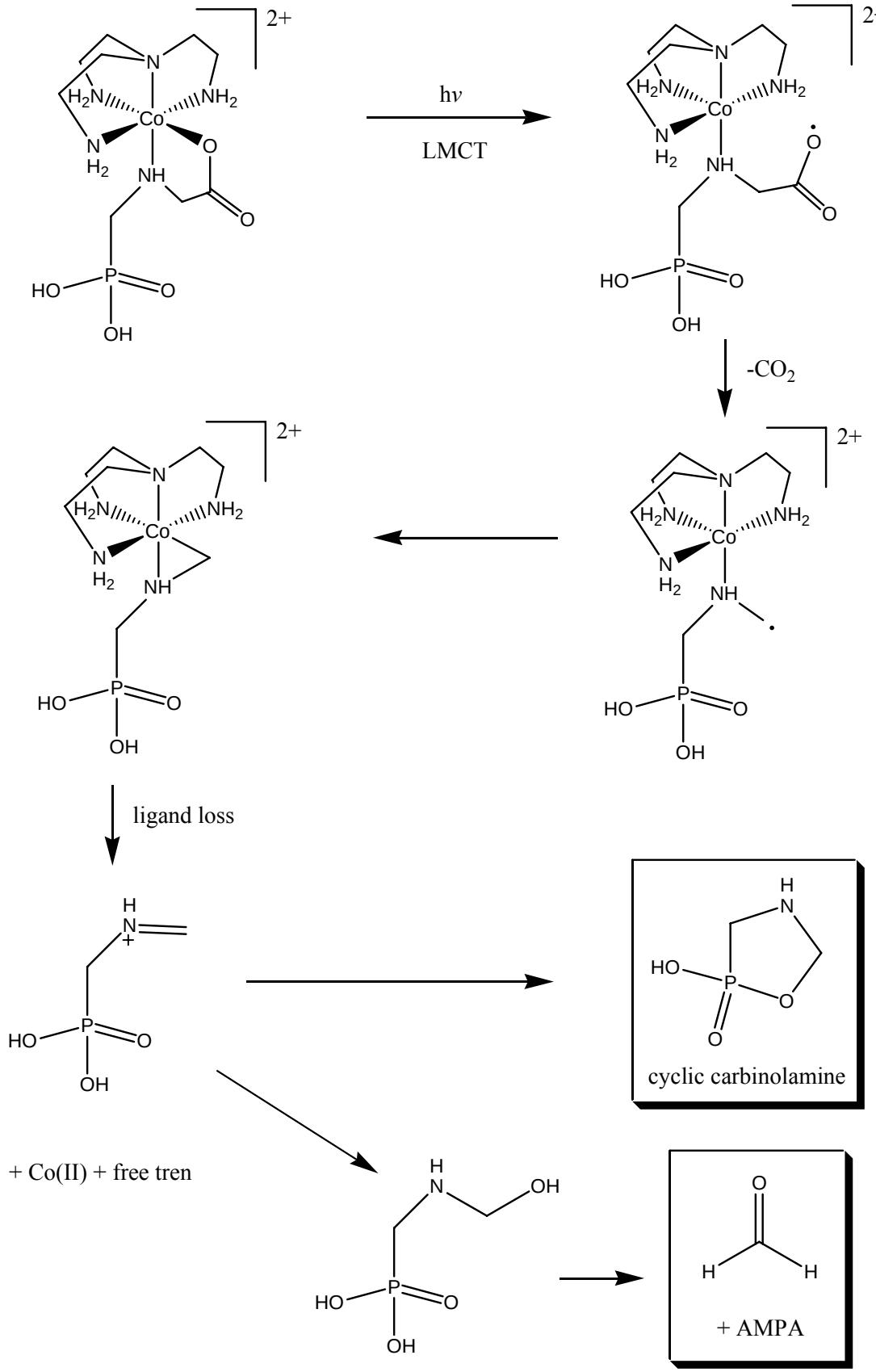

Figure 3.7: The possible route to a cyclic carbinolamine, *via* a metallacycle and imine, upon the photolysis of $[Co(tren)(PMGH)]Cl_2 \cdot 0.5CH_3OH$.

formaldehyde and AMPA, but it is unlikely that these species lead to a peak at 84.5 ppm in the ^{13}C NMR spectrum.

3.2.1.4 Photolysis of [Co(bamp)(PMG)]Cl·2.5H$_2$O

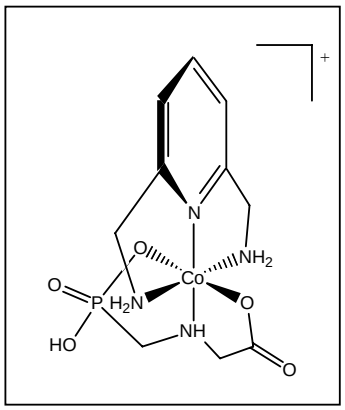

It was noted that over the period of photolysis of this complex the colour of the solution changed from pink-purple to orange-red. The ^{1}H NMR spectra does not show a lot of change over this time, apart from gradual broadening of the peaks, and a change in the signals in the aromatic region. The spectrum of the non-photolysed starting material shows two peaks in this region: a triplet at 8.2 ppm and a doublet at 7.8 ppm. Shortly after photolysis was initiated two new triplets began to grow, at 7.9 ppm and 7.4 ppm.

The ^{13}C NMR spectra show the rapid loss of the doublet assigned to the carbon atom attached to the phosphonate group of the PMG, normally centred at 50.1 ppm. Continued photolysis leads to a much-diminished carbonyl peak, at 184.5 ppm. There are many new "satellite" peaks surrounding the signals assigned to the carbon atoms of coordinated bamp, while the signals corresponding to the coordinated bamp itself reduce in intensity. The signal for the methylene carbon atom of the carboxylate arm of the PMG is very small by the end of the experiment, and new peaks are observed at 81.7 and 63.0 ppm.

The ^{31}P NMR spectrum of the photolysate after four hours of irradiation shows that the peak for the starting material has disappeared, while the growth of several new peaks is observed. New signals continue to appear in the ^{31}P NMR spectra throughout the period of irradiation. The extra peaks that develop in the ^{31}P NMR spectra are depicted in Figure 3.15.

It appears that this complex is reactive under photolytic conditions. It is likely that some Co(II) is produced in the experiment, leading to the broadening of the peaks in the ^{1}H NMR spectra. The only significant change in the spectra over time is the development of two new multiplets in the aromatic region of the spectrum, at 7.9 and 7.4 ppm. It was

thought that this might be a response to the development of free bamp in the solution (a possible consequence of the generation of the labile Co(II) ion). Free bamp gives rise to a doublet at 8.0 ppm and a triplet at 7.5 ppm, a plausible match to the new signals appearing at 7.9 and 7.4 ppm. But this free ligand would also lead to a signal at 4.4 ppm, which is not observed. We can conclude from the change in the ^{1}H NMR spectra that a new species of some kind has been formed.

The ^{13}C NMR spectra of the photolysed complex show the eventual decrease in the intensity of the carbonyl peak at 184.5 ppm. It is possible that this is due to decarboxylation of the PMG ligand. Certainly, the presence of Co(II) in the ^{1}H NMR spectra is supportive of this, since the reduction of Co(III) to Co(II) is thought to be the first step in the photo-induced decarboxylation process.

The signal that develops at 81.7 ppm in the ^{13}C NMR spectra can possibly be assigned to a carbinolamine, as previously described in Section 3.2.1.1. In the case of the $[Co(bamp)(PMG)]^{+}$ complex, the rapid formation of a coordinated carbinolamine from the Co-C-N metallacycle is likely to be on account of strain. Figure 3.8 depicts a possible Co-C-N metallacycle that could form when $[Co(bamp)(PMG)]^{+}$ is photolysed. On examination of the structure it becomes apparent that the Co-C-N ring would be very strained due to the meridional coordination of the PMG ligand – the central amine is tethered by its phosphonyl arm which offers the coordinated amine little “give” in the direction of the Co-C-N ring. There is no evidence of the Co-C-N ring in the ^{13}C NMR spectra.

Keeping in mind the strain that would exist in the Co-C-N species depicted in Figure 3.8, it is possible that a carbinolamine, as described in previous sections, is formed. The strained Co-C-N ring would easily undergo reductive elimination, resulting in a coordinated imine. The imine could then be attacked by water from the surrounding solution to produce a carbinolamine (Figure 3.9).

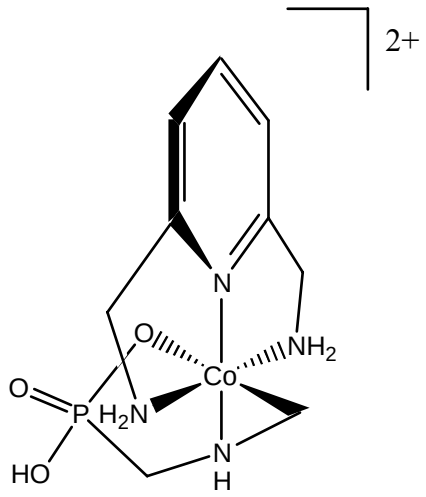

Figure 3.8: Possible structure of a metallacycle formed from the photolysis of $[Co(bamp)(PMG)]^{+}$.

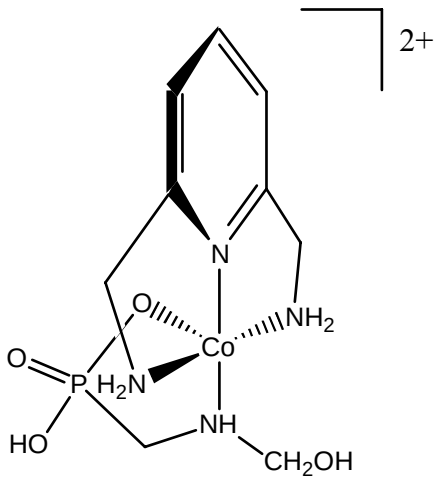

Figure 3.9: Possible structure of a carbinolamine resulting from the reductive elimination of a Co-C-N structure.

According to the ^{13}C NMR spectra, free bamp is not present in the photolysate at any stage. The ^{13}C NMR spectrum of the free ligand exhibits to four peaks at 153.7, 142.2, 125.1, and 45.1 ppm, none of which are detectable in the ^{13}C NMR of the photolysate. However, the signal-to-noise ratio appears to be low (unfavourable for detecting small peaks in the NMR spectrum), so it is possible that free bamp has been produced but the peaks corresponding to this free ligand cannot be seen.

It is not known what species might give rise to the peak at 63.0 ppm in the ^{13}C NMR spectra.

The first ^{31}P NMR spectrum was obtained after four hours of photolysis and exhibits the loss of the signal corresponding to the [Co(bamp)(PMG)]Cl·2.5H_2O starting material. The development of several new peaks is noted over the course of irradiation. These are depicted in Figure 3.15 and discussed afterwards.

3.2.1.5 Photolysis of [Co(bamp)(IDA)]Cl

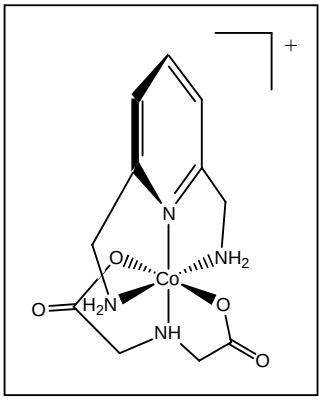

This complex is the only non-phosphorus-containing compound to have been tested photolytically in this research.

Over the period of photolysis the colour of the solution did not change from the original shade of peach-orange. The ^{1}H NMR spectra obtained intermittently during the six hours of photolysis show gradual broadening of the signals, as well as the development of two extra peaks. These peaks are major and occur at 5.0 ppm and 2.2 ppm. The increase in intensity of the existing multiplets at 4.5 ppm and 4.2 ppm is also observed.

The ^{13}C NMR obtained after six hours of photolysis shows a significant reduction in the intensity of the signal that represents the carboxylate carbon atom. There are five new peaks appearing at 153.6 ppm, 141.4 ppm, 124.4, 85.0 ppm and 45.1 ppm. The signal that has been assigned to the methylene carbon atom of the coordinated IDA ligand, which normally appears at 58.4 ppm, gradually moves downfield to a new position of 60.2 ppm in the photolysed product.

It can be seen from the data described above that this complex is certainly reactive towards photolysis. The gradual broadening of the signals in the ^{1}H NMR spectra indicates that some of the Co(III) centres are being reduced to Co(II). It is not known what species give(s) rise to the new peaks at 5.0 ppm and 2.2 ppm. The ^{1}H NMR

spectrum of free bamp consists of a triplet at 8.0 ppm, a doublet at 7.5 ppm, and a singlet at 4.4 ppm, so the new peaks at 5.0 and 2.2 ppm cannot be assigned to this free ligand.

The decrease in the intensity of the carbonyl signal in the ^{13}C NMR spectra suggest that decarboxylation of the IDA ligand could be occurring.

It is possible that the photolysis of this complex results in carbinolamine, as this would account for the new peak in the ^{13}C NMR spectrum at 85.0 ppm. The issue of carbinolamine formation was first introduced in Section 3.2.1.1. As explained in the discussion of the $[Co(bamp)(PMG)]^+$ photolysis experiment, a Co-C-N metallacycle involving meridional PMG would be a very strained species. The possible metallacycle that could result from the photolysis of [Co(bamp)(IDA)]Cl is illustrated in Figure 3.10. This would most likely be short-lived due to the strained ring, and ring opening could eventually give rise to a carbinolamine (Figure 3.11).

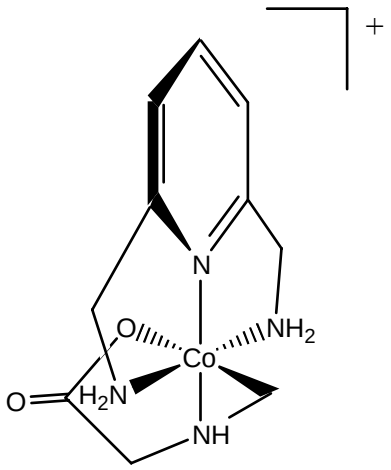

Figure 3.10: The possible structure of a metallacycle formed from the photolysis of $[Co(bamp)(IDA)]^+$.

Further examination of the ^{13}C NMR spectra leads to the conclusion that a significant proportion of bamp ligand has fallen off the labile Co(II) centre. Free bamp gives rise to peaks at 153.7, 142.4, 125.1, and 45.1 ppm. All of these signals are easily detectable in the ^{13}C NMR spectrum of the photolysate after only one hour of irradiation.

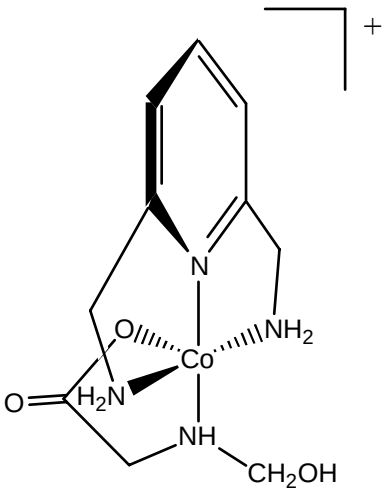

Figure 3.11: The possible structure of a carbinolamine resulting from the ring opening of a Co-C-N species.

3.2.2 Summary of ^{31}P NMR spectra obtained during photolysis

For this research, phosphorus NMR is a useful technique in that each phosphorus-containing species gives rise to just one signal in the spectrum. The development of numerous peaks, as observed in the photolysis reactions, suggests that many phosphorous-containing species are being produced. Inspection of Figure 3.12 to Figure 3.15 leads to the observation that all of the photolysates of the complexes give rise to several common peaks in their ^{31}P NMR spectra. These common peaks are coloured red in the figures below. Due to their widespread occurrence, it makes good sense to identify what species may give rise to these peaks. It is likely, due to their recurring nature, that they are important species that arise during the photodecomposition of Co-PMG complexes, and in the degradation of the ligand itself. It is, therefore, of interest to attempt to identify these common phosphorous-containing species. The signals of significance appear at the following chemical shifts in the ^{31}P NMR spectra: 161, 25, 20, 18, 16, 11, and -53 ppm.

Figure 3.12 to Figure 3.15 show the development of many different peaks during the photolysis of the four phosphorus-containing complexes. The loss of the peaks representing the starting material is gradual for [Co(tacn)(PMG)]Cl·HCl·2.5H_2O and [Co(tacn)(PMG)$ZnCl_3$]·3H_2O, and is signified by the depletion of the peaks over time. The [Co(tren)(PMGH)]Cl_2·0.5CH_3OH and [Co(bamp)(PMG)]Cl·2.5H_2O complexes appear to react more rapidly, the signals for the starting materials vanishing over the first four hours of photolysis.

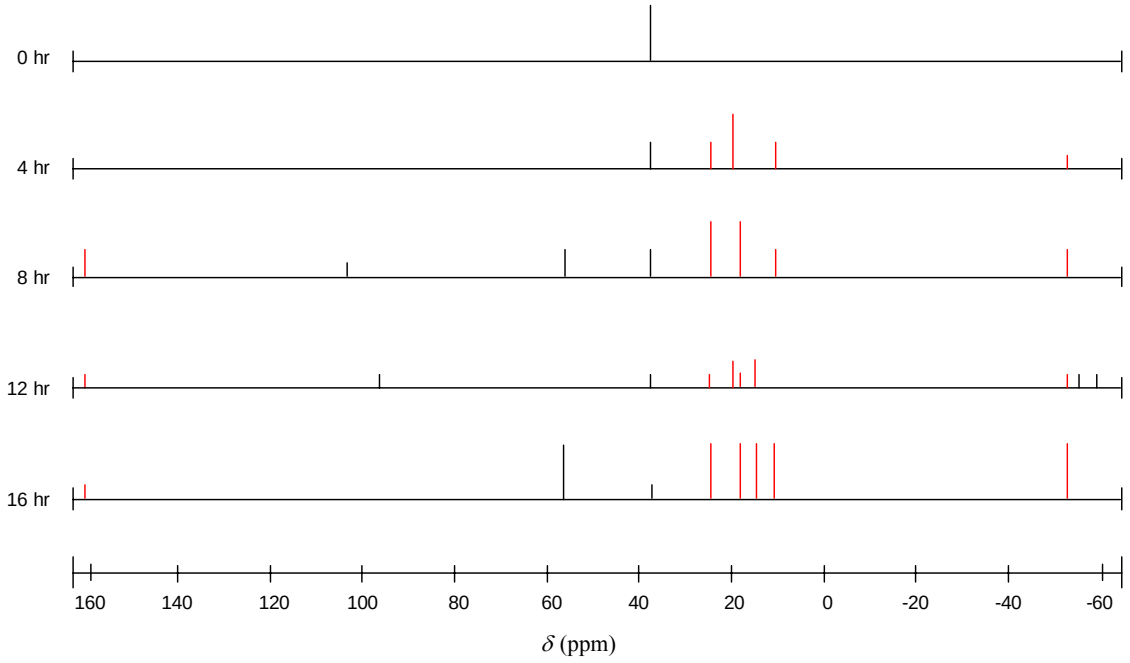

Figure 3.12: The peaks observed in the ^{31}P NMR spectra of the photolysed Co(tacn)(PMG)]Cl·HCl·2.5H_2O complex.

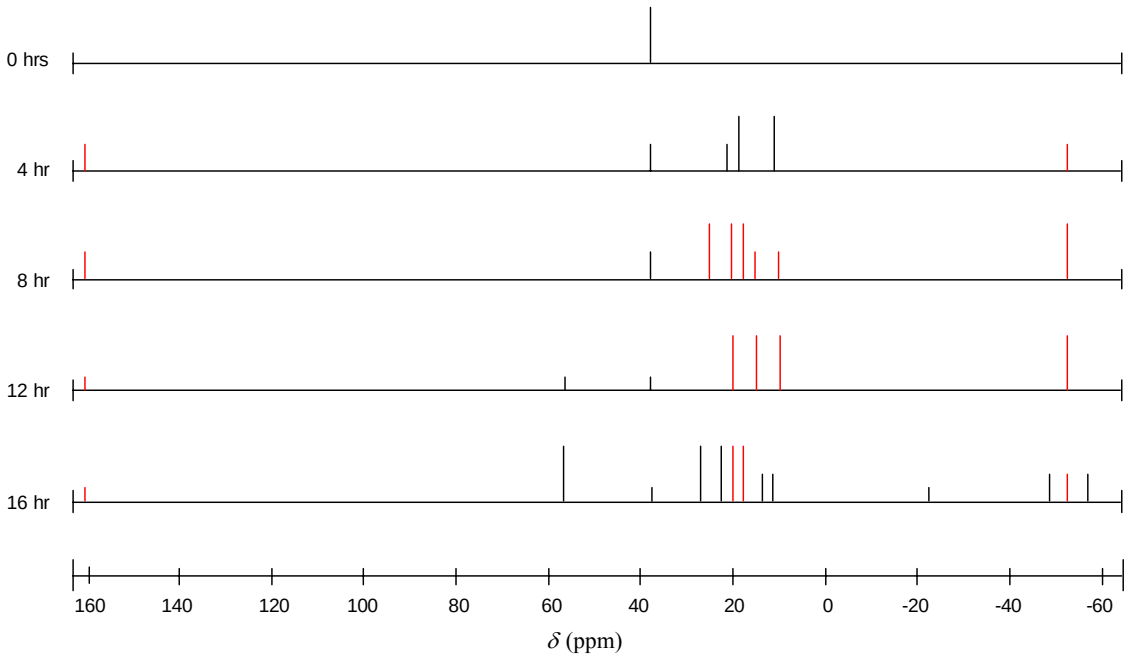

Figure 3.13: The peaks observed in the ^{31}P NMR spectra of the photolysed [Co(tacn)(PMG)$ZnCl_3$]·3H_2O complex.

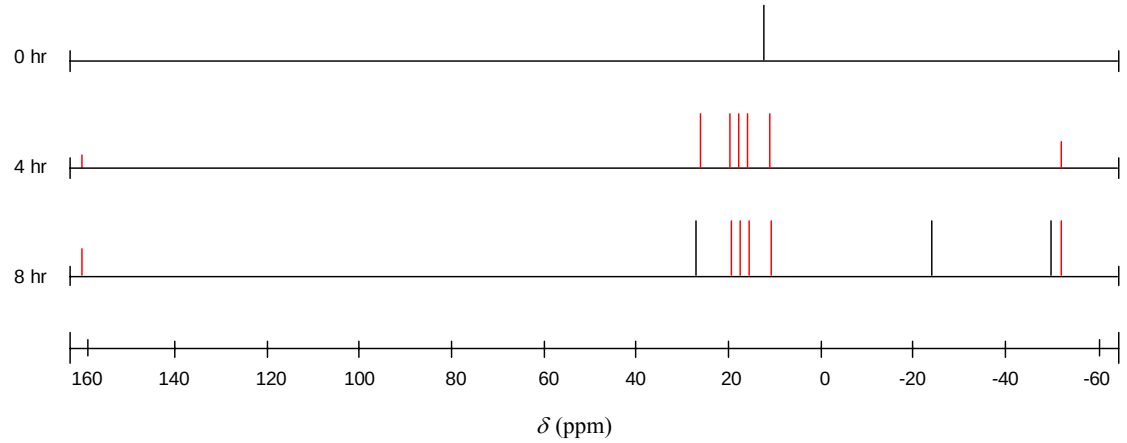

Figure 3.14: The peaks observed in the ^{31}P NMR spectra of the photolysed $[Co(tren)(PMGH)]Cl_2 \cdot 0.5CH_3OH$ complex.

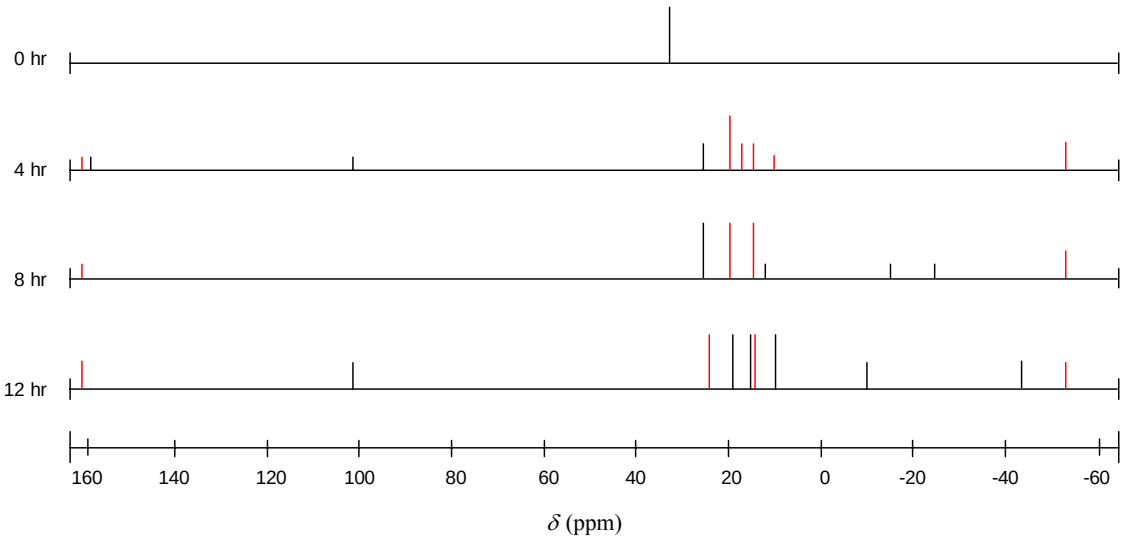

Figure 3.15: The peaks observed in the ^{31}P NMR spectra of the photolysed $[Co(bamp)(PMG)]Cl \cdot 2.5H_2O$ complex.

A search through ^{31}P NMR spectroscopy tables of phosphorus-containing compounds[62] has allowed an attempt to identify the kinds of compounds that may give rise to the peaks at 25 and 20 ppm. The structures that possibly represent the signals at 25 and 20 ppm, and their reported chemical shifts, are depicted in Figure 3.16.

The phosphorus-oxygen bond is very strong, so it can be expected that at least as many P-O bonds will be seen in the products as were in the starting material. Since PMG has three P-O bonds, it is expected that any decomposition product would also have at least three P-O bonds. Accordingly, the methyl phosphonic acid species, in Figure 3.16, is a likely candidate to lead to the observed peaks at 25 ppm in the ^{31}P spectra. The undertaking of a spiking experiment is one method of ascertaining that the signals at 25 ppm are due to the presence of methyl phosphonic acid. This experiment entails the addition of a small amount of methyl phosphonic acid to the photolysates, then recollection of the ^{31}P NMR spectrum. If the peaks at 25 ppm have increased in intensity, then we can propose that methyl phosphonic acid is indeed a product of the photolysis reactions. Unfortunately, this phosphorus containing species was not available to us in our laboratory, so the spiking experiment could not be carried out.

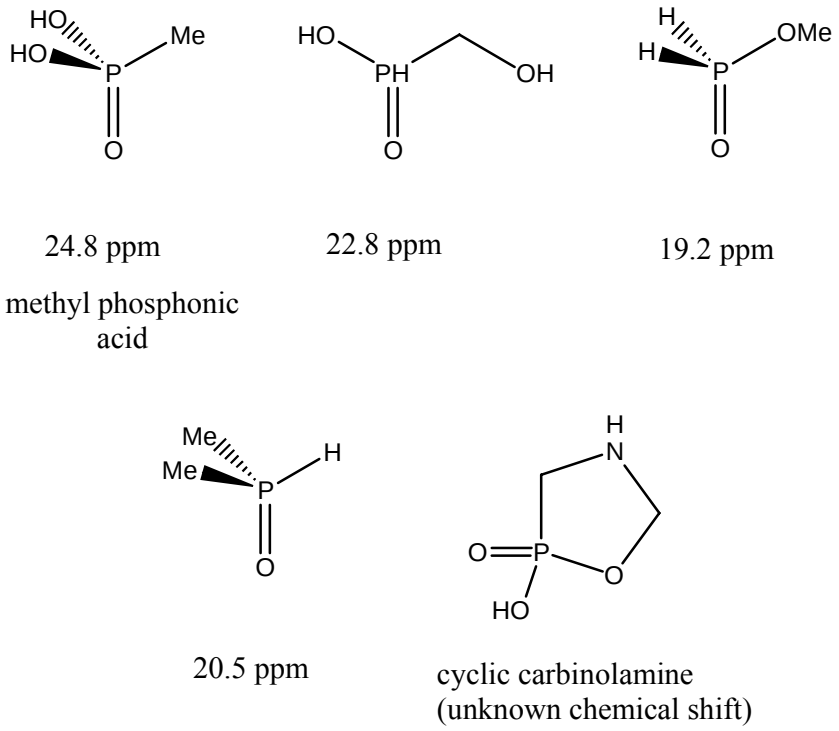

Figure 3.16: Various phosphorus-containing compounds that may lead to the observed signals at 25 and 20 ppm in the ^{31}P NMR spectra.

It is not known what phosphorus-containing compound would give rise to the other regularly occurring peaks. Study of the tables of phosphorus-containing species[62] have proved futile, offering few species of compound that could give rise to the (as yet) unassigned peaks in the ^{31}P NMR spectra.

3.2.3 Summary of photolysis reactions

The results of the photolysis reactions are summarised in Table 3.1.

Complex	Colour change?	Evidence of Co(II)?	Evidence of decarboxy-lation?	New peaks in ^{13}C NMR (ppm)	Additional observations/ comments
[Co(tacn)(PMG)]Cl·HCl·2.5H_2O	no	yes	yes	79.1 (carbin-olamine), 45.2 (free tacn)	possible formation of carbinolamine
[Co(tacn)(PMG)$ZnCl_3$]·3H_2O	no	yes	yes	79.1 (carbin-olamine), 45.2 (free tacn)	possible formation of carbinolamine
[Co(tren)(PMGH)]Cl_2·0.5CH_3OH	orange to red	yes	yes	52.9,39.5 (free tren), 84.5 (carbinolamine)	possible formation of carbinolamine
[Co(bamp)(PMG)]Cl·2.5H_2O	pink-to orange	yes	yes	63.0 (unassigned), 81.7 (carbinol-amine)	possible formation of carbinolamine
[Co(bamp)(IDA)]Cl	no	yes	yes	153.6, 141.4, 124.4, 45.1 (free bamp), 85.0 (carbinol-amine), 60.2 (unassigned)	possible formation of carbinolamine

Table 3.1: A summary of the results for the photolysis reactions, at 500 W, of five complexes.

As can be concluded from the descriptions of the ^{1}H NMR and ^{13}C NMR spectra above, all of the complexes were reactive under photolytic conditions. All of the irradiated samples underwent a small temperature rise, from room temperature to around 30˚C, during these experiments. As far as we are aware, heating to this temperature is not harmful to the starting materials. As described in Chapter 2, at the end of the synthetic and isolation procedures each complex was dried on a rotary evaporator at around 35-40˚C. But we cannot be so sure of the stability of any intermediates or products formed during the photolysis reactions. It is possible that these species may be temperature-sensitive such that their thermal decomposition occurs.

The reactivity that we are interested in is the decomposition of the ligands associated with the complexes, in particular, PMG and IDA. Such reactivity might be induced by the photo-reduction of the Co(III) centres to Co(II). The reduction of Co(III) to Co(II) implies that another species must be oxidised. As explained by Poznyak and Pavlovski,[30] the first step of any photochemical reaction of a transition metal complex is a LMCT which results in a reduced metal centre. It is possible that the PMG or IDA ligand is supplying the electron for the reduction *i.e.* being oxidised. If this is the case, such oxidation could induce the decomposition of the PMG or IDA compounds.

Since Co(II) is kinetically labile, the loss of ligands from the reduced metal centre is one possible result. This outcome is certainly evident in the $[Co(tacn)(PMG]^{+}$, $[Co(tren)(PMGH)]^{2+}$ and $[Co(bamp)(IDA)]^{+}$ photolysis examples, where the experiments result in a considerable amount of free tacn, tren and bamp, respectively in the samples.

Although all of the samples photolysed show evidence of Co(II) in their ^{1}H NMR spectra, there is little evidence of the PMG or IDA ligand being released into solution. The ^{31}P NMR spectrum of the $[Co(tren)(PMGH)]Cl_2 \cdot 0.5CH_3OH$ complex after nine hours of photolysis does show a peak at 8.9 ppm, which could possibly correspond to free PMG. However, contrary to this, the ^{13}C NMR spectrum obtained at the same time interval shows no evidence of free PMG. On the basis of phosphorus NMR being a more sensitive technique than ^{13}C NMR spectroscopy, it is possible that free PMG is present.

Another possible result of these photolysis experiments is the decarboxylation of the five-membered chelate ring formed by PMG or IDA. This can lead to the eventual formation of a carbinolamine. There is evidence in the ^{13}C NMR spectra of carbinolamine species in all of the photolysates. These compounds give rise to signals between 85 and 90 ppm in the ^{13}C NMR spectra. In the complexes tested in this research, the carbinolamine may be either coordinated (tacn and bamp complexes) or non-coordinated (tren complex). The carbinolamine species can be formed when a three-membered Co-C-N ring undergoes reductive elimination to form an imine, then hydration.

The development of such ring would lead to a change in chemical shift of the methylene carbon atom that bonds to the cobalt centre to form the Co-C-N species. In Telfer's[41] experiment involving the photolysis of $[Co(dpg)(phen)]^{2+}$ complex to yield a Co-C-N ring (Section 3.2), the signal representing the methylene carbon underwent an upfield shift of 24.6 ppm. The photolysis of other complexes by Telfer[41] led to the upfield movement of the signals for the methylene carbon atoms of 18.5 and 21.4 ppm. We used these outcomes as a yardstick by which to measure our results, but no Co-C-N rings that were sufficiently long-lived to be detectable by NMR spectroscopy were evident in the photolysates of our complexes.

It is possible that the cyclic carbinolamine (Figure 3.18) is a product of photolysis of the $[Co(tren)(PMGH)]Cl_2 \cdot 0.5CH_3OH$ complex. A search of SciFinder Scholar, an international, online database of chemical compounds and literature, was undertaken. The search for the cyclic carbinolamine was unsuccessful, as the compound has not been documented. Thus, we are not able to obtain NMR spectroscopic data on the compound, but this would be a useful measure by which to identify the peaks the compound may give rise to in the NMR spectra of the photolysed complexes.

Most of the complexes tested photolytically appear to be fairly robust against these conditions, compared with the results of the UV irradiation of other amino acid complexes. The $[Co(dpg)(phen)]^{2+}$ complex described in Figure 3.3 (Section 3.2) required photolysis for only 80 minutes to yield the decarboxylated product.[41] The complexes tested in our research appear to require hours of irradiation with UV light before broadening of the signals in the ^{1}H NMR spectra and a decrease in the intensity of the carbonyl peaks in the ^{13}C NMR spectra is observed.

We have attempted to explain the development of the new signals in the ^{1}H, ^{13}C, and ^{31}P NMR spectra of the photolysates, but many of these remain unassigned. Therefore, our understanding of the chemistry that is occurring within the complexes is incomplete.

3.3 Reaction of Complexes Under Basic Conditions

During the first attempts by Hartshorn[39] to synthesise the complex $[Co(tren)(IDAH)]^{2+}$, it was found that the complex was pH-sensitive (this topic was introduced in Section 1.4.1). If the synthesis was carried out at a pH greater than 8, *N*-dealkylation of the coordinated IDA ligand occurred. The result was the production of the $[Co(tren)(gly)]^{2+}$ complex. It appeared that the IDA ligand was undergoing some kind of bond cleavage to yield glycine. It was thought that this cleavage was occurring in the IDA after coordination, and not to the free IDA before coordination took place (it was found in a separate experiment that free IDA was unreactive under basic conditions). To support the notion that it was the coordinated ligand that reacted under basic conditions, Hartshorn successfully prepared the $[Co(tren)(IDAH)]^{2+}$ complex at a lower pH then subjected it to a pH greater than 8. The same result was obtained as in the first instance, *i.e.* the IDA ligand underwent *N*-dealkylation to yield the $[Co(tren)(gly)]^{2+}$ complex. The conclusion was made that it was the coordinated, and not free, IDA that reacted to the basic conditions. This is in line with expectation, since coordinated ligands are generally more reactive than the free species.

This result sheds some light on the reactions that other IDA complexes and its related compounds might undergo when deprotonated. PMG is structurally related to IDA, as was covered in Section 1.4.1, and it seems justifiable that coordinated PMG could undergo similar reactivity when deprotonated.

To test the reactivity of glyphosate that has lost a proton from an α-carbon, it is necessary to use a PMG-containing species where deprotonation of the ligand is relatively easy. For this, we need to test such complexes as were described in Chapter 2. These complexes contain coordinated PMG or IDA. It is likely that coordinated PMG/IDA is more reactive than the free ligands towards deprotonation. A coordinated species such as PMG or IDA shares some of the positive charge of the metal centre, and it becomes easier to deprotonate an α-carbon on the ligand.

Deprotonation of a substance is often the first step in a chemical reaction. Hence, if coordination of PMG to a metal centre facilitates the deprotonation of the ligand it is

possible that further reactions of the ligand can occur. Such further reactions could be significant factors in the degradation of PMG.

During the studies into the base-induced dealkylation of the $[Co(tren)(IDAH)]^{2+}$ complex[39] it was found that the addition of sacrificial Co(III) complexes increased the yield of the $[Co(tren)(gly)]^{2+}$ product. Examination of Figure 1.29 in Section 1.4.1 shows that the mechanism of the dealkylation process includes the oxidation of the amine group of the IDA ligand to an imine. This oxidation is a two-electron process – the Co(III) of the $[Co(tren)(IDAH)]^{2+}$ complex could accept one electron from the ligand, but at some stage another Co(III) centre is required to accept the second electron from the ligand. Therefore, to allow a similar reaction to occur in our complexes we need to supply an excess of oxidant to the reaction mix, particularly if we hope to isolate Co(III) complexes. For this work, the $[Co(tren)Cl_2]Cl{\cdot}H_2O$ complex is an ideal choice of oxidant, and has the additional benefit of being relatively cheap and easy to prepare. This complex was present in excess quantity in all the reactions described below.

The Co-PMG complexes described in Chapter 2 were subjected to basic conditions during this component of the research. The pH of the reaction solutions was raised with aqueous sodium hydroxide, and $[Co(tren)Cl_2]Cl{\cdot}H_2O$ was added as a sacrificial metal complex. These experiments were carried out with the aim of exploring how these complexes, and the ligands they consist of, might behave under basic conditions.

3.3.1 Results and discussion

Provided below are the observations of the reactions of the complexes under basic conditions, and an interpretation of the NMR data obtained from these. A discussion of the results is presented in Section 3.3.2.

3.3.1.1 Base reaction of [Co(tacn)(PMG)]Cl·HCl·2.5H_2O

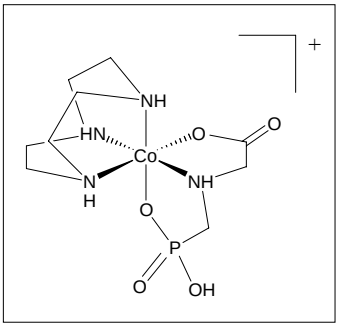

The aqueous mixture of the [Co(tacn)(PMG)]Cl·HCl·2.5H_2O and [Co(tren)Cl_2]Cl·H_2O complexes was adjusted to a pH of 9.5. The mixture was then placed on a steam bath for three hours, then cooled, acidified, and loaded onto a Dowex ion exchange column. Elution with HCl solution began, and two main pink bands developed. The ^{13}C NMR spectrum of the first dried band found it to be starting material, *i.e.* [Co(tacn)(PMG)]$^+$, while the second band was found to be [Co(tren)Cl_2]Cl·H_2O. Two minor bands that proved to be Co(II) also eluted from the column. The presence of Co(II) is indicated by the colour change of the band upon drying – usually from a shade of purple or yellow to a green/blue colour. The retrieval of the starting material ([Co(tacn)(PMG)]Cl·HCl·2.5H_2O) informs us that this complex is not reactive at pH 9.5.

3.3.1.2 Base reaction of [Co(tacn)(PMG)$ZnCl_3$]·3H_2O

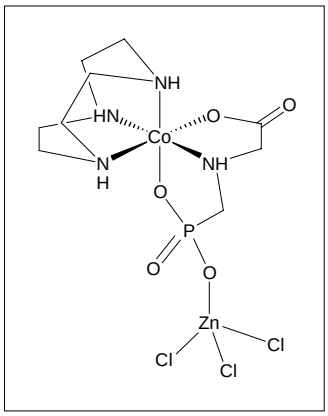

A similar procedure to the reaction of [Co(tacn)(PMG)]Cl·HCl·2.5H_2O under basic conditions was carried out for this complex.

At the end of the heating the reaction solution on a steam bath, it was noticed that a precipitate, most likely $Zn(OH)_2$, had formed in the reaction vessel. The precipitate dissolved when the pH was adjusted to 2.

Column chromatography yielded two major bands: the ^{13}C NMR of the first band showed it to be the [Co(tacn)(PMG)]$^+$ starting material, while the second band was proven to be [Co(tren)Cl_2]Cl·H_2O. A small amount of Co(II) was also isolated from the column.

The NMR results of this experiment indicate that the [Co(tacn)(PMG)$ZnCl_3$]·3H_2O complex is not reactive when subjected to a pH of 9. As expected, given the similarity

between this complex and [Co(tacn)(PMG)]Cl·HCl·2.5H_2O (the reason behind this similarity was explained in Section 3.2.1.2), the results for the two reactions are identical.

3.3.1.3 Base reaction of [Co(tren)(PMGH)]Cl_2·0.5CH_3OH

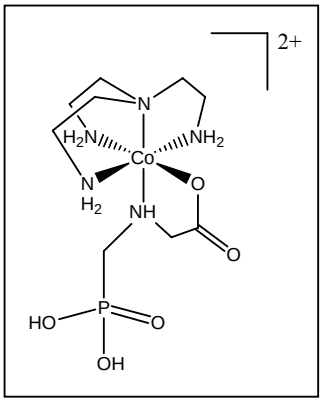

Storer[40] originally carried out this reaction, but duplication of the procedure was needed to ensure reproducibility of the results obtained.

An aqueous solution of [Co(tren)(PMGH)]Cl_2·0.5CH_3OH and [Co(tren)Cl_2]Cl·H_2O complexes was adjusted to a pH of 9.5, before being heated for three hours then cooled, acidified, and eluted on a ion exchange column. The main bands to elute were shown, *via* NMR, to be [Co(tren)(PMGH)]$^{2+}$, [Co(tren)Cl_2]$^{+}$ and a small amount of decomposition matter (Co(II)).

In agreement with the results documented by Storer,[40] the [Co(tren)(PMGH)]Cl_2 complex is not reactive at pH 9.5.

3.3.1.4 Base reaction of [Co(bamp)(PMG)]Cl·2.5H_2O

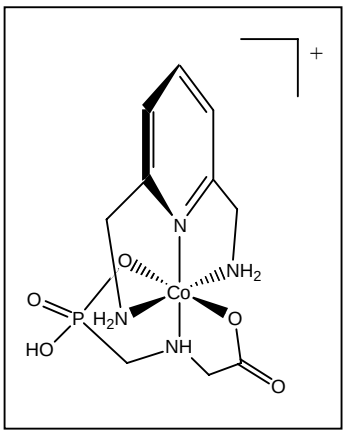

The [Co(bamp)(PMG)]Cl·2.5H_2O complex and [Co(tren)Cl_2]Cl·H_2O were dissolved in water and the pH was adjusted to 9.5. This task proved to be challenging as the pH had a tendency to drop rapidly upon the addition of base. After ten minutes of heating the pH had decreased to 6.4 – it was adjusted to 9.5 before heating for a further three hours. The solution was cooled, acidified, and loaded onto a Dowex column. When elution with HCl was initiated one major orange band developed. The ^{13}C NMR spectrum of the band showed it to be a mixture of compounds.

It is not evident what species are present in the main band. We can rule out free bamp, free PMG and starting material ([Co(bamp)(PMG)]Cl·2.5H_2O), as the spectrum does not display peaks representative of these three species. This is not to say that free bamp and PMG were not produced during the reaction: being colourless species, they would not have intentionally been collected from the chromatography column.

3.3.1.5 Base reaction of [Co(bamp)(IDA)]Cl

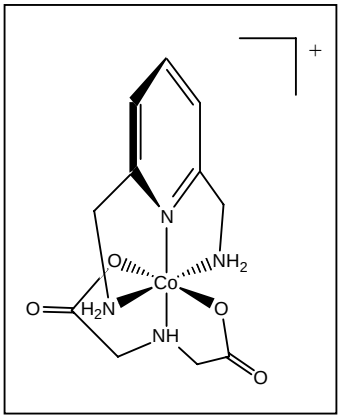

A solution of [Co(bamp)(IDA)]Cl and [Co(tren)Cl_2]Cl·H_2O was adjusted to a pH of 9.5 and heated for three hours on a steam bath. Half an hour into the reaction time the pH of the solution had dropped to 6.5, and the solution was readjusted to pH 9.5 before heating continued. The solution was cooled, diluted, and loaded onto a Dowex column. The major band to leave the column was red-brown in colour. The ^{1}H NMR spectrum of the band shows significant broadening of the peaks, signifying the presence of Co(II). The ^{13}C NMR spectrum of the dried band proved it to be a mixture of products.

The main band to leave the column showed no evidence of containing [Co(bamp)(IDA)]Cl, indicating that the complex has undergone degradation of some kind.

There is there is an indication in the ^{13}C NMR spectrum that $[Co(tren)(gly)]^{2+}$ has been produced. The ^{13}C NMR spectrum of a freshly prepared sample of $[Co(tren)(gly)]^{2+}$ was obtained to verify these results. The ^{13}C NMR spectrum of the product of the base reaction exhibits five peaks that closely match that of $[Co(tren)(gly)]^{2+}$. A peak at 187.3 ppm can be assigned to the carbonyl carbon atom of coordinated glycine, while the signal at 49.3 ppm possibly corresponds to the methylene carbon atom of the glycine. Two peaks with a 2:1 intensity ratio, at 64.4 and 61.7 ppm, probably represent the carbon atoms next to the tertiary amine of the coordinated tren ligand. Another set of peaks, also with a 2:1 ratio, appearing at 48.2 and 47.6 ppm, are likely to correspond to the carbon atoms neighbouring the primary amines of the coordinated tren ligand.

A signal observed in the band, at 185.3 ppm, suggests the presence of another carbonyl-containing compound. This peak appears at the same chemical shift as the carbonyl atoms of the coordinated IDA ligand in the starting material. However, since the remainder of the signals for the $[Co(bamp)(IDA)]^+$ complex are absent from the ^{13}C NMR spectrum, it is probable that the complex has decomposed. It is possible that the signal is due to the presence of one of the isomers of the $[Co(bamp)(gly)Cl]^+$ complex (this complex can exist as two isomers – the amine of the glycine ligand can attach in a *cis* or *trans* fashion with respect to the quaternary nitrogen atom of the bamp ligand).

3.3.1.6 Reactivity of [Co(tpa)(PMGH)]Cl$_2$

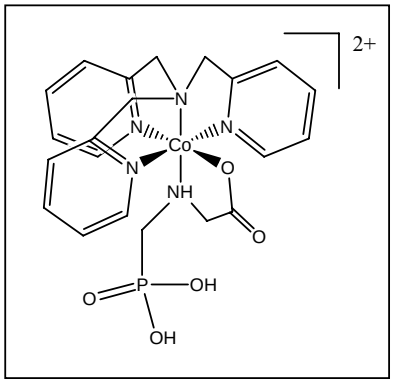

Initial attempts to synthesise this complex were unsuccessful when carried out at a pH of 7. As described in Chapter 2, the synthesis was only fruitful when the pH was maintained at a value of 6. It appears that this complex is very sensitive to the slightest of basic conditions. After the complex was isolated from the chromatography column, it exhibited great instability when dried down. At first, it was thought that the complex was being oxidised by atmospheric oxygen, but even samples of the complex held under an inert atmosphere, *i.e.* argon, underwent rapid decomposition.

Attempts to grow crystals, *via* vapour diffusion and slow evaporation, for X-ray crystallographic structure determination resulted in the decomposition of the complex. This was first evident by the colour change of the samples used – a change from orange-peach to purple-blue. The ^{13}C NMR spectrum of the decomposed complex exhibits a great deal of symmetry. It can be deduced from these results, and from the outcome of the mass spectrometry on the sample, that the $[Co(tpa)(PMGH)]Cl_2$ complex has undergone ligand exchange to form $[Co(tpa)(H_2O)_2]^{3+}$. These results were discussed briefly in Section 2.2.4.2. It appears that the PMG ligand may have fallen off the cobalt centre, to be replaced by two water molecules, while the tpa has remained in its original tripodal position. From examination of the ^{13}C NMR spectrum it could be deduced that the PMG ligand has decomposed, as there are no signals present at all that correspond to the free

ligand. This is in contrast to the ^{31}P NMR spectrum of the decomposed sample that shows one major, but broad, signal at 9.0 ppm, the chemical shift for the phosphorus atom of the free PMG species. This discrepancy is possibly due to the sensitivity of the ^{31}P NMR technique compared to its ^{13}C counterpart, so it is quite possible that free PMG is in fact present in the band.

With regard to the instability of the $[Co(tpa)(PMGH)]Cl_2$ complex, it can be postulated that this complex would be very reactive when subjected to basic (and photolytic) conditions. It is difficult to speculate, however, whether the decomposition of the complex would lead to the degradation of the PMG ligand.

3.3.1.7 Reactivity of [Co(bpa)(IDA)]Cl

The attempts to synthesise $[Co(tpa)(IDAH)]^{2+}$ were described in Section 2.2.6.1. It was documented that the synthesis was unsuccessful at pH 7, resulting in a large amount of decomposition material and some free tpa ligand. A repeat of the synthesis with the pH maintained at 6 appeared to be more successful, leading to the isolation and characterisation of the $[Co(bpa)(IDA)]^+$ complex.

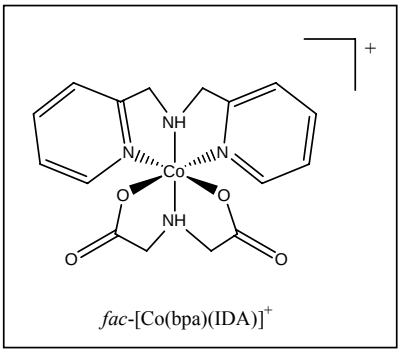

fac-$[Co(bpa)(IDA)]^+$

3.3.2 Summary of reaction of complexes under basic conditions

The results of the reactions of the complexes under basic conditions are outlined in Table 3.2.

Complex	Charge on complex when in base	л-acidic ancillary ligand?	Reaction products
$[Co(tacn)(PMG)]Cl{\cdot}HCl{\cdot}2.5H_2O$	0	no	Major: $[Co(tacn)(PMG)]^{+}$
$[Co(tacn)(PMG)ZnCl_3]{\cdot}3H_2O$	0	no	Major: $[Co(tacn)(PMG)]^{+-}$
$[Co(tren)(PMGH)]Cl_2{\cdot}0.5CH_3OH$	0	no	Major: $[Co(tren)(PMG)]^{2+}$
$[Co(bamp)(PMG)]Cl{\cdot}2.5H_2O$	0	yes	Unknown
[Co(bamp)(IDA)]Cl	1+	yes	Major: $[Co(tren)(gly)]^{2+}$

Table 3.2: A summary of the results of the reactions on the complexes at pH 9.5.

It appears, from the reactions carried out at elevated pH, that the type of ancillary ligand attached to the complex, and the ease with which the PMG or IDA can be deprotonated, might govern the reactivity of the complexes.

It was found that the complexes with amine-containing ancillary ligands, such as $[Co(tacn)(PMG)]Cl{\cdot}HCl{\cdot}2.5H_2O$, $[Co(tacn)(PMG)ZnCl_3]{\cdot}3H_2O$ and $[Co(tren)(PMGH)]Cl_2{\cdot}0.5CH_3OH$ were non-reactive at pH 9.5.

Meanwhile, the two complexes with pyridine-containing ancillary ligands, $[Co(bamp)(PMG)]Cl{\cdot}2.5H_2O$ and [Co(bamp)(IDA)]Cl, did react at pH 9.5. Similarly, the synthesis of the $[Co(tpa)(PMGH)]Cl_2$ complex was found to be a pH-sensitive reaction, in that if the synthesis was carried out at a pH greater than 6, decomposition of the complex occurred. This suggests that the $[Co(tpa)(PMGH)]Cl_2$ complex is also susceptible to basic conditions. The tpa ligand is also a pyridine-containing ligand, a detail that supports the postulate that such ligands might promote the degradation of $[Co(L)(PMG)]^{n+}$ or $[Co(L)(IDA)]^{n+}$ complexes at elevated pH.

It is possible that the π-acidity of the pyridine-containing ligands is the basis for the reactivity of the complexes consisting of these ligands. Figure 3.17 depicts the possible

mechanism that may occur when $[Co(L)(PMG)]^{n+}$ or $[Co(L)(IDA)]^{n+}$ complexes are subjected to base.[39]

When L_m is π-acidic, *e.g.* bamp or tpa, the electron-accepting nature of the ligand stabilises the Co(II) species shown in Figure 3.17. Step 2 will probably be relatively fast as the π-acidic ligands make electron transfer easier. This implies that there will be little carbanion present in the reaction, so the reverse of Step 1 is a trivial contribution to the process occurring.

In complexes with amine-containing ancillary ligands such as tacn and tren, Step 2 is likely to be slower due to the lack of π-acidity of the ligands. Thus, the reverse of Step 1 is probably a significant step, and this may help explain why such complexes are not reactive under basic conditions.

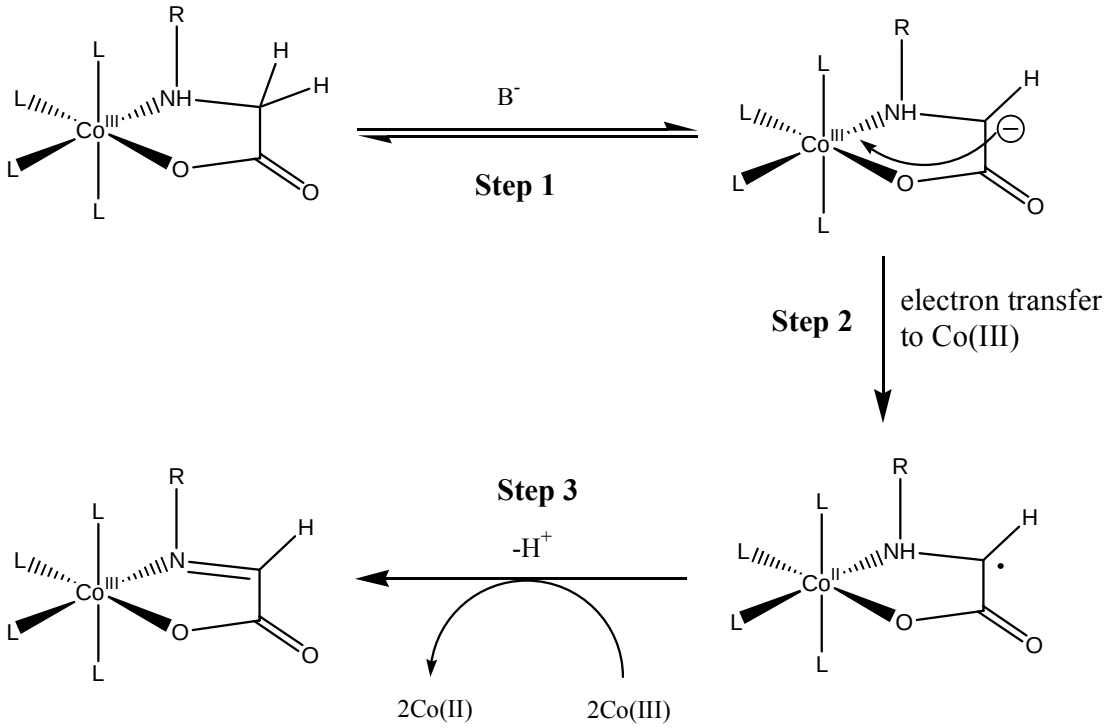

Figure 3.17: Possible steps in the treatment of $[Co(L_m)(PMG)]^{n+}$ and $[Co(L_m)(IDA)]^{n+}$ with base (m = 3 or 4 depending on ancillary ligand used, R = $CH_2PO_3H_2$ (PMG complexes) or CH_2CO_2H (IDA complexes)).

It was found in this research that PMG-containing complexes are less reactive than IDA-containing complexes, *e.g.* $[Co(bamp)(PMG)]Cl{\cdot}2.5H_2O$ was less reactive in basic conditions than [Co(bamp)(IDA)]Cl. There was no evidence of $[Co(tren)(gly)]^{2+}$ being

produced in the reaction of [Co(bamp)(PMG)]Cl·2.5H_2O, whereas this was a major product in the similar reaction of [Co(bamp)(IDA)]Cl. This trend of coordinated IDA being more reactive than coordinated PMG has been reflected in the tren system,[39,40] and can possibly be explained on account of charge difference between the PMG and IDA ligands.

PMG has three acidic protons, while IDA has two. Figure 3.18 depicts two complexes comprising these ligands, and the resulting charge on the complexes when placed in base.

It is possibly easier to deprotonate the IDA complex ('b', Figure 3.18) at the α-carbon due to its positive charge. The PMG complex, 'a', is neutral and will be less likely to deprotonate. Thus, the forward reaction of Step 1 in Figure 3.17 will be more likely to occur in the IDA complex. This perhaps helps to explain the difference in reactivity of the two ligands when coordinated to cobalt and subjected to basic conditions.

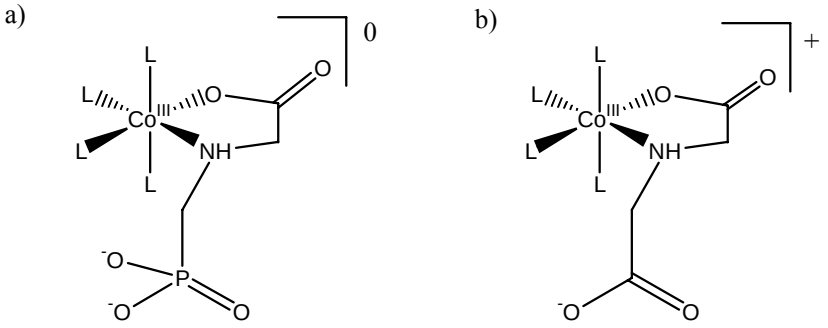

Figure 3.18: a) a [Co(L_4)(PMG)] complex. The deprotonated complex is neutral; b) a [Co(L_4)(IDA)]$^+$ complex, with a 1+ charge when deprotonated.

When [Co(bamp)(IDA)]Cl reacts under basic conditions and in the presence of [Co(tren)Cl_2]$^+$ it is not known what mechanism is occurring. We do know, however, that the result is [Co(tren)(gly)]$^{2+}$. There are two possible processes that could occur: a) the coordinated IDA is oxidised to an imine which then falls off the cobalt centre. The free imine perhaps undergoes hydrolysis to give glycine, which then coordinates to a cobalt-tren complex to give [Co(tren)(gly)]$^{2+}$ (this is similar to Pathway B, Figure 1.29); b) the IDA falls off the [Co(bamp)(IDA)]$^+$ complex and coordinates to a cobalt-tren species. The [Co(tren)(IDAH)]$^{2+}$ complex that results could then react under basic conditions to give [Co(tren)(gly)]$^{2+}$ (Pathway A or B, Figure 1.29).

3.4 Conclusions and Future Work

The research portrayed in this chapter has involved the photolytic and deprotonation studies of some of the complexes previously described in Chapter 2.

It is evident that the photolysis reactions result in the decomposition of the complexes and possibly the PMG and IDA ligands. This conclusion has been aided by the scrutiny of NMR data. The loss of carbonyl peaks (suggesting decarboxylation), the decrease in intensity of starting material (evidence that reaction of some kind is occurring), and the development of new peaks in the ^{13}C NMR spectra imply that the complexes may undergo decarboxylation, then formation of a short-lived Co-C-N metallacycle, then degradation of the metallacycle to a carbinolamine.

The reactions under basic conditions have shown a dependence on the nature of the ancillary ligand present, and a general charge-reactivity relationship. Complexes containing л-acidic ancillary ligands seem to be more reactive than complexes with amine-containing ligands, and PMG complexes appear to be less reactive than their IDA counterparts.

To allow more conclusions to be drawn, further work needs to be completed in the area of glyphosate reactivity. A repeat of the photolysis experiments on a larger scale than those described in this thesis is possibly a sensible road to take. Column chromatography of the photolysates to separate their components would be a good method of further characterising what species may occur under photolytic conditions. If X-ray crystal structure determination of the components can be obtained, this would be a reliable way of determining their nature.

The preparation of the cyclic carbinolamine, depicted in Figure 3.19, might help with the assignment of the unknown peaks in the ^{13}C and ^{31}P NMR spectra from the photolysis experiments. Thus far, here is no report on the synthesis of this cyclic compound on the database SciFinder Scholar.

The synthesis of a cobalt-tren-diester species (Figure 3.19) would be an obvious objective in terms of future studies of glyphosate under basic conditions.

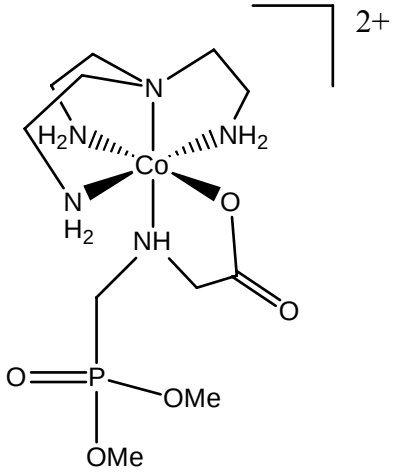

Figure 3.19: The $[Co(tren)diester]^{2+}$ species.

The outcome of reacting a cobalt-tren-diester complex under basic conditions might give us an insight into the significance of any deprotonation steps that occur when glyphosate degrades. We know that $[Co(tren)(PMGH)]^{2+}$ is unreactive under basic conditions, and that this may be due to its charge (when initially placed in base the phosphonate group deprotonates, yielding a neutral complex). A diester species as depicted above is not prone to deprotonation when first subjected to base, and would retain its 2+ charge. This charge may make it easier to deprotonate an α-carbon which might lead to the reactivity of the diester ligand. On this account, it would be expected to be more reactive than its $[Co(tren)(IDAH)]^{2+}$ equivalent. However, it is also possible that the esters could hydrolyse under basic conditions, so this experiment may prove futile.

A comparison of the reactivities of $[Co(tren)(PMGH)]^{2+}$ and a $[Co(tren)(diester)]^{2+}$ species when subjected to base would allow us to investigate the charge-reactivity relationship that may exist between them. The results of such research may give us an indication as to how important the deprotonation of PMG (and glyphosate) is in terms of its degradation.

The preparation of $[Co(tacn)(IDA)]^{+}$ would allow us to test this complex under basic conditions. We could then compare the results with its PMG-containing equivalent, which showed no reactivity when subjected to base. It is probable that $[Co(tacn)(IDA)]^{+}$ would

be reactive under these conditions on account of it containing the more reactive IDA ligand.

Further study of the bamp complexes under basic conditions is necessary to determine the chemistry that is occurring in this system. A repeat of the reaction of the [Co(bamp)(PMG)]Cl·2.5H_2O complex at pH 9.5 might help to identify the products that occur. In this research, the base reaction of [Co(bamp)(IDA)]Cl in the presence of [Co(tren)Cl_2]Cl·H_2O yielded $[Co(tren)(gly)]^{2+}$. Repeating the reaction in the absence of [Co(tren)Cl_2]Cl·H_2O could give us more information on the mechanisms occurring.

A repeat of the synthesis of the $[Co(tpa)(PMGH)]^{2+}$ and $[Co(bpa)(IDA)]^{+}$ complexes, plus their IDA and PMG counterparts (respectively), would enable us to explore the reactivities of these complexes and make comparisons between them.

It is hoped that the outcome of this research will be an increased understanding of the degradation processes of PMG, and that the results obtained can be applied to the mechanisms that occur when Roundup® herbicide degrades in nature.

Chapter 4 - Experimental

4.1 Materials and Methods

Reagent-grade solvents and reagents were purchased from a commercial supplier and were used in the syntheses and reactivity experiments without purification. Dowex 50W-X2 ion-exchange resin was used in column chromatography procedures. The column dimensions are given as height × diameter. A Buchi rotary evaporator equipped with a vacuum pump and water bath (< 40°C) was used to remove solvent from solutions. For the photolysis of the complexes a high-pressure mercury lamp equipped with a 254 nm transmission Pyrex filter (Corning, 7-54) was used.

4.2 Measurements

^{1}H, ^{13}C and ^{31}P NMR spectra were recorded at 23°C on a Varian Unity 300 Spectrometer with a broadband probe. D_2O was used as a solvent, and sodium trimethylsilyl-1-propanesulfonate (TPMS, δ 0, singlet) was used as an internal reference for ^{1}H and ^{13}C NMR spectroscopy. ^{31}P NMR chemical shifts were reported relative to external 85 % H_3PO_4. The University of Otago Microanalytical Service performed elemental analyses. A Varian Cary 50-Probe Uv/vis spectrometer was used to record UV/vis spectra of the complexes dissolved in 0.01 M HCl solution. The data is reported in the format of λ_{max} (ε_{max}, L $mol^{-1}cm^{-1}$). The mass spectrometry experiments were run on a Micromass LCT coupled to a Waters 2790 LC.

4.3 Synthesis of Complexes

Unless otherwise stated, the syntheses of the complexes all followed the same basic procedure: an aqueous solution of the starting material and phosphonomethylglycine isopropylamine was adjusted to a pH of 7 with 4 M NaOH solution and heated on a steam bath. The pH was readjusted to 7 after 10 min, after a further 30 min, and finally after a further 60 min. Heating continued for a total of 3 hr. The reaction solution was cooled,

acidified to pH 2 with 3 M HCl solution. The solution was loaded onto a Dowex 50W-X2 column and elution with HCl solution promoted the development of bands on the column.

4.3.1 [Co(tacn)(PMG)]Cl·HCl·2.5H_2O

[Co(tacn)Cl_3][46] (2.07 g, 7.2 mmol) and 40 % phosphonomethylglycine isopropylamine solution (11.57 g, 20 mmol) were dissolved in 85 mL H_2O to give a green slurry. The slurry soon became a solution upon heating. After 3 hr reaction time, the solution was loaded onto a Dowex column (150 × 50 mm). Good band separation occurred with elution of 0.5 M HCl solution. The first band to leave the column was minor and pink in colour and was discarded. The second and major band was dried down on a rotary evaporator to give bright pink crystals. Yield 2.48 g (73 %). ^{13}C NMR: δ 187.0, 60.6, 56.8, 54.5, 53.5, 52.9, 52.3, 51.5, 50.9. ^{31}P NMR: δ 38.4. Calc. for [$CoC_9H_{21}N_4PO_5$]Cl·HCl·2.5H_2O: C 22.90, H 5.56, N 11.89. Found: C 23.22, H 5.69, N 11.74%. UV/vis: 355 nm (68), 500 nm (37). TOF MS ES+ *m/z (%)*; 355.1185 (100) M^+ $CoPN_4O_5C_9H_{21}$.

4.3.2 [Co(tacn)(PMG)$ZnCl_3$]·3H_2O

Crystals of [Co(tacn)(PMG)$ZnCl_3$]·3H_2O were prepared according to a literature procedure,[47] using [Co(tacn)(PMG)]Cl·HCl·2.5H_2O as a starting material. The crystals were grown from slow evaporation and from vapour diffusion of acetone into an aqueous, acidified (1 M) solution of the complex. Both methods yielded crystals that were of ideal quality for analytical studies. ^{13}C NMR: δ 187.0, 60.7, 54.6, 53.6, 53.0, 52.4, 51.6, 51.0. ^{31}P: δ 38.3. Calc for [$CoZnC_9H_{20}N_4PO_5Cl_3$]·3H_2O: C 18.67, H 4.52, N 9.67. Found: C 18.43, H 4.43, N 9.30. UV/vis: 355 nm (98), 500 nm (61). TOF MS ES+ *m/z (%)*; 355.1185 (100) M^+ $CoPN_4O_5C_9H_{20}$.

4.3.3 [Co(dien)(PMG)]Cl

[Co(dien)Cl_3][48] (1.4 g, 5.2 mmol) and phosphonomethylglycine isopropylamine solution (4.76 g, 8.3 mmol) were dissolved in 75 mL water to give a red-brown solution. When the reaction was complete, the solution was deep cherry red in colour. The diluted solution

was loaded onto a Dowex column (150 × 50 mm). Elution with 0.5 M HCl solution led to the good separation of three bands. The first and major band was removed with 0.5 M HCl solution and was cherry red in colour. The band was dried to a red solid on a rotary evaporator. Yield 2.14 g (113 %). The ^{13}C NMR spectrum showed the band to be a mixture of isomers and that it was contaminated with isopropyl ammonium ion. Various chromatographic methods were used in attempts to separate the isomers and free the band of its contaminant. Efforts to separate the isomers were unsuccessful. Yield 1.4 g (74 %). ^{13}C NMR: δ 185.2, 184.6, 59.9, 59.7, 59.5, 59.4, 53.4, 53.3, 53.0, 52.8, 51.5, 51.2, 50.2, 50.1, 49.9, 49.6, 49.3. ^{31}P NMR: δ 38.3, 37.3. UV/vis: 365 nm (0.899), 525 nm, (0.178). TOF MS ES+ m/z (%); 329.1016 (100) M^+ $CoPN_4O_5C_7H_{19}$.

4.3.4 [Co(tren)(PMGH)]Cl_2·0.5CH_3OH

This complex was synthesised according to a previously described method,[40] so that further characterisation and reactivity studies could be carried out. [Co(tren)Cl_2]Cl·H_2O[50] (9.69 g, 29 mmol) and phosphonomethylglycine isopropylamine (24.69 g, 43 mmol) were dissolved in 300 mL water. After the reaction was complete the cooled and acidified solution was loaded onto a Dowex column (300 × 50 mm). The first and major orange band was dried to an orange solid. Yield 3.56 g (28 %). ^{13}C NMR: δ 185.1, 64.7, 64.5, 62.2, 59.8, 59.7, 54.5, 52.7, 48.2, 47.4, 47.0. ^{31}P NMR: δ 12.1. Calc. for [$CoC_9H_{24}PO_5N_5$]Cl_2·0.5H_2O: C 24.80, H 5.91, N 15.22. Found: C 24.51, H 6.20, 14.88.

4.3.5 [Co(tpa)(PMGH)]Cl_2

Initial attempts to synthesise this complex were carried out at pH 7 and were unsuccessful. Repeating the procedure at pH 6 resulted in the successful synthesis of the complex.

40 % phosphonomethylglycine isopropylamine solution (4.3 g, 7.5 mmol) and [Co(tpa)Cl_2]ClO_4 (2.39 g, 4.6 mmol) were dissolved in water (40 mL) to give a purple solution. The pH of the solution was adjusted to 6 with 4 M NaOH and the solution was placed on a steam bath. After the reaction time was reached, the dark brown solution was cooled, diluted and acidified before being loaded onto a Dowex column (150 × 50 mm). Elution with 0.5 M HCl began, and four major bands developed. The first, third and

fourth bands were found to be either free tpa ligand or $[Co(tpa)Cl_2]^+$. The second band was yellow in colour, and was dried down to give an orange oil. Yield 0.4 g (15 %). ^{13}C NMR: δ 184.7, 165.1, 164.6, 164.0, 153.0, 151.5, 145.5, 145.4, 143.9, 131.0, 130.5, 129.8, 128.7, 128.5, 124.5, 74.9, 72.1, 71.7, 59.5. TOF MS ES+ m/z (%); 516.1371 (10) M^{++} $CoPN_5O_5C_{21}H_{24}$.

4.3.6 [Co(bamp)(PMG)]Cl·2.5H$_2$O

$[Co(bamp)Cl_3]$ (2.31 g, 7.6 mmol) and 40 % phosphonomethylglycineisopropylamine solution (15 g, 26.0 mmol) were dissolved in 100 mL water to give a brown slurry. When the synthesis was completed, the acidified and diluted solution was loaded onto a Dowex column (150 × 50 mm) and elution with HCl began. One major, dark red band eluted quickly from the column and was dried on a rotary evaporator. NMR studies proved the complex to be contaminated with isopropylammonium ion, so the band was rechromatographed and found (*via* ^{13}C NMR spectroscopy) to be free of contaminant. Yield 1.2 g (38 %). ^{13}C NMR: δ 184.5, 165.8, 165.7, 144.4, 124.0, 123.9, 59.4, 59.2, 55.0, 54.4, 51.0, 49.2. ^{31}P NMR: δ 36.0. Calc. for $[CoC_{10}H_{16}N_4PO_5]2.5H_2O$: C 29.53, H 5.20, N 13.7. Found: C 29.61, H 5.11, N 13.61. Uv/vis: 360 nm (182), 460 nm (120), 520 nm (129). TOF MS ES+ m/z (%); 363.0033 (100) M^+ $CoPN_5O_5C_{10}H_{16}$.

4.3.7 [Co(tpa)(IDAH)]Cl$_2$ and [Co(bpa)(IDA)]Cl

Initial attempts to synthesise the $[Co(tpa)(IDAH)]Cl_2$ complex at pH 7 were unsuccessful, the outcome being the production of free tpa. Repeating the procedure at pH 6 resulted in the successful synthesis of the [Co(bpa)(IDA)]Cl complex, and a small amount of the $[Co(tpa)(IDAH)]Cl_2$ species.

$[Co(tpa)Cl_2]ClO_4$ (2.58 g, 4.9 mmol) and iminodiacetic acid (2.65 g, 19.5 mmol) were dissolved in 50 mL water and the pH was adjusted to 6 with 4 M NaOH solution. The red-pink solution was placed on a steam bath. At the end of the reaction time, the diluted and acidified solution was loaded onto a Dowex column (150 × 25 mm) and elution with HCl began. The main band to leave the column was pink-purple in colour. The band was dried by rotary evaporation to give a purple solid. Yield 0.73 g (35 %)

([Co(bpa)(IDA)]Cl). ^{13}C NMR: δ 187.3, 186.4, 166.8, 166.7, 164.7, 164.6, 152.9, 150.7, 143.9, 143.8, 129.2, 128.7, 125.7, 64.3, 64.2, 63.5, 63.4, 62.7, 61.4. UV/vis: 342 nm (1.007), 474 nm (0.658). TOS MS ES+ m/z (%); 389.0194 (100) M^+ $CoN_4O_4C_{16}H_{17}$.

The second band to leave the column was pink-orange in colour and minor in quantity. The ^{13}C NMR spectrum of the band showed it to be a mixture of [Co(tpa)(IDAH)]Cl_2 (major) and another species. NMR data for [Co(tpa)(IDAH)]Cl_2: ^{13}C NMR δ 185.2, 153.7, 152.9, 151.3, 145.5, 145.4, 143.9, 130.9, 130.2, 129.7, 128.6, 128.5, 124.5, 74.9, 72.1, 71.9, 59.5, 58.7.

4.3.8 [Co(bamp)(IDA)]Cl

Initial attempts to synthesise this complex were carried out at pH 7 and were unsuccessful. Repeating the procedure at pH 6 resulted in the successful synthesis of the complex.

[Co(bamp)Cl_3] (0.51 g, 1.7 mmol) and iminodiacetic acid (1.02 g, 7.7 mmol) were dissolved in 25 mL H_2O, and the pH of the solution was adjusted to 6. The solution was placed on a steam bath. When the reaction time was over the solution was diluted, acidified and loaded onto a Dowex column (100 × 50 mm). One major, red band eluted from the column and was dried by rotary evaporation. Yield 0.43 g (70 %). ^{13}C NMR: δ 185.2, 165.8, 165.4, 144.3, 123.8, 58.4, 54.8, 54.3. UV/vis: 360 nm, 495 nm. TOF MS ES+ m/z (%); 327.0805 (100) M^+ $CoN_4O_4C_{11}H_{16}$.

4.4 Photolysis of the Complexes

A solution of each complex was dissolved in D_2O with an internal reference (TPMS) and placed in a glass quartz cuvette. Photolysis began with the lamp power set to 200 W, and ^{1}H NMR spectra were collected at regular intervals (*i.e.* half-hourly or hourly). If little change was observed in the ^{1}H NMR spectra after 2 or 3 hours the lamp power was increased to 500 W and photolysis continued. ^{1}H, ^{13}C, and ^{31}P (if required) spectra were collected at hourly intervals, or at longer intervals (*i.e.* 4 hourly) if the complex being monitored appeared to be slow to react.

Abbreviated results are presented in Table 3.1, while a more descriptive discussion into the results of the experiments is given in Section 3.2.

4.5 Reaction of the Complexes under Basic Conditions

The reactions of the complexes under basic conditions all followed the same procedure: A solution of the complex and excess $[Co(tren)Cl_2]Cl{\cdot}H_2O$ was adjusted to pH 9.5 with 4 M NaOH solution before being heated on a steam bath for three hours. The pH was adjusted from time to time and readjusted to 9.5 if necessary. When the reaction time was completed the solution was cooled, diluted and acidified to pH 2 with 3 M HCl solution before being loaded onto a Dowex 50W-X2 column. Elution with HCl solution was then initiated to induce band separation on the column.

4.5.1 $[Co(tacn)(PMG)]Cl{\cdot}HCl{\cdot}2.5H_2O$

$[Co(tacn)(PMG)]Cl{\cdot}HCl{\cdot}2.5H_2O$ (0.93 g, 2.8 mmol) and $[Co(tren)Cl_2]Cl{\cdot}H_2O$ (1.47 g, 4.5 mmol) were dissolved in water (100 mL) to give a purple solution, the pH of which was adjusted to 9.5 with 4 M NaOH solution. When the reaction was completed the solution was loaded onto a Dowex column (150 × 25 mm). Elution with HCl began and two major bands developed. The bands were removed with increasing concentrations of HCl solution, and dried on a rotary evaporator. The first band was pink and was shown, by ^{13}C NMR spectrosocpy, to be $[Co(tacn)(PMG)]^+$. The second, purple, band was found to be $[Co(tren)Cl_2]^+$.

4.5.2 $[Co(tacn)(PMG)ZnCl_3]{\cdot}3H_2O$

$[Co(tacn)(PMG)ZnCl_3]{\cdot}3H_2O$ (0.27 g, 0.5 mmol) and $[Co(tren)Cl_2]Cl{\cdot}H_2O$ (0.36 g, 1.0 mmol) were dissolved in 40 mL water to give a purple solution. The pH was adjusted to 9.5. After the reaction was completed the solution was loaded onto a Dowex column (100 × 25 mm). Elution with 0.5 M HCl solution saw the development of two major bands. The first band to elute was pink and was dried down on a rotary evaporator to give a pink solid. The solid was shown to be $[Co(tacn)(PMG)]^+$ by ^{13}C NMR. The second band was

also pink but dried down to give a purple solid. The ^{13}C NMR spectrum of the solid showed it to be $[Co(tren)Cl_2]^+$.

4.5.3 [Co(tren)(PMGH)]Cl_2·0.5CH_3OH

$[Co(tren)(PMGH)]Cl_2·0.5CH_3OH$ (1.75 g, 3.8 mmol) and $[Co(tren)Cl_2]Cl·H_2O$ (2.45 g, 7.4 mmol) were dissolved in 200 mL water. The pH of the solution was adjusted to 9.5. When the reaction time was over, the acidified solution was loaded onto a Dowex column (200 × 50 mm). Several bands developed when elution with 0.5 M HCl solution began, and were removed from the column with increasing concentrations of HCl. The major bands were taken to dryness by rotary evaporation. The ^{13}C NMR spectra showed the bands to be $[Co(tren)(PMGH)]^{2+}$ and $[Co(tren)Cl_2]^+$. The minor bands were found to be Co(II).

4.5.4 [Co(bamp)(PMG)]Cl·2.5H_2O

$[Co(bamp)(PMG)]Cl·2.5H_2O$ (0.52 g, 1.3 mmol) and $[Co(tren)Cl_2]Cl·H_2O$ (0.85 g, 2.6 mmol) were dissolved in water (80 mL) to give a purple solution. The pH was adjusted to 9.5 and the reaction was commenced. When the reaction time was complete, the cooled and acidified solution was loaded onto a Dowex column (70 × 25 mm). Elution with 0.5 M HCl solution began. One main orange band eluted from the column and was dried down. A ^{13}C NMR spectrum was obtained but it is not clear what the product is.

4.5.5 [Co(bamp)(IDA)]Cl

[Co(bamp)(IDA)]Cl (0.75 g, 1.8 mmol) and and $[Co(tren)Cl_2]Cl·H_2O$ (1.95 g, 6 mmol) were dissolved in 70 mL water. The pH of the solution was adjusted to 9.5 and the reaction was initiated. At the end of the reaction time the reaction solution was loaded onto a Dowex column (50 × 25 mm). One major, red-brown band developed when the column was eluted with 0.5 M HCl solution. The band was removed from the column and dried, and was found to consist of $[Co(tren)(gly)]^{2+}$ plus an identified complex.

References

1. C. K. Mathews, K. E. van Holde and K. G. Ahern, *Biochemistry***,** Addison-Wesley Publishing Company, 2000, p 762.
2. S. F. Araujo, R. T. R. Monteiro and R. B. Abarkeli, *Chemosphere*, 2003, **52**, 799-804.
3. F. Veiga, J. M. Zapata, M. L. Fernandez Marcos and E. Alvarez, *The Science of the Total Environment*, 2001, **271**, 135-144.
4. U. Cheah, R. C. Kirkwood and K. Lum, *J. Agric. Food Chem*., 1998, **46**, 1217-1223.
5. R. E. Hoagland, *Weed Sci.*, 1980, **28**, 393-400, and references therein.
6. J. E. Franz, M. K. Mao and J. A. Sikorski, *Glyphosate: a Unique Global Herbicide*, American Chemical Society, 1997.
7. S. M. Carlisle and J. T. Trevors, *Water, Air, and Soil Pollut*., 1988, **39**, 409-420, and references therein.
8. C. Accinelli, C. Screpanti, A. Vicari and P. Catizone, *Agric., Ecosystems and Environ.*, 2004, **103**, 497-507.
9. M. Klimek, B. Lejczak, P. Kafarski and G. Forlani, *Pest. Manag. Sci*., 2001, **57**, 815-821.
10. G. Forlani, A. Mangiagalli, E. Nielsen and C. M. Suardi, *Soil Biol. and Biochem*., 1999, **31**, 991-997.
11. J. P. Giesy, S. Dobson and K. R. Solomon, *Rev. Environ. Contam. Toxicol*., 2000, **167**, 35-120.
12. E. Mallat, D. Barcelo, *J. Chromatogr. A*, 1998, **823**, 129-136.
13. M. F. Zaranyika and M. G. Nyandoro, *J. Agric. Food Chem*., 1993, **41**, 838-842.
14. E. Grossbard and D. Atkinson, *The Herbicide Glyphosate*, Butterworth and Co. (Publishers) Ltd., 1985, and references therein.
15. N. A. Campbell, J. B. Reece and L. G. Mitchell, *Biology*, Addison Wesley Longman Inc., Menlo Park, CA, 1999.
16. P. Sprankle, W. F. Meggitt and D. Penner, *Weed Sci.*, 1975, **23**, 224-228.
17. D. L. Hensley, D. S. N. Beuerman and P. L. Carpenter, *Weed Res.*, 1978, **18**, 287-291.
18. P. Sprankle, W. F. Meggitt and D. Penner, *Weed Sci.*, 1975, **23**, 229-234.

19. Handbook of Chemistry and Physics, CRC Press, Inc., Boca Raton, Florida, 1983.
20. P. W. Stahlman and W. M. Phillips, *Weed Sci.*, 1979, **27**, 38-41.
21. P. J. Shea and D. R. Tupy, *Weed Sci.*, 1984, **32**, 802-806.
22. P. H. Smith and K. R. Raymond, *Inorg. Chem.*, 1988, **27**, 1056-1061, and references therein.
23. R. L. Glass, *J. Agric. Food Chem*., 1987, **35**, 497-500.
24. R. J. Hance, *Pestic. Sci*., 1976, **7**, 363-366.
25. L. C. Salazar and A. P. Appleby, *Weed Sci.*, 1982, **30**, 463-466, and references therein.
26. *Oxford Dictionary of Science*, Oxford University Press, Oxford, UK, 1999.
27. R. L. Haney, S. A. Senseman, F. M. Hons and D. A. Zuberer, *Weed Sci.*, 2000, **48**, 89-93.
28. N. S. Nomura and H. W. Hilton, *Weed Res.*, 1977, **17**, 113-121.
29. L. J. Moshier and D. Penner, *Weed Sci.*, 1978, **26**, 686-691.
30. L. Poznyak and V. I. Pavlovski, *Angew. Chem. Int. Ed. Engl.*, 1988, **27**, 789-796.
31. J. A. P. Marsh, H. A. Davies and E. Grossbard, *Weed Res.*, 1977, **17**, 77-82.
32. http://sis/agr.gc.ca/cansis/glossary/texture,_soil.html
33. G. Ye, P. T. J. Hajdukiewicz, D. Broyles, D. Rodriguez, C. W. Xu, N. Nehra and J. M. Staub, *The Plant Journal*, 2001, **25**, 261-273, and references therein.
34. W. P. Ridley, R. S. Sidhu, P. D. Pyla, M. A. Nemeth, M. L. Breeze and J. D. Astwood, *J. Agric. Food Chem*., 2002, **50**, 7235-7243.
35. D. S. Sagatys, C. Dahlgren, G. Smith, R. C. Bott and A. C. Willis, *Aust. J. Chem*, 2000, **53**, 77-81.
36. T. G. Appleton, K. A. Byriel, J. R. Hall, C. H. L. Kennard, D. E. Lynch, J. A. Sinkinson and G. Smith, *Inorg. Chem.*, 1994, **33**, 444-455.
37. E. Clarke, P. R. Rudolf, A. E. Martell and A. Clearfield, *Inorg. Chim. Acta*, 1989, **164**, 59-63.
38. D. Heineke, S. J. Franklin and K. N. Raymond, *Inorg. Chem.*, 1994, **33**, 2413-2421.
39. R. M. Hartshorn, *J. Chem. Soc., Dalton Trans*., 2002, **16**, 3214-3218.
40. M. K. Storer, Honours Thesis, Chemistry Department, University of Canterbury, 2000.

41. S. G. Telfer, Ph. D. thesis, Chemistry Department, University of Canterbury, 1999, and references therein.
42. H. Koyama and T. Yoshino, *Bull .Chem. Soc. Jpn.*, 1972, **45**, 481-484.
43. M. Ouchi, Y. Inoue, J. Liu, S. Nagamune, S. Nakamura, K.Wada and T. Hakushi, *Bull. Chem. Soc. Jpn.*, 1990, **63**, 1260-1262.
44. D. Parker, *Macrocycle Synthesis – A Practical Approach*, ed. B. Delmon, Oxford University Press, New York, 1996, p 4.
45. B. Wu, Ph. D. Thesis, Flinders University, Adelaide, Australia, 2005.
46. M. S. Okamoto and E. K. Barefield, *Inorg. Chim. Acta*, 1976, **17**, 91-96.
47. R. M. Hartshorn and C. Otter, *Aust. J. Chem.*, 2003, **56**, 1179-1186.
48. P. Crayton, *Inorg. Synth.*, 1963, **7**, 20-213.
49. R. M. Hartshorn, personal communication.
50. E. Kimura, S. Young and J. P. Collman, *Inorg. Chem.*, 1970, **9**, 1183-1191.
51. J. B. Mandel, C. Maricondi and B. E. Douglas, *Inorg. Chem.*, 1988, **27**, 2990-2996.
52. C. A. Otter and R. M. Hartshorn, *J. Chem Soc., Dalton Trans.*, 2004, **1**, 150-156.
53. H. Chaouk and M. T. W. Hearn, *J. Biochem. Biophys. Methods*, 1999, **39**, 161-177.
54. G. Lee, M. Oka, H. Takemura, Y. Miyahara, N. Shimizu and T. Inazu, *J. Org. Chem.*, 1996, **61**, 8304-8306.
55. G. Schwarzenbach, J. Boesch and H. Egli, *J. Inorg. Nucl. Chem.*, 1971, **33**, 2141-2156.
56. D. G. Lonnon, D. C. Craig and S. B. Colbran, *Inorg. Chem. Commun.*, 2003, **6**, 1351-1353.
57. E. Natarajan and P. Natarajan, *Inorg. Chem.*, 1992, **31**, 1215-20.
58. F. A. Cotton and G. Wilkinson, *Advanced Inorganic Chemistry – A Comprehensive Text*, Interscience Publishers, New York, 1966.
59. J. Lilie, N. Shinohara and M. Simic, *J. Am. Chem. Soc.*, 1976, **98**, 6516-20.
60. J. M. Browne, Masters thesis, Chemistry Department, University of Canterbury, 2000.
61. I. Rosenthal, M. M. Mossoba and P. Riesz, *J. Phys. Chem.*, 1981, **85**, 2398-2403.
62. J. D. Verkade and L. D. Quin, *Phosphorus-31 NMR Spectroscopy in Stereochemical Analysis – Organic Compounds and Metal Complexes*, ed. A. P. Marchand, VCH Publishers Inc., Deerfield Beach, Florida, 1987.

Appendix

X-ray Crystallographic Tables

The X-ray data were collected on a Siemens P4 four circle diffractometer, using a Siemens SMART 1K CCD area detector. The crystals were mounted 5.5 cm from the detector and irradiated with graphite monochromated Mo-Kα(λ = 0.71073) X-rays. The data were collected by the SMART program[1] and processed with the help of SAINT[2] to apply Lorentz and Polarisation corrections to the diffraction spots (integrated 3 dimensionally). SADABS[3] was used to scale the diffraction data, apply empirical adsorption corrections and to apply decay corrections if needed. Literature values for the neutral scattering factors and the anomalous dispersion corrections were used. The structures were solved by direct methods and refined using the SHELXTL[4] program. Hydrogen atoms were calculated at ideal positions and refined using a riding model.

Table A1.1 [Co(tacn)(PMG)]Cl·2O

Co-investigator	Professor Ward Robinson
Empirical formula	$C_8 H_{20} Cl Co N_4 O_8 P_2$
Formula weight	456.60
Temperature	88(2) K
Wavelength	0.71073 Å
Crystal system, space group	Orthorhombic, Pna2(1)
Unit cell dimensions	a = 10.5756(14) Å alpha = 90° b = 11.4738(14) Å beta = 90° c = 13.3690(18) Å gamma = 90°
Volume	1622.2(4) $Å^3$
Z	4
Calculated density	1.870 Mg/m^3
Absorption coefficient	1.467 mm^{-1}

F(000)	936
Crystal size	0.47 x 0.40 x 0.35 mm^3
Theta range for data collection	2.34 to 26.39°
Limiting indices	-12<=h<=13, -14<=k<=14, -16<=l<=15
Reflections collected / unique	13375 / 3220 [R(int) = 0.0287]
Completeness to theta = 26.39	99.3 %
Absorption correction	None
Refinement method	Full-matrix least-squares on F^2
Data / restraints / parameters	3220 / 1 / 217
Goodness-of-fit on F^2	1.583
Final R indices [I>2sigma(I)]	R_1 = 0.0960, wR_2 = 0.3070
R indices (all data)	R_1 = 0.1014, wR_2 = 0.3216
Absolute structure parameter	0.39(5)
Largest diff. peak and hole	3.688 and -2.808 e.$Å^{-3}$

Table A1.2 Bond lengths (Å) and angles (°) for [Co(tacn)(PMG)]Cl·2O

Co-O(6)	1.930(7)
Co-N(2)	1.929(9)
Co-N(4)	1.938(5)
Co-O(1)	1.935(6)
Co-N(3)	1.958(8)
Co-N(1)	1.993(5)
N(4)-C(7)	1.471(18)
N(4)-C(6)	1.471(15)
N(3)-C(5)	1.455(14)
N(3)-C(4)	1.461(14)
N(2)-C(3)	1.49(2)
N(2)-C(8)	1.500(14)
N(1)-C(1)	1.466(11)
N(1)-C(2)	1.504(11)
P(1)-O(1)	1.415(7)
P(1)-O(2)	1.406(10)
P(1)-O(3)	1.537(13)

P(1)-C(1)	1.800(11)
P(2)-O(5)	1.312(9)
P(2)-O(6)	1.448(7)
P(2)-O(4)	1.497(14)
P(2)-C(2)	1.689(10)
C(4)-C(3)	1.385(18)
C(8)-C(7)	1.46(2)
C(6)-C(5)	1.445(18)
O(3)-O(4)	1.601(17)

O(6)-Co-N(2)	91.3(4)
O(6)-Co-N(4)	89.6(3)
N(2)-Co-N(4)	87.1(3)
O(6)-Co-O(1)	92.00(19)
N(2)-Co-O(1)	176.0(4)
N(4)-Co-O(1)	90.7(3)
O(6)-Co-N(3)	174.2(3)
N(2)-Co-N(3)	85.4(3)
N(4)-Co-N(3)	85.5(4)
O(1)-Co-N(3)	91.1(3)
O(6)-Co-N(1)	88.1(3)
N(2)-Co-N(1)	95.6(3)
N(4)-Co-N(1)	176.5(2)
O(1)-Co-N(1)	86.7(3)
N(3)-Co-N(1)	97.0(3)
C(7)-N(4)-C(6)	116.2(14)
C(7)-N(4)-Co	106.5(6)
C(6)-N(4)-Co	111.5(7)
C(5)-N(3)-C(4)	117.5(9)
C(5)-N(3)-Co	109.2(7)
C(4)-N(3)-Co	109.6(7)
C(3)-N(2)-C(8)	102.5(12)
C(3)-N(2)-Co	110.7(9)
C(8)-N(2)-Co	110.1(6)
C(1)-N(1)-C(2)	112.2(5)
C(1)-N(1)-Co	112.1(6)
C(2)-N(1)-Co	105.5(5)
O(1)-P(1)-O(2)	111.3(5)
O(1)-P(1)-O(3)	116.6(6)
O(2)-P(1)-O(3)	108.0(7)
O(1)-P(1)-C(1)	103.4(5)
O(2)-P(1)-C(1)	107.1(5)
O(3)-P(1)-C(1)	110.0(6)
O(5)-P(2)-O(6)	116.9(5)
O(5)-P(2)-O(4)	103.1(6)
O(6)-P(2)-O(4)	112.4(5)
O(5)-P(2)-C(2)	111.2(6)
O(6)-P(2)-C(2)	101.1(4)
O(4)-P(2)-C(2)	112.5(7)
P(1)-O(1)-Co	117.1(4)

P(2)-O(6)-Co	117.5(4)
C(3)-C(4)-N(3)	114.5(14)
C(4)-C(3)-N(2)	114.7(13)
C(7)-C(8)-N(2)	111.9(10)
N(4)-C(7)-C(8)	113.2(14)
C(5)-C(6)-N(4)	113.4(10)
N(3)-C(5)-C(6)	113.7(11)
N(1)-C(1)-P(1)	105.4(6)
N(1)-C(2)-P(2)	111.8(5)
P(1)-O(3)-O(4)	121.4(10)
P(2)-O(4)-O(3)	125.1(10)

Table A2.1 [Co(tacn)(PMG)ZnCl$_3$]·H$_2$O

Co-investigator	Professor Ward Robinson
Empirical formula	$C_9 H_{23} Cl_3 Co N_4 O_6 P Zn$
Formula weight	544.93
Temperature	197(2) K
Wavelength	0.71073 Å
Crystal system, space group	Orthorhombic, Fdd2
Unit cell dimensions	a = 14.4192(9) Å alpha = 90° b = 50.313(3) Å beta = 90 ° c = 10.1290(6) Å gamma = 90°
Volume	7348.4(8) Å^3
Z	16
Calculated density	1.970 Mg/m^3
Absorption coefficient	2.766 mm^{-1}
F(000)	4416
Crystal size	0.85 x 0.36 x 0.10 mm
Theta range for data collection	2.49 to 26.39 deg.
Limiting indices	-17<=h<=15, -62<=k<=61, -12<=l<=5
Reflections collected / unique	8187 / 2825 [R(int) = 0.0271]

Completeness to theta = 26.39	99.4 %
Absorption correction	None
Refinement method	Full-matrix least-squares on F^2
Data / restraints / parameters	2825 / 3 / 236
Goodness-of-fit on F^2	1.110
Final R indices [I>2sigma(I)]	$R_1 = 0.0421$, $wR_2 = 0.1119$
R indices (all data)	$R_1 = 0.0425$, $wR_2 = 0.1122$
Absolute structure parameter	0.00
Largest diff. peak and hole	2.131 and -1.407 e.Å $^{-3}$

Table A2.2 Bond lengths (Å) and angles (°) for $[Co(tacn)(PMG)ZnCl_3]\cdot H_2O$

N(1)-C(3)	1.495(9)
N(1)-C(2)	1.497(8)
N(1)-Co	2.027(5)
N(2)-C(9)	1.476(9)
N(2)-C(4)	1.492(9)
N(2)-Co	1.914(5)
N(3)-C(5)	1.489(9)
N(3)-C(6)	1.516(8)
N(3)-Co	1.943(6)
N(4)-C(7)	1.476(9)
N(4)-C(8)	1.513(8)
N(4)-Co	1.927(5)
Co-O(1)	1.909(4)
Co-O(3)	1.910(5)
O(1)-C(1)	1.440(7)
O(2)-C(1)	1.315(8)
O(3)-P	1.472(5)
P-O(5)	1.488(6)
P-O(4)	1.582(7)
P-C(3)	1.777(8)
O(4)-H(6D)	1.57(4)
O(5)-Zn	1.982(5)
Zn-Cl(1)	2.2391(18)
Zn-Cl(2)	2.2488(17)
Zn-Cl(3)	2.2739(19)
C(1)-C(2)	1.614(9)

C(4)-C(5)	1.527(10)
C(6)-C(7)	1.488(10)
C(8)-C(9)	1.496(10)
C(3)-N(1)-C(2)	112.1(5)
C(3)-N(1)-Co	108.4(4)
C(2)-N(1)-Co	106.9(4)
C(9)-N(2)-C(4)	112.7(5)
C(9)-N(2)-Co	106.9(4)
C(4)-N(2)-Co	111.8(4)
C(5)-N(3)-C(6)	113.0(5)
C(5)-N(3)-Co	106.6(4)
C(6)-N(3)-Co	110.6(4)
C(7)-N(4)-C(8)	113.4(5)
C(7)-N(4)-Co	107.4(4)
C(8)-N(4)-Co	110.3(4)
O(1)-Co-O(3)	93.4(2)
O(1)-Co-N(2)	90.1(2)
O(3)-Co-N(2)	89.0(2)
O(1)-Co-N(4)	175.0(2)
O(3)-Co-N(4)	90.1(2)
N(2)-Co-N(4)	86.5(2)
O(1)-Co-N(3)	89.9(2)
O(3)-Co-N(3)	174.5(2)
N(2)-Co-N(3)	86.6(3)
N(4)-Co-N(3)	86.2(2)
O(1)-Co-N(1)	86.7(2)
O(3)-Co-N(1)	89.0(2)
N(2)-Co-N(1)	176.2(2)
N(4)-Co-N(1)	96.8(2)
N(3)-Co-N(1)	95.6(2)
C(1)-O(1)-Co	115.4(3)
P-O(3)-Co	115.6(3)
O(3)-P-O(5)	113.3(3)
O(3)-P-O(4)	112.1(3)
O(5)-P-O(4)	114.4(4)
O(3)-P-C(3)	102.8(3)
O(5)-P-C(3)	105.2(3)
O(4)-P-C(3)	107.9(4)
H(6D)-O(4)-P	119(3)
P-O(5)-Zn	122.7(3)
O(5)-Zn-Cl(1)	111.02(18)
O(5)-Zn-Cl(2)	104.75(17)
Cl(1)-Zn-Cl(2)	120.06(7)
O(5)-Zn-Cl(3)	110.43(16)
Cl(1)-Zn-Cl(3)	106.32(7)
Cl(2)-Zn-Cl(3)	103.93(7)
O(2)-C(1)-O(1)	113.5(6)
O(2)-C(1)-C(2)	114.1(6)
O(1)-C(1)-C(2)	105.3(5)

N(1)-C(2)-C(1)	109.7(5)
N(1)-C(3)-P	107.2(5)
N(2)-C(4)-C(5)	108.8(5)
N(3)-C(5)-C(4)	107.0(6)
C(7)-C(6)-N(3)	109.1(6)
N(4)-C(7)-C(6)	108.9(5)
C(9)-C(8)-N(4)	109.0(5)
N(2)-C(9)-C(8)	107.7(6)

Table A3.1 [Co(bamp)(PMG)]·3H_2O·OH·O·C_2·C

Co-investigator	Professor Ward Robinson	
Empirical formula	C_{13} H_{23} Co N_4 O_{10} P	
Formula weight	485.25	
Temperature	112(2) K	
Wavelength	0.71073 Å	
Crystal system, space group	Monoclinic, P2(1)/c	
Unit cell dimensions	a = 10.375(2) Å b = 9.158(2) Å c = 20.287(5) Å	alpha = 90° beta = 101.445(4)° gamma = 90°
Volume	1889.3(8) $Å^3$	
Z	4	
Calculated density	1.706 Mg/m^3	
Absorption coefficient	1.157 mm^{-1}	
F(000)	816	
Crystal size	0.65 x 0.32 x 0.13 mm	
Theta range for data collection	2.00 to 26.57 deg.	
Limiting indices	-13<=h<=13, -10<=k<=11, -25<=l<=25	
Reflections collected / unique	16416 / 3898 [R(int) = 0.0330]	
Completeness to theta = 26.57	98.8 %	
Absorption correction	None	

Max. and min. transmission	0.8642 and 0.5201
Refinement method	Full-matrix least-squares on F^2
Data / restraints / parameters	3898 / 10 / 302
Goodness-of-fit on F^2	1.073
Final R indices [I>2sigma(I)]	$R_1 = 0.0457$, $wR_2 = 0.1206$
R indices (all data)	$R_1 = 0.0558$, $wR_2 = 0.1257$
Largest diff. peak and hole	1.618 and -0.739 e.Å^{-3}

Table A3.2 Bond lengths (Å) and angles (°) for [Co(bamp)(PMG)] $3H_2O{\cdot}OH{\cdot}O{\cdot}C_2{\cdot}C$

Co-N(2)	1.860(3)
Co-O(1)	1.886(2)
Co-O(3)	1.907(2)
Co-N(1)	1.925(3)
Co-N(3)	1.937(3)
Co-N(4)	1.951(3)
N(1)-C(2)	1.463(4)
N(1)-C(3)	1.470(4)
N(2)-C(4)	1.319(5)
N(2)-C(8)	1.332(5)
N(3)-C(9)	1.470(4)
N(4)-C(10)	1.486(4)
C(1)-O(2)	1.227(4)
C(1)-O(1)	1.279(4)
C(1)-C(2)	1.495(5)
C(3)-P	1.805(3)
C(4)-C(5)	1.378(5)
C(4)-C(10)	1.489(5)
C(5)-C(6)	1.374(6)
C(6)-C(7)	1.372(6)
C(7)-C(8)	1.375(5)
C(8)-C(9)	1.479(5)
P-O(5)	1.496(2)
P-O(4)	1.498(2)
P-O(3)	1.545(2)
O(5)-H(1")	2.59(3)
C(12)-C(13)	1.72(3)
C(12)-C(11)	1.799(19)
O(1")-H(3")	1.01(2)
O(1")-H(1")	1.249(18)
N(2)-Co-O(1)	91.60(11)

N(2)-Co-O(3)	93.81(11)
O(1)-Co-O(3)	173.95(10)
N(2)-Co-N(1)	174.73(12)
O(1)-Co-N(1)	84.08(10)
O(3)-Co-N(1)	90.65(10)
N(2)-Co-N(3)	82.51(12)
O(1)-Co-N(3)	91.11(11)
O(3)-Co-N(3)	92.28(11)
N(1)-Co-N(3)	94.52(12)
N(2)-Co-N(4)	83.57(12)
O(1)-Co-N(4)	90.66(11)
O(3)-Co-N(4)	87.26(11)
N(1)-Co-N(4)	99.46(12)
N(3)-Co-N(4)	166.01(11)
C(2)-N(1)-C(3)	116.5(3)
C(2)-N(1)-Co	107.7(2)
C(3)-N(1)-Co	110.8(2)
C(4)-N(2)-C(8)	123.2(3)
C(4)-N(2)-Co	118.8(2)
C(8)-N(2)-Co	117.9(2)
C(9)-N(3)-Co	109.2(2)
C(10)-N(4)-Co	108.9(2)
O(2)-C(1)-O(1)	123.6(3)
O(2)-C(1)-C(2)	120.3(3)
O(1)-C(1)-C(2)	116.1(3)
N(1)-C(2)-C(1)	107.8(3)
N(1)-C(3)-P	103.7(2)
N(2)-C(4)-C(5)	119.7(3)
N(2)-C(4)-C(10)	112.9(3)
C(5)-C(4)-C(10)	127.4(3)
C(6)-C(5)-C(4)	118.3(4)
C(7)-C(6)-C(5)	120.8(3)
C(6)-C(7)-C(8)	118.5(4)
N(2)-C(8)-C(7)	119.5(3)
N(2)-C(8)-C(9)	112.8(3)
C(7)-C(8)-C(9)	127.6(3)
N(3)-C(9)-C(8)	108.0(3)
N(4)-C(10)-C(4)	109.1(3)
C(1)-O(1)-Co	114.6(2)
O(5)-P-O(4)	115.05(13)
O(5)-P-O(3)	111.02(13)
O(4)-P-O(3)	111.54(13)
O(5)-P-C(3)	107.48(15)
O(4)-P-C(3)	109.59(14)
O(3)-P-C(3)	101.16(13)
P-O(3)-Co	112.30(13)
P-O(5)-H(1")	117.7(7)
C(13)-C(12)-C(11)	97.4(9)
H(3")-O(1")-H(1")	89(2)

References for X-ray data

1. SMART Version 5.045, Data Collection Software, Siemens Analytical Instruments Inc., Madison, Wisconsin, 1998.
2. SAINT Version 5.01, Data Integration Software, Siemens Analytical Instruments Inc., Madison, Wisconsin, 1998.
3. G. M. Sheldick, SADABS Version 5.01, Program for Empirical Absorption Correction of Area Detector Data, University of Göttingen, Germany, 1996.
4. SHELXTL Reference Manual, Version 5.1, Bruker AXS, Madison, Wisconsin, 1997.